OFFICE OF ADVANCED RESEARCH AND TECHNOLOGY
SPACE VEHICLES DIVISION

4 B 145

PROCEEDINGS OF CONFERENCE ON

SPACECRAFT COATINGS DEVELOPMENT

MAY 6, 1964

NASA HEADQUARTERS

WASHINGTON, D.C.

Table of Contents

CONFERENCE ON SPACECRAFT COATINGS DEVELOPMENT

May 6, 1964

List of Attendees

Name	Center
Conrad P. Mook	Hdqt (RV-1)
Warren Keller	Hdqt (RV-1)
Wm F Carroll	JPL
John Lucas	JPL
Wm. Hagemeyer	JPL
W. L. Gill	MSC
R. A. Vogt	MSC
N. Ackerman	GSFC
John Rogers	GSFC
Nelson Hyman	GSFC
Jack Triolo	GSFC
John Schutt	GSFC
B. Seidenberg	GSFC
Joe Colony	GSFC
Archie Cunningham	GSFC
S. Ollendorf	GSFC
R. H. Hoffman	GSFC
M. Schach	GSFC
T. G. James	Langley
G. F. Pezdirtz	Langley -AMPD
R. A. Jewell	Langley -AMPD
R. L. Turner	Langley -AMPD
D. E. Wornom	Langley
Wm. R. Wade	Langley
V. L. Vaughan, Jr.	Langley
Walter T. Myers	MSFC R-P&VE-PTP
Wm. E. Murphy	MSFC R-Aero-ATA
R. L. Elkin	MSFC R-Aero-ATA
Klaus Schocken	MSFC R-RP-T
Gary Arnett	MSFC R-RP-T
Edgar R. Miller	MSFC R-RP-T
Eugene C. McKannan	MSFC R-P&VE-ME
Jackson C. Horton	MSFC R-P&VE-ME
D. W. Gates	MSFC R-RP
Morris Perlmutter	LeRC
Henry Curtis	LeRC
O. W. Uguccini	LeRC
Jack Howell	LeRC
Carr Neel	Ames RC
Elmer Streed	Ames RC

AGENDA

Space Vehicles Division
Office of Advanced Research and Technology
NASA Headquarters
Washington, D. C.

SPACECRAFT COATINGS DEVELOPMENT INCLUDING
UV DEGRADATION AND a/e MEASUREMENT PROBLEMS

Review and Planning Conference - May 6, 1964, to be held in OART Conference Room 6036, Federal Office Building 10B, 600 Independence Avenue, S.W.

Wednesday, May 6, 1964

9:00	Coatings Development and Environmental Effects - W. F. Carroll - JPL
9:45	Measurements of Hemispherical Total Emittance and Normal Solar Absorptance For Selected Materials in the Temperature Range 280° to 600°K - Henry B. Curtis - LeRC
10:15	BREAK
10:30	The Effect of Ultraviolet and Gamma Rays on Thermal Control Coatings - Robert A. Jewell and George F. Pezdirtz - LRC
11:15	Status Report on a/e Measurements at Goddard - Jack Triolo - GSFC
11:45	Spacecraft Coatings from a Temperature Control Point of View - W. A. Hagemeyer - JPL
12:15	LUNCH
1:30	Progress Report on Development of Thermal Control Coatings - Dr. John Schutt - GSFC
2:30	Spectral Emittance of Metals after Damage by Particle Impact - Dr. Klaus Schocken - MSFC
3:00	BREAK
3:15	Preliminary Results from a Round-Robin Study of Ultraviolet Degradation of Spacecraft Thermal Control Coatings - Carr B. Neel - ARC
4:00	Some Poly-Basic Phosphate Conversion Coatings for Thermal Control - Noel T. Wakelyn and George F. Pezdirtz - LRC
4:30	Round Table Discussion - Moderator - Conrad P. Mook

Conference Notes

The papers published herein were presented at a conference attended by NASA thermal control coating specialists and others with similar interests on May 6, 1964. The meeting was one of a series held in NASA Headquarters in Washington, D.C. during the first half of 1964, dealing with the subject "Thermal Radiation and Temperature Control."

Near the close of the conference a round table discussion took place in which it was decided that the most important matter facing the thermal control coating program was the need for thermal radiation measurement standards. Jack Triolo of Goddard volunteered to take the first steps toward the preparation and measurement of samples which would be submitted to other NASA laboratories for comparison. The various centers agreed to participate.

The second most important matter seemed to be the need for studies of the effects of high energy particle radiations on thermal control surfaces. In this connection a pro-tem committee, consisting of Dr. George Pezdirtz, William Carroll, Milton Schach, and the undersigned, agreed to look into the matter of holding a national conference of working specialists to examine this problem.

One additional paper, not listed on the original agenda, that by E. R. Streed, is included herein.

Conrad P. Mook
Office of Advanced Research
and Technology
NASA Headquarters (Code RV-1)
Washington, D.C.

COATINGS DEVELOPMENT AND ENVIRONMENTAL EFFECTS

William F. Carroll
Jet Propulsion Laboratory

Abstract

This presentation consists of three aspects of the JPL temperature control coatings work:

1. White coatings development and ultraviolet effects - IIT Research Institute Contract.

Since the significant results of this program are fully covered in an IIT Research Institute Report only a brief summary is presented. Plans for investigation of rate, wave length, and temperature dependence of ultraviolet degradation during the current year are discussed.

2. Proton and Other Effects

A limited study of the effects of protons on temperature control surfaces is now under way. Results indicate no serious effects on metallic surfaces (for temperature control), but very significant changes for white coatings. Available data is included. A serious need exists for further work in the area of charged particle effects.

3. Related Investigations in Progress

A list of programs in progress on effects other than those due to ultraviolet is presented.

I. WHITE COATINGS DEVELOPMENT AND ULTRAVIOLET EFFECTS (IIT RESEARCH INSTITUTE CONTRACT)

A. SUMMARY OF PAST WORK

The program has resulted in three basic coatings. The results through 1963 are summarized in Refs. 1 and 2. The formulations and properties of the three coatings are summarized in Appendix A of Ref. 1. All

three coatings are pigmented with zinc oxide but have varying physical properties and degrees of stability.

The ZnO-Potassium silicate coating is the most stable formulation developed, but, like all non-vitreous inorganic coatings, has adverse physical properties which limit its use. The coating is porous and therefore easily soiled and difficult to reclean. Therefore, use should be limited to applications where surfaces can be easily protected from contamination or where requirements for maximum stability justify extreme precautions for prevention of contamination. Like all inorganic coatings it is brittle and therefore not applicable where extreme flexure is anticipated.

The ZnO-silicone coating designated S-33 has stability nearly equivalent to the inorganic coating and has superior (but not optimum) flexability, cleanability and resistance to soiling. The vehicle, a pure methyl silicone, synthesized in the IITRI laboratory, is not available except in laboratory quantities. Part of the effort during the current year will be directed to adequate characterization of the synthesis to permit larger scale "production" of the resin.

The third coating, designated S-13, is also pigmented with ZnO and has a commercial silicone resin vehicle (General Electric LTV 602). Although less stable than the other two, it is more stable than most other white coatings and can be formulated from commercially available materials. It is non-porous so is resistant to contamination and is easily cleanable. A primer is required for adherence to most substrates.

B. CURRENT PROGRAM

The work during the current year will emphasize ZnO pigmented coatings (silicone and silicate) but utilizing other materials in addition to gain information on and understanding of U.V. damage.

The problem of laboratory simulation of space U.V. radiation will receive more attention. Irradiation rate as related to temperature effects, interplanetary projects (with changing solar constant), and practical testing and quality control will be investigated. Similarly, direct temperature effects will be studied. Simple tests will be conducted on the wavelength dependence of degradations to evaluate the validity of laboratory simulation and to attempt to correlate with other aspects of the program and to increase the understanding of U.V. damage. The latter will include study of the practical problems of possible catastrophic degradation of ZnO after prolonged periods. Other potential pigments and vehicles for coatings will be sought.

As mentioned earlier, one of the areas of investigation will be further work with the synthesis of silicone resins. The ultimate goal is practical production of coating materials but will include the effects of synthesis parameters, composition and structure on the resin and ultimately on the U.V. stability.

II. PROTON AND OTHER EFFECTS

A. INTRODUCTION

Environmental factors other than U.V. can now be important. The NRC work of 1960-61 concluded that the effects of $<2000\text{Å}$ U.V. radiations were similar to that produced by 2000-4000Å energy but less signi-

ficant due to the relatively lower total energy levels present. Now that more stable white coatings are available, additional work is required in this area.

The total energy is also low for other high energy electromagnetic radiation except in the case of flight reactors. Some work has been done as reported recently in Ref. 3. Additional work is required to define possible synergistic effects with other types of radiation.

The effects of the charged particle environment can be a significant problem as indicated by the test results to follow. These results are preliminary and are presented to demonstrate the types and magnitudes of effects to be anticipated.

The program resulted from Ref. 4 which reported discoloration of metallic surfaces by protons. Although it was recognized that the effect demonstrated was possibly (or probably) a contamination phenomenon, it was decided to pursue a limited program with the following objectives (listed strictly in their order of importance): (1) Prove whether or not the phenomenon could be attributed to contaminants and if not, the quantitative effects on thermal radiative properties; (2) If the effect was due to contaminants, could it occur at typical spacecraft contamination levels (either residual materials on the surface or as a result from outgassing of components); and (3) Check the effects to be expected on some of the coatings used on the spacecraft.

B. EQUIPMENT

The original tests used in the submitted proposal were conducted with the samples in the target end of the Van de Graff generator.

All tests reported here were irradiated in a high vacuum chamber attached to the Van de Graff through a differentially pumped system.

The proton beam was passed through a pair of slits, which constituted the terminals of a differentially pumped section of the system, into the high vacuum chamber. Electrical deflection of the proton beam permitted rastering the slit image beam across the surface of the sample to achieve uniform irradiation so that measurements of optical properties could be made. In addition, the sample was placed off the line-of-sight of the slits to reduce the probability of contamination effects.

C. RESULTS

The results presented are incomplete and are included only to indicate types of changes produced and the magnitude of the problem.

The Z-93 coating (ZnO-Potassium silicate) has a change in solar absorptance of .08 at 10^{15} particles per cm^2. At the same total dose, PV 100, the TiO_2-silicone alkyd white, changes .04-.05. As with ultraviolet effects, the only black tested showed no significant change. The Boeing barrier anodize coating showed slight changes in reflectance at wavelengths $< 4000\text{Å}$ at 10^{17} particles/cm^2.

No changes in total reflectance were seen for metallic surfaces, even when intentional contaminants were introduced into the system.

D. CHARACTER OF RESULTS

The magnitudes of changes of the Z-93 coating as a result of the 200 Kev protons used in this program are strikingly similar to the results obtained by Boeing at 1 mev on the same coating (Ref. 5).

The results with PV 100 are similarly comparable to those found by General Electric Co. with 400 Kev protons (Ref. 6). In addition, the spectral character of the changes in the S-13 coating are similar to those reported by Wehner in orally presenting Ref. 6 (however, they are not included in the written version). No quantitative comparison of change for equivalent dose for Wehner's work is available.

In all cases, the spectral nature of the reflectance change is similar to that encountered with ultraviolet effects. All white coatings tested decreased in reflectance in the short wavelength end of the visible, adjacent to the absorption edge (i.e., the coatings "yellowed").

The nature and reasons for the measured changes have not been established. Strictly chemical effects of H^+ (and possibly H_x^+) may be a factor. Secondary radiation produced at the surface may also contribute or be the real cause of the changes observed.

E. QUESTIONS AND DISCUSSION OF RESULTS AND TEST PROCEDURE

Although calculations can show that no significant temperature gradients can exist in the samples on a gross basis, at the irradiation rates used, these do not rule out the possibility of thermal effects on a crystallographic or instantaneous level.

During these tests, several months of space exposure were simulated in minutes or hours. Possible time, temperature or radiation dependent reversal (or promotion) of darkening reactions cannot be overlooked in considering results obtained.

Many problems exist in simulation testing of this type. A phenomenon referred to as "chasing," indicated by fluctuations in

measured beam current at the sample, and probably caused by deflection of the beam by static charge build-up at the sample surface, was encountered at some of the higher irradiation rates. Rates which appeared satisfactory for the Z-93 coating resulted in "chasing" with the organic coatings. Although tests which showed significant fluctuations were terminated, it is possible that less pronounced and therefore undetected similar effects were responsible for some of the differences in relative stability of the coatings tested.

A related but different rate problem was encountered on one test of the Boeing barrier anodize where a high irradiation rate was used. Visual examination of the surface after test indicated physical disruption of the anodic coating. Comparison of before and after reflectance curves showed a damping of the interference reflectance pattern which would result if part of the aluminum surface were bare after the test. Apparently, the charge build-up arced through the coating and caused fracture and removal of the anodic layer. Although this would not be encountered in space, it is discussed here because it represents a potential simulation problem.

To reiterate, although the results presented here indicate a significant problem with proton irradiation, possible synergistic or anergistic effects with other aspects of the space environment (i.e., U.V., electrons, etc.) should not be overlooked.

III. RELATED INVESTIGATIONS IN PROGRESS

Following is a list of programs, not necessarily complete, in progress or completed which are concerned with the effects on temperature control surfaces of environmental effects other than U.V.

1. Lockheed - Pile radiation (Ref. 3)
2. General Electric - Protons, electrons, $< 2000\text{Å}$ ultraviolet (Ref. 6)
3. Northrup Space Laboratory - X-rays (Dr. Robert Johnson)
4. Litton - Low energy protons (Ref. 7)
5. NASA-Ames Research Center - Low energy protons (Anderson)
6. Boeing - Protons, pile radiation (Ref. 5)

It is suggested that a meeting of people working in these related areas be held in an attempt to avoid a repeat of the duplication and confusion which occurred in U.V. testing 2 or 3 years ago.

References

1. Zerlaut, G. A., and Y. Harada, IIT Research Institute Report C-207-25, August 27, 1963.

2. Zerlaut, G. A. and Y. Harada, IIT Research Institute Report C-207-27, January 9, 1963.

3. Gilligan, J. E. and R.P. Caren, "Some fundamental aspects of nuclear radiation effects in spacecraft thermal control materials," presented in Session IV on Space Environmental Effects at the Symposium on Thermal Radiation of Solids, San Francisco, California, March 4-6, 1964.

4. AVCO Corp. Space Program Office, "An investigation of the discoloration of metal surfaces by ions in the solar system," Technical Proposal No. 414-1, June 3, 1963, to Jet Propulsion Laboratory.

5. Private communication from Roger Gillette, The Boeing Co.

6. Personal communication from Mr. Steve Drabeck, General Electric Co.

7. Wehner, G. K., "Solar-wind bombardment of a surface in space," Presented in Session IV on Space Environmental Effects at the Symposium on Thermal Radiation of Solids, San Francisco, California, March 4-6, 1964.

E-2397

MEASUREMENT OF HEMISPHERICAL TOTAL EMITTANCE AND NORMAL SOLAR ABSORPTANCE OF SELECTED MATERIALS IN THE TEMPERATURE RANGE 280° TO 600° K

By Henry B. Curtis

Lewis Research Center
National Aeronautics and Space Administration
Cleveland, Ohio

SUMMARY

A steady-state heat-balance method is used in making measurements of thermal-radiation parameters. The hemispherical total emittance and normal solar absorptance are measured in the temperature range 280° to 600° K. Results are given for the following surfaces which are applied to an aluminum substrate: four plasma-sprayed ceramics, zirconium silicate, strontium titanate, calcium titanate, and barium titanate; two ceramics applied by the Rokide Process, Rokide MA and Rokide ZS; anodized aluminum, plain and electrophoretically blackened; two multiple layer coatings; Tile Coat paint; and two pigmented coatings.

INTRODUCTION

The temperature control of space systems is primarily dependent on the thermal-radiation parameters of the materials used on the vehicle surface viewing the space environment. The important radiation parameters are hemispherical total emittance and normal solar absorptance, (hereinafter referred to as emittance and absorptance). The relative importance of these parameters depends on the temperature level and the environment of the space system. For example, the size of a radiator with a required heat-rejection rate and given temperature level is primarily dependent on the emittance. The absorptance is of importance to any space system of moderate temperature (under 600° K) with a view of the sun. The choice of materials for a space system is also governed by the overall space environment, the desired temperature range, and the expected useful life of the space system.

This paper describes measurements of emittance, absorptance, and their ratio for a variety of applicable materials. The temperature range covered by the measurements is 280° to 600° K. The radiation parameters of such materials as plasma-sprayed ceramics, painted coatings and composite coatings

consisting of thin layers of vapor deposited compounds were measured. The ultimate uses of such materials include low temperature radiators (under 600° K) and temperature control surfaces of space systems and experiments.

Measurements are made on an apparatus designed and built at the Lewis Research Center. This paper gives a brief description of the apparatus and methods used in making these measurements. A more complete description is given in reference 1. Results are given for several different materials together with descriptions of the materials.

MEASURING TECHNIQUE

A steady-state heat-balance method is used in measuring the radiation parameters. A test specimen is placed in a controlled environment and isolated in such a manner that the only form of heat transfer out of the specimen is accomplished by radiation, that is, the test surface radiates to a cold sink of known temperature. With a test specimen of known area, the specimen temperature and power required to maintain that temperature constant are measured. With this data, the emittance can be calculated by means of the Stefan-Boltzmann Law.

The absorptance is determined in a two-stage measurement. The power required to maintain the specimen at the same temperature is measured under two conditions; first, with and, then, without simulated solar energy incident normally on the specimen. The difference in the two power measurements is the rate at which solar energy is being absorbed. By knowing the incident solar flux the absorptance is calculated.

DESCRIPTION OF APPARATUS

A cutaway view of the test specimen assembly and heat shield is shown in figure 1. The test specimen consists of a 1-inch square substrate of aluminum with the test surface applied or bonded to one side. A heater plate with resistive heating is attached to the other side of the substrate. The test specimen assembly is placed in a heat shield, which covers the back and edges of the heater plate and the specimen. The heat shield and the heater plate are controlled to the same temperature with two similar automatic temperature controllers. This assures that there is no heat loss by radiation from the back and edges of the test specimen assembly. The power and thermocouple leads from the test specimen assembly are routed such that only a negligible amount of power is lost. A thermocouple is placed directly on the specimen substrate for temperature measurement of the test specimen. It has been found that if a thin layer of vacuum grease is spread between the heater plate and the specimen substrate, the thermal conduction

across the interface is greatly increased. No adverse effects on radiation parameters due to contamination by the grease have been observed.

The specimen assembly and the heat shield are placed in a test chamber evacuated to approximately 10^{-7} torr. A schematic of the test chamber is given in figure 2. The chamber is a hollow cylinder with the test specimen assembly and the heat shield mounted from one end flange. A quartz window is placed on the opposite end of the chamber to admit simulated solar radiation when needed. A hollow sleeve with blackened walls is built into the chamber, and liquid nitrogen is circulated through it to obtain a known low temperature sink. About 99 percent of the total solid angle viewed by the test surface is occupied by the cold sink.

The solar simulator for the absorptance tests utilizes a carbon arc lamp as an energy source. The output of the simulator is a collimated beam with a flux density equal to that of solar radiation outside the atmosphere of the earth (0.14 $w/cm^2 \pm 2\%$). The irradiance in the test plane is maintained within the indicated limits by an automatic controller, which continuously positions a pair of condensing lenses in the simulator. The normalized spectral distribution of the irradiance of the simulator has been measured, and the best known value is plotted in figure 3. Due to difficulties in measuring such spectral distributions, some error could be present in this curve. For comparison, the Johnson curve is also plotted in figure 3. The Johnson curve is the spectral distribution of solar energy outside the atmosphere of the earth (ref. 2). The area under each curve is equivalent to one solar constant (0.14 w/cm^2). A complete discussion of a similar solar simulator is given in reference 3.

The total output of the simulator is calibrated to one solar constant by two different methods. One method uses a narrow angle pyrheliometer, and the second uses a blackbody absorptance reference. The absorptance reference is a surface of notches formed by stacking razor blades side by side in a manner similar to that described in reference 4. The absorptance of the reference has been computed to be greater than 0.99 with the assumption of specular reflection. Tests have shown that the absorptance is independent of the inclination from the normal of the reference surface up to an angle of 30°. The inclination angle is generated by rotating the reference about an axis parallel to the razor blade edges. The two methods of calibration agree to within 2 percent.

An accuracy of ±5 percent (ref. 1) for the emittance is estimated with temperature measurement and power losses as the main sources of error. The inaccuracy in absorptance can be attributed to two basic sources of error. The first is associated with temperature control and power measurement, and is estimated to be ±5 percent. The second source of error is due to the solar simulator. This is caused by day-to-day shifts in the calibration and the spectral mismatch between the Johnson curve and the spectral distribution of the simulator. An example of the latter form of error would occur when the spectral absorptance of a specimen was high in a wavelength band where

the simulator had an excess of output energy. In this case, more energy would be absorbed in the test than under a true solar source. This leads to an error in the measured absorptance. This type of error occurs in the absorptance measurement of Tile Coat paint reported in this paper.

RESULTS

Ceramic Coatings

Measurements of emittance and absorptance have been made on several ceramic coatings applied to aluminum substrates. These coatings are being investigated for possible use on radiators in both low and high temperature ranges. Measurements were made on various thicknesses of six different materials. Figures 4 to 9 show emittance as a function of temperature for the six different ceramics. Table I gives the emittance at 500° K for each specimen. The ceramic coatings that were measured are barium titanate, calcium titanate, Rokide MA, Rokide ZS, strontium titanate, and zirconium silicate. On each graph, the coating mass per unit area and the approximate thickness are given for each specimen. The coating mass was determined by weighing the specimen before and after application of the coating. The approximation thickness is presented only to give an indication of the coating thickness. The error in these measurements is estimated at ±0.02 millimeter. It is seen that there is little temperature dependence of emittance; however, there is an increase in emittance as coating mass increases. This can be seen in figure 10, in which emittance at 500° K is plotted against coating mass. For any of these specific coatings, increasing the coating mass up to approximately 15 milligrams per centimeter squared increases the emittance of the coating. Beyond 15 milligrams per centimeter squared, there is little further change in emittance. Comparison of the emittance values with those published in reference 5 show a general agreement in the overlapping temperature region.

The absorptance data of each specimen is given in Table I. In general the absorptance is constant with temperature over the measured range 400° to 600° K. Some of the coatings, however, showed a marked drop in absorptance during the first heating to 600° K. After the initial heating, these specimens exhibited no further change in absorptance. This change is always a drop in absorptance, never an increase. The decrease is approximately 0.10 and is noticed in the barium and calcium titanates. The final stabilized absorptance values are those given in Table I. Table II denotes the general appearance of the specimens before and after testing. All specimens had a matted texture finish. A few of the specimens acquired a few dark specks during testing.

Anodized Aluminum

Measurements of emittance and absorptance were made on four anodized aluminum specimens. Two of the specimens had a layer of carbon electrophoretically deposited into the pores of the anodized aluminum. Two other anodized specimens were left plain. The purpose of the carbon black coating is to obtain a lightweight, high emittance coating. It was desired to determine the increase in emittance caused by adding the carbon layer to the anodized aluminum specimens.

The emittance measurements were made in the temperature range 300° to 600° K. Emittance against temperature plots for the two plain anodized specimens are given in figure 11. Specimen 1 in figure 11 was duller in appearance than specimen 2. This could account for the difference in emittance between the two. The emittance data for the two blackened specimens is given in figure 12. These two specimens were similar in appearance and were black in color.

The addition of the carbon layer has a definite effect on emittance. The two plain specimens both exhibit decreasing emittance with increasing temperature, while the black specimens have increasing emittance with increasing temperature. The difference in emittance between plain and blackened specimens at 600° K is on the order of 25 percent with the black specimens around emittance of 0.95. A summary of data for the anodized specimens is presented in Table III. The absorptance values were constant over the measured temperature range. A large increase in absorptance occurs because of the addition of the carbon layer.

Tile Coat Paint

Measurements of emittance and absorptance have been made on aluminum substrates coated with Tile Coat, a white epoxy-based paint. Measurements were made on two specimens around 320° K. In order to apply the paint to one specimen, the substrate was dipped into the paint and the excess was allowed to drain off. This resulted in a smooth even coating. The paint was sprayed on the other substrate resulting in a whiter coating. The thickness of the paint coatings were both about 0.2 millimeter. The data for the two specimens is given in Table III.

The emittance is consistent and agrees with previous results published in reference 6. From Table III it is seen that the method of application affects the absorptance values. The sprayed coating had an absorptance that was 11 percent lower than the dipped coating. The absorptance data reported herein is much higher than that in reference 6 (absorptance $\alpha = 0.20$). Part of this difference can be attributed to spectral mismatch between the

solar simulator used in the measurements reported herein and the Johnson Curve.

An attempt was made to estimate the error in absorptance readings due to this spectral mismatch. An analysis using the spectral absorptance of Tile Coat paint given in reference 6 and the spectral distribution of the solar simulator given in figure 3 accounts for approximately one third of the difference in absorptance measurements. The remaining difference is probably due to inaccuracies in the measured spectral distribution of the simulator and similar inaccuracies in the data of reference 3.

Multiple Layer Coatings

A series of measurements of absorptance and emittance in the temperature range 300° to 415° K was made on a proposed coating for a micrometeoroid satellite. The purpose of these measurements was to select a coating with a desired absorptance to emittance ratio. The coating consisted of four layers of material. Figure 13 shows a cross section of the coating. The base was 0.25-millimeter stainless steel with 12 microns of Mylar cemented to it. Vapor-deposited coatings of aluminum and silicon monoxide of various thicknesses were applied over the Mylar for thermal control purposes. The silicon monoxide layer was the outer surface of the coating. The data in the following table are emittance, absorptance, and the absorptance to emittance ratio for specimens with various thicknesses of aluminum and silicon monoxide. The silicon monoxide coating is the most important in determining the radiation parameters of the surface. Increasing thicknesses of silicon monoxide cause increasing emittance and decreasing absorptance to emittance ratios. The absorptance does not change much or show any trend with aluminum or silicon monoxide thicknesses. All data were consistent over the narrow temperature range, and no temperature dependence could be noted.

Thickness of coating, micron		Emittance, ϵ	Absorptance, α	Absorptance to emittance ratio, α/ϵ
Silicon monoxide	Aluminum			
0	1.0	0.06		
.6	1.0	.15	0.18	1.2
.6	1.0	.16	.19	1.2
.7	.1	.15	.13	.86
1.1	.1	.26	.13	.50
1.2	1.0	.46	.15	.33

Measurements have been made of emittance and absorptance on a 65-micron foil bonded to an aluminum substrate. The foil is of a layered construction with a coating of aluminum covered on both sides by Mylar. The foil was to be used as a covering for the insulation of the Centaur cryogenic fuel tanks. It is required to hold boil-off to a minimum during an extended parking orbit; however, charing and discoloration would occur during take-off because of aerodynamic heating. Therefore, measurements were made to determine the change in radiation parameters due to the color change. The temperature level associated with aerodynamic heating was simulated by heating samples of the foil in an oven at atmospheric pressure. The samples were heated to a given temperature, held at that temperature for a given time, and then allowed to cool. The different samples were then bonded to aluminum substrates and measurements of the radiation parameters were made in the temperature range 300° to 375° K. The results are:

Heating cycle		Surface color	Emittance	Absorptance
Temperature, °K	Time, min			
---	---	Clear	0.67	0.23
440	3	Clear	.66	.27
540	1	Yellow	.69	.38
660	1	Orange-brown	.69	.50

The data show that the emittance stays almost constant, but the absorptance greatly increases because of higher temperature preheating treatments. This makes the foil ineffective for the desired purpose.

Pigmented Coatings

Measurements are being made currently on a series of coatings under investigation for possible use on a solar Brayton cycle radiator. Table IV gives absorptance and emittance in the indicated temperature range for two different coatings. The first is a stannic oxide coating with an aluminum metaphosphate binder. The coating thickness is approximately 2 mils including a nickel-chrome-cobalt spinel subcoat. The emittance values rise steadily from 0.90 to 0.96 in the temperature range 300° to 550° K. The absorptance values show no trend with temperature. The second coating is a zinc oxide pigmented paint with a methyl silicone vehicle. This is one of the paints developed by Zerlaut at Illinois Tech. The coating is approximately 5 mils thick and white in color. The emittance data increases from 0.92 to 0.96 over the indicated temperature range while the absorptance data is constant at approximately 0.20 to 0.21.

CONCLUDING REMARKS

The apparatus is capable of making measurements of the radiation parameter

of a wide variety of materials. All measurements were made with aluminum substrates for the surface to be tested. For a given specimen, the emittance measurements are repeatable to within $\pm 1\frac{1}{2}$ percent, while the absorptance values repeat to within ±5 percent. In general, where comparisons are available, the measured emittance data agree with published results. There is a large difference, however between measured and published absorptance data for Tile Coat paint, which is the only absorptance data comparison made. This seems to indicate that if any error is inherent in the measurements reported herein it is with the irradiance of the solar simulator or with application and handling techniques. It can be concluded that there is a thickness of ceramic coating beyond which additional application of ceramic has little effect on emittance. Similarly, emittance values over a large range can be achieved with proper selection of thicknesses of the vapor-deposited layers for the multiple layer coating.

REFERENCES

1. Nyland, Ted W.: Apparatus for the Measurement of Hemispherical Emittance and Solar Absorptance from 270° to 650° K. Presented at the Symposium on Measurement of Thermal Radiation Properties of Solids at Dayton, Ohio, Sept. 5-7, 1962.

2. Johnson, Francis S.: The Solar Constant. J. Meteorol. vol. 11, no. 6, Dec. 1954, pp. 431-439.

3. Uguccini, Orlando W., and Pollack, John L.: A Carbon-Arc Solar Simulator. ASME paper 62-Wa-241, Nov. 1962.

4. Neal, Carr B.: Measurement of Thermal Radiation Characteristics of Temperature-Control Surfaces During Flight in Space. Presented at the Ninth National ISA Aerospace Instrumentation Symposium, San Francisco (Calif), May 6-8, 1963.

5. Askwyth, W. H., and Hayes, R. J.: Quarterly Progress Report, Determination of the Emissivity of Materials. PWA-2128, Pratt and Whitney Aircraft. Report Period: July 1 - Sept. 30, 1962.

6. Brock, C. L., and Ernst, W. A.: Solar Reflective Finish for Space Applications. Westinghouse Electric Corp., Report AA-3276, Dec. 1962.

TABLE 1. - EMITTANCE AND ABSORPTANCE

FOR CERAMIC COATINGS

Substance	Mass/unit area, mg/cm^2	Emittance,[a] ϵ	Absorptance,[b] α
Barium titanate	5.9	0.75	0.65
	17	0.82	0.61
	49	0.87	0.74
Calcium titanate	6.2	0.75	0.72
	11.3	0.82	0.70
	23	0.88	0.70
Rokide MA	2.3	0.55	0.55
	6.0	0.71	0.58
	31	0.82	0.41
Rokide ZS	6.5	0.79	0.54
	32	0.89	0.45
Strontium titanate	12	0.81	0.73
	28	0.82	0.76
	40	0.83	0.64
Zirconium silicate	8.3	0.83	0.46
	9.5	0.83	0.38
	29	0.86	0.37

[a]At 500° K.

[b]Measurement at 400° to 600° K.

TABLE II. - DESCRIPTION OF CERAMIC COATINGS

Substance	Method of application	Appearance	
		Before test	After test
Barium titanate	Plasma-arc spraying	Dark grey	No change
Calcium titanate	Plasma-arc spraying	Grey with red tint	Grey
Rokide MA	Rokide process	Grey with blue tint	No change
Rokide ZS	Rokide process	Light grey with blue tint	No change
Strontium titanate	Plasma-arc spraying	Dark grey	No change
Zirconium titanate	Plasma-arc spraying	Light grey	No change

TABLE III. - EMITTANCE AND ABSORPTANCE FOR ANODIZED ALUMINUM AND TILE COAT PAINT

Coating	Emittance, ϵ		Absorptance, α	
	Value	Measured temperature	Value	Temperature range
Anodized plain 1	0.83	500° K	0.57	400° to 600° K
Anodized plain 2	0.71	500° K	0.48	400° to 600° K
Anodized blackened 1	0.94	500° K	0.97	400° to 600° K
Anodized blackened 2	0.97	500° K	0.97	400° to 600° K
Dipped Tile Coat	0.89	330° K	0.38	320° K
Sprayed Tile Coat	0.89	330° K	0.34	320° K

TABLE IV. - EMITTANCE AND ABSORPTANCE OF ZINC-OXIDE AND STANNIC OXIDE PIGMENTED COATINGS

TEMPERATURE RANGE 300° TO 550° K

Coating	Thickness, mils	Emittance, ϵ	Absorptance, α
SnO pigmented coating Aluminum metaphosphate binder Ni-Cr-Co spinel subcoat	2	0.90-0.96	0.40-0.43
ZnO pigmented paint Methyl silicone vehicle	5	0.92-0.96	0.20-0.21

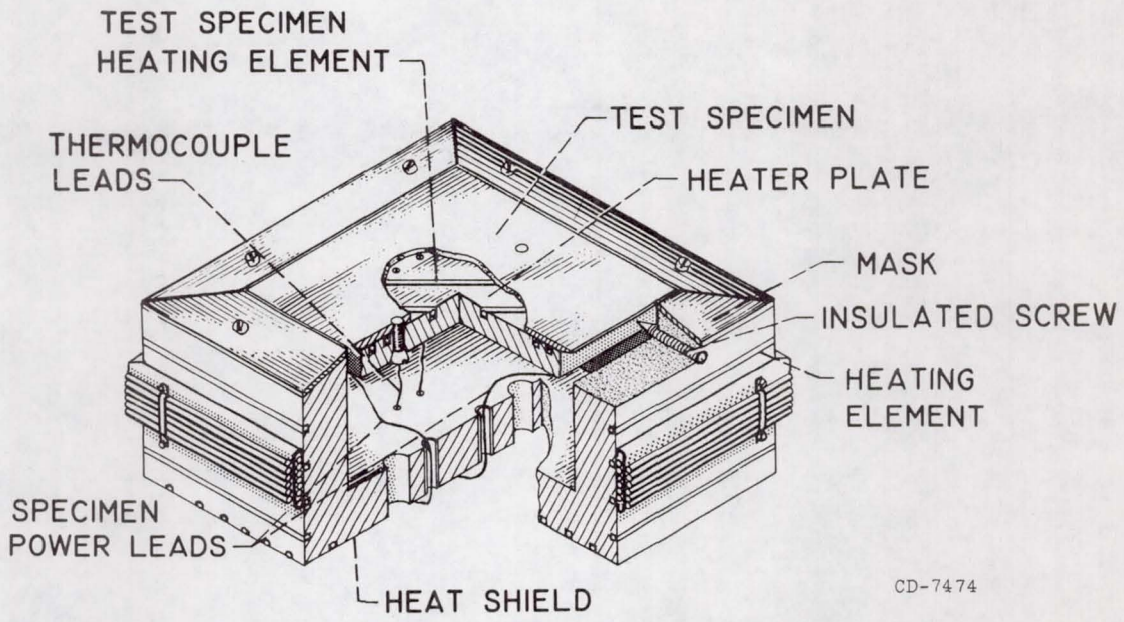

Figure 1. - Test specimen assembly and heat shield.

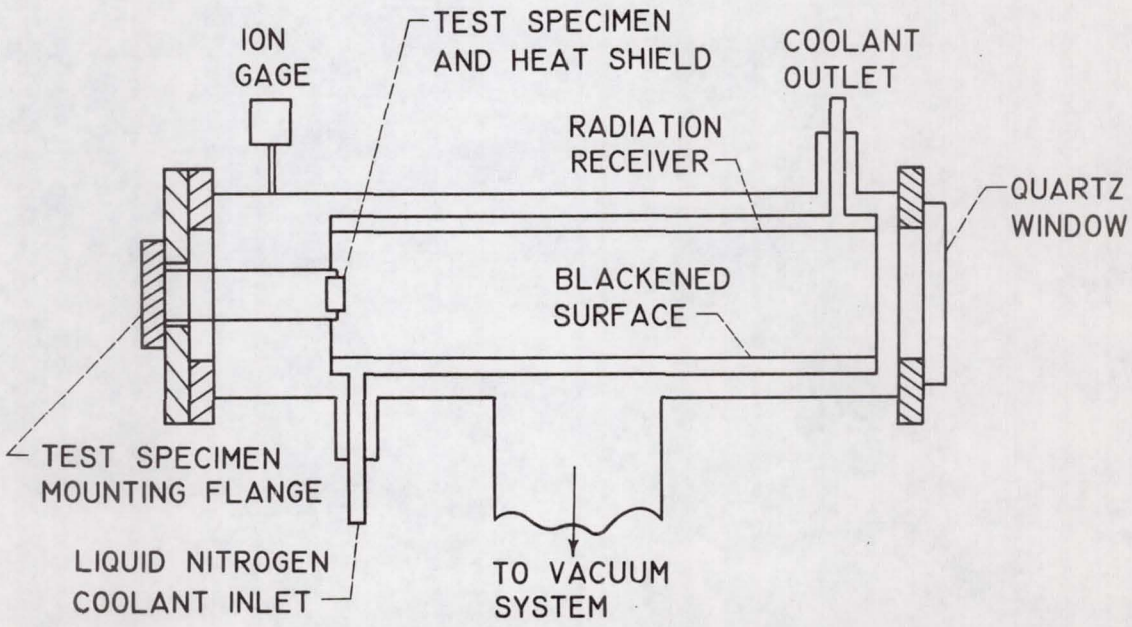

Figure 2. - Schematic of test chamber.

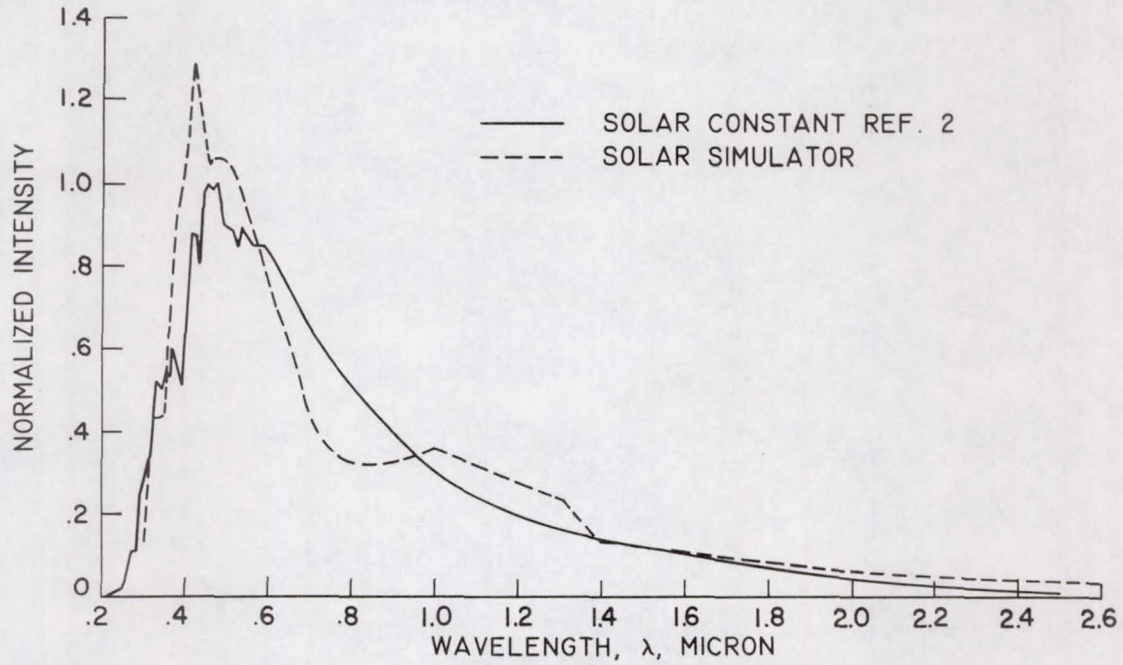

Figure 3. - Normalized spectral distribution of solar simulator irradiance.

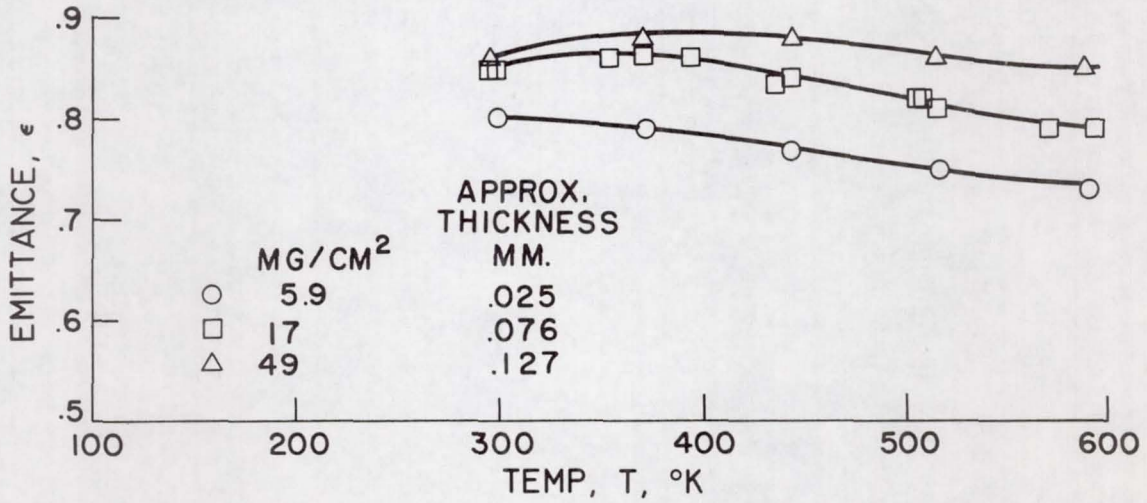

Figure 4. - Emittance as a function of temperature (barium titanate).

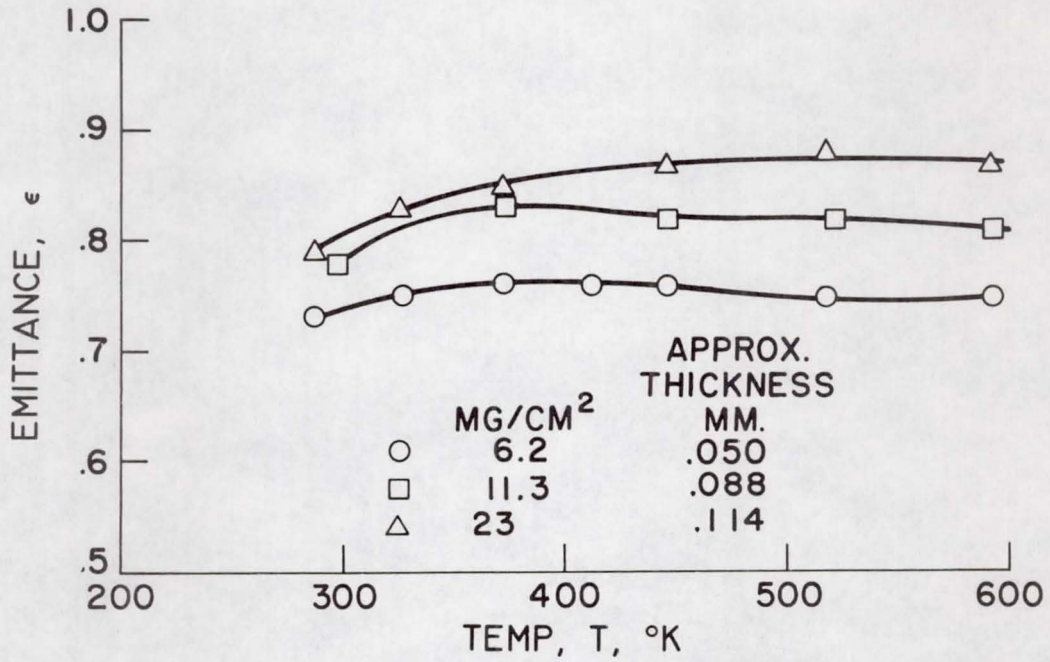

Figure 5. - Emittance as a function of temperature (calcium titanate).

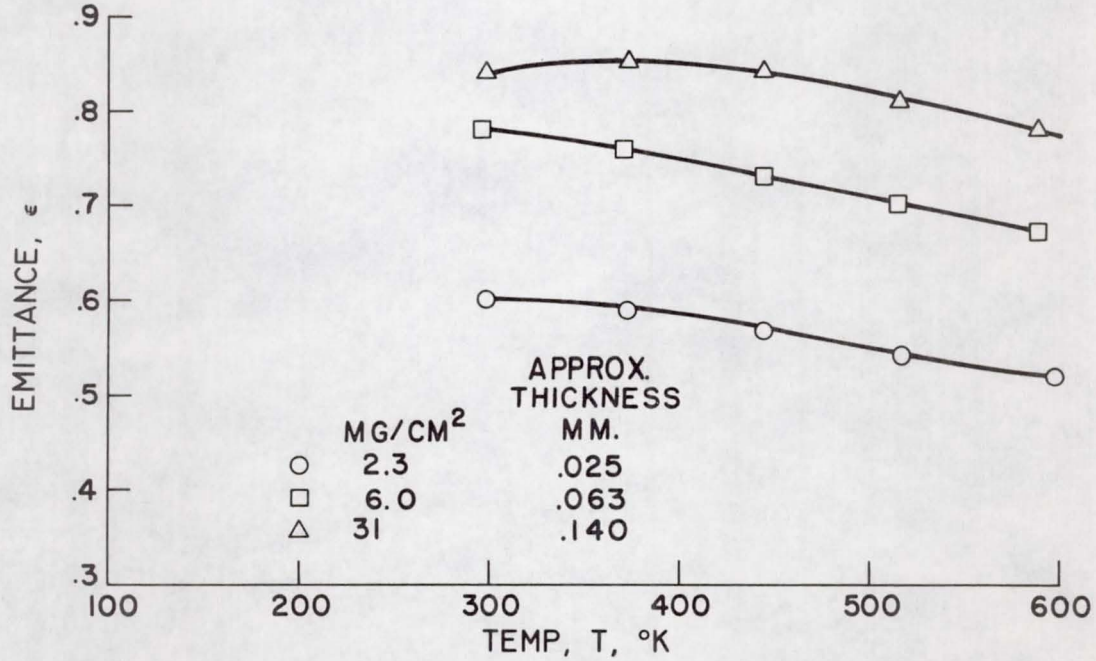

Figure 6. - Emittance as a function of temperature (Rokide MA).

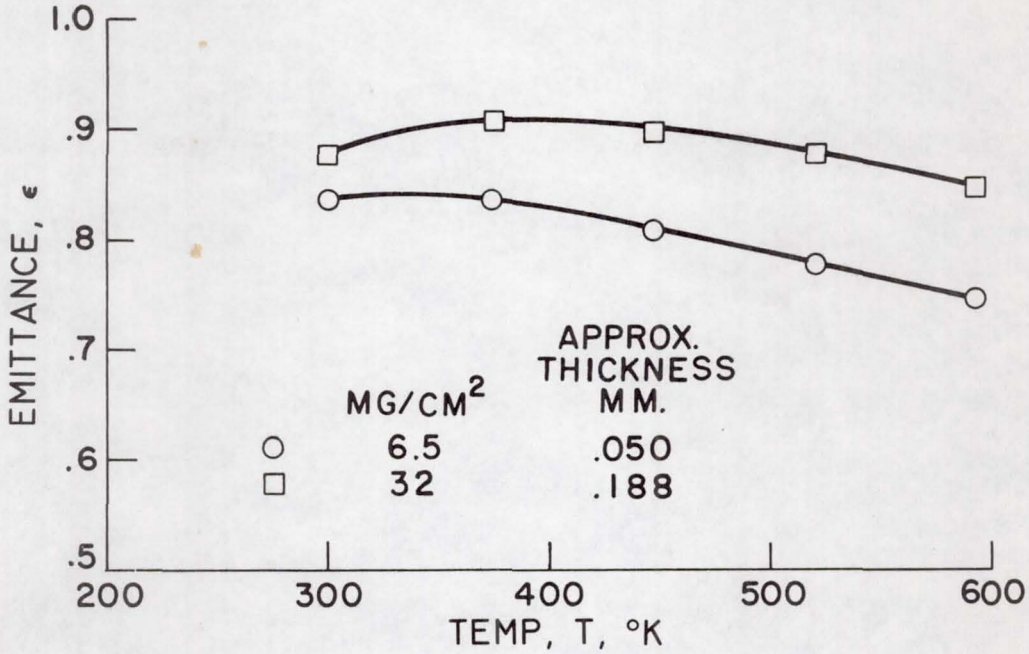

Figure 7. - Emittance as a function of temperature (Rokide ZS).

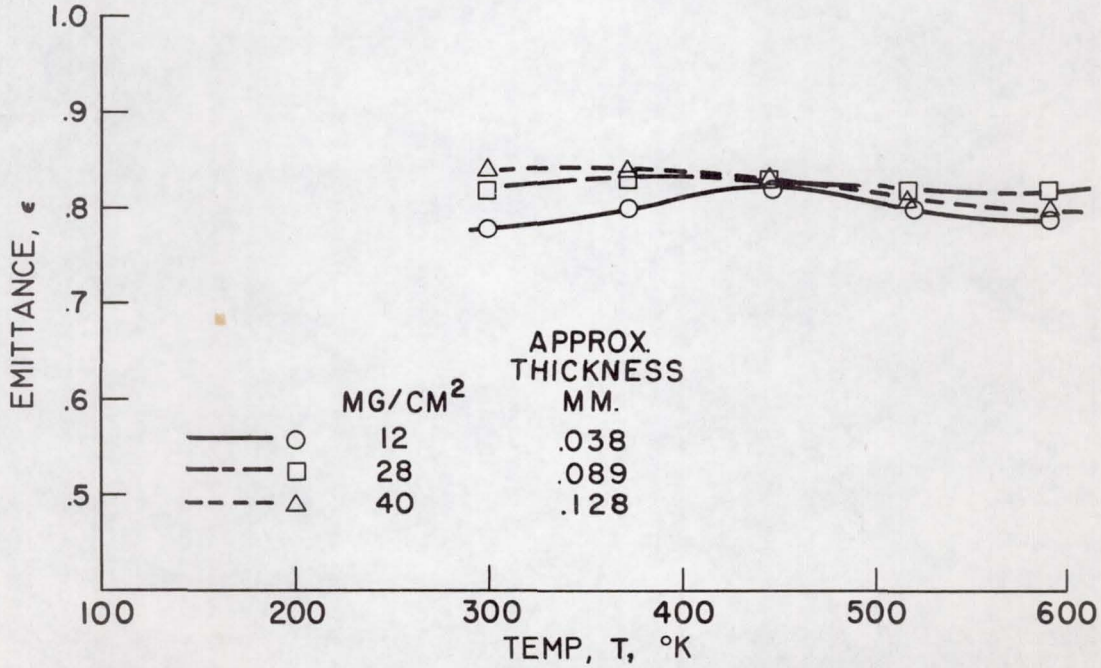

Figure 8. - Emittance as a function of temperature (strontium titanate).

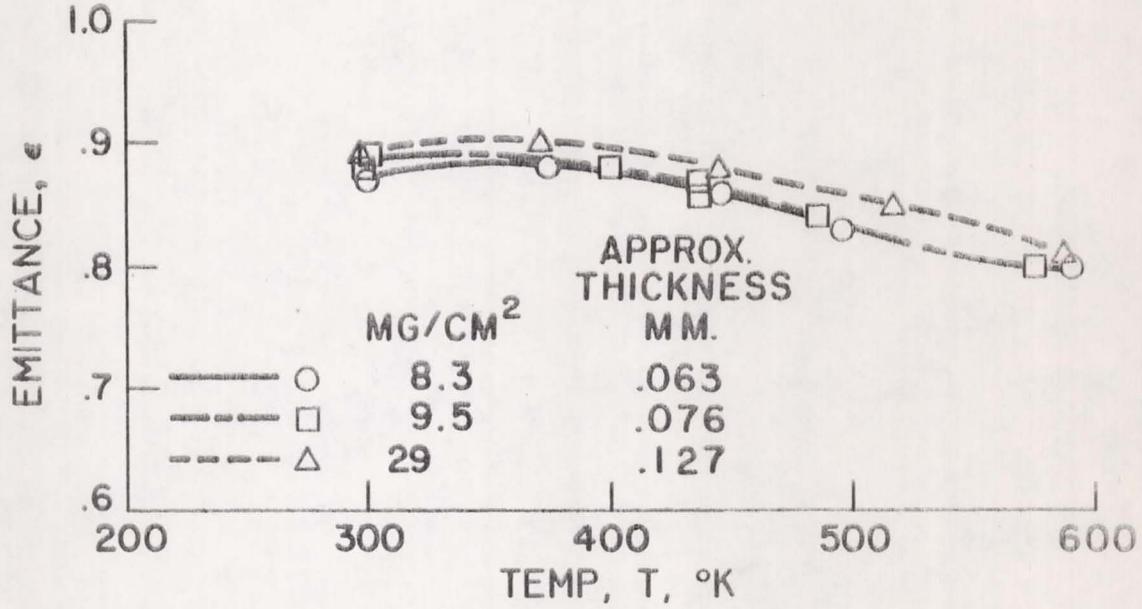

Figure 9. - Emittance as a function of temperature (zirconium silicate).

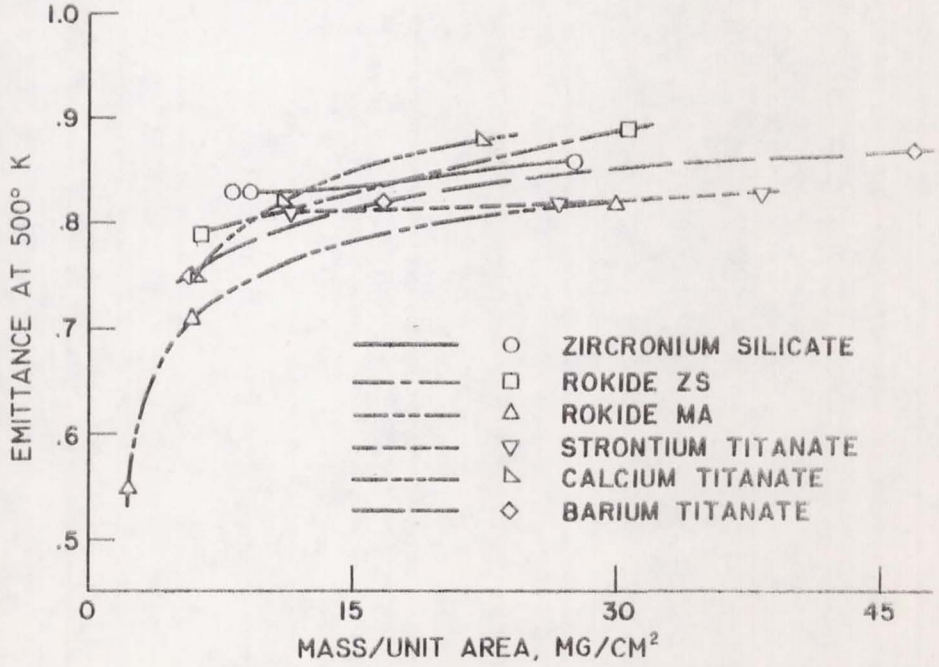

Figure 10. - Emittance of ceramics at 500° K as a function of coating mass per unit area.

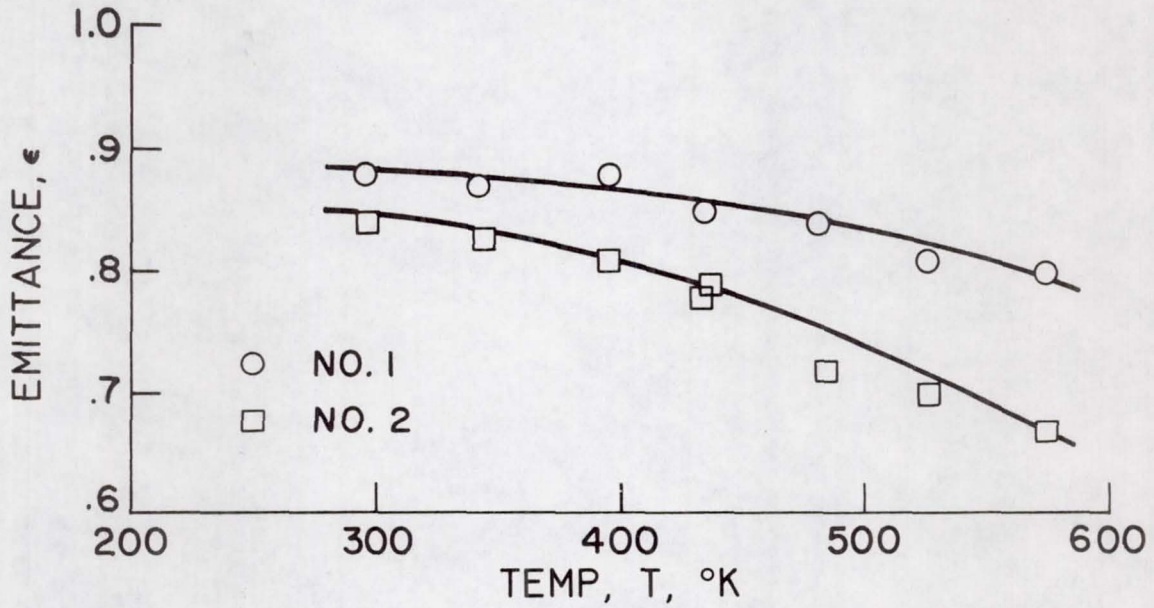

Figure 11. - Emittance as a function of temperature (plain anodized aluminum).

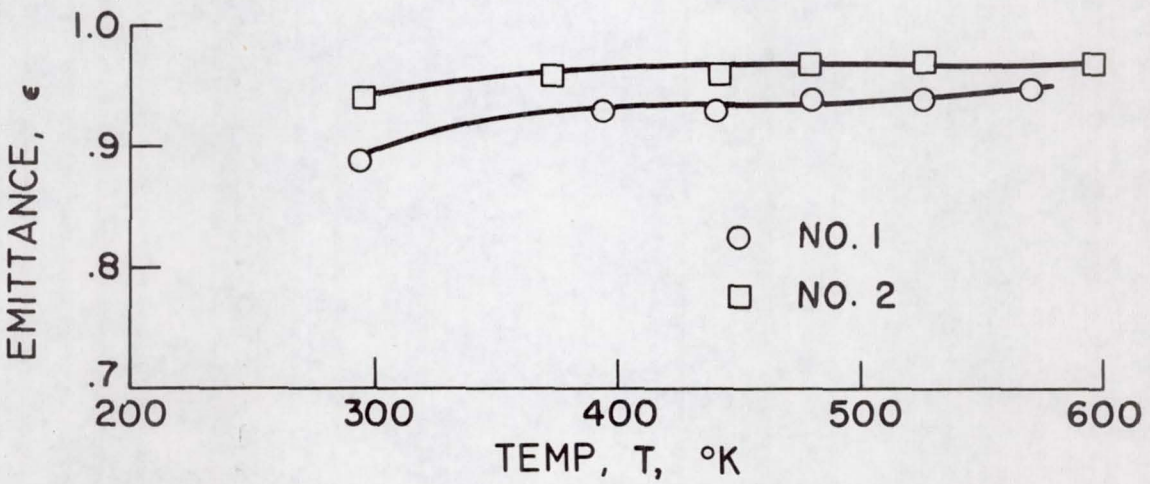

Figure 12. - Emittance as a function of temperature (blackened anodized aluminum).

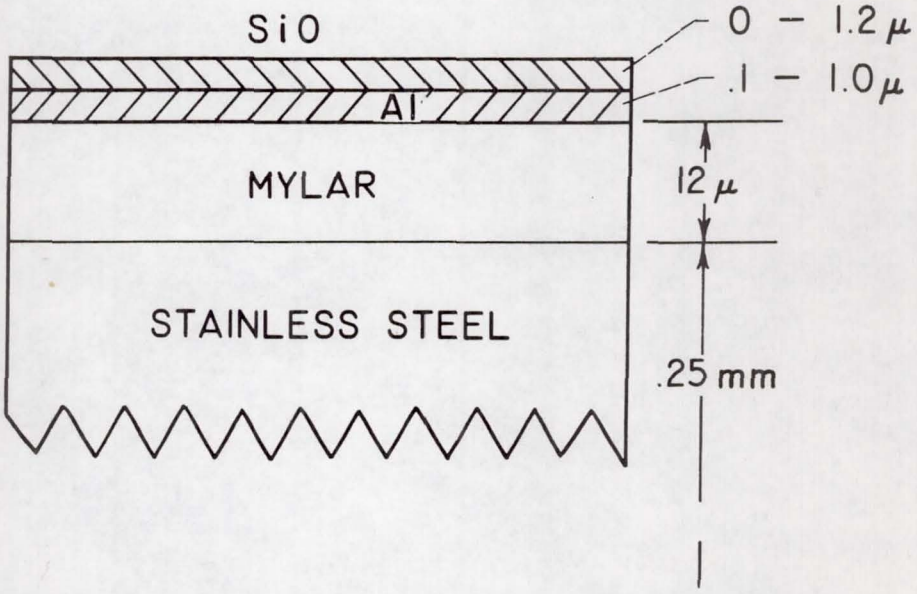

Figure 13. - Cross section of multiple layer coating with vapor-deposited aluminum and silicon monoxide.

A SURVEY OF α_s- $\bar{\epsilon}$ INSTRUMENTATION AT GODDARD SPACE FLIGHT CENTER

by

Jack J. Triolo

Introduction

There are a number of different methods of measuring α_s, the solar absorptance, and $\bar{\epsilon}$, the thermal emittance. One way of classifying these methods is by the type and variety of data obtained. Optical methods measure α_s and $\bar{\epsilon}$ by the radiation reflected from, or emitted by, materials; this radiation may be either spectrally resolved or integrated. Thermal methods measure α_s and $\bar{\epsilon}$ by the temperature, or rate of change of temperature, of materials. Optical methods require the elimination of, or the control of, background radiation. Thermal methods require, in addition, a high vacuum surrounding the sample of the material being measured. Also, to obtain α_s values by thermal methods, a light source whose spectral distribution is similar to that of the sun ("solar simulator") is necessary, plus instrumentation for measuring the intensity of the light from the solar simulator.

The different methods for measuring α_s and $\bar{\epsilon}$, then, are classified as follows:

A. Optical methods

1. Reflectance measurements

a. Spectrally resolved

(1) 0.3 to 2.5 microns, for α_s

(2) 5 to 35 microns, for $\bar{\epsilon}$

b. Integrated

(1) Light source spectral intensity times detector spectral response must match solar spectrum approximately, for α_s.

(2) Light source spectral intensity times detector spectral response must match 300°K blackbody approximately, for $\bar{\epsilon}$.

2. Emitted radiation measurements, for $\bar{\epsilon}$ only

a. Spectrally resolved

(1) 5 to 35 microns

b. Integrated

B. Thermal Methods

1. Equilibrium measurements

   a. With electrical heating for $\bar{\varepsilon}$

   b. With solar simulator as heater, for $\alpha_s/\bar{\varepsilon}$

   c. With solar simulator, for α_s (water calorimeter

   d. With sun (flight experiment in orbit), for $\alpha_s/\bar{\varepsilon}$

2. Dynamic measurements

   a. With solar simulator as heater, for $\bar{\varepsilon}$

   b. Adiabatic cooling, for $\bar{\varepsilon}$

   c. With sun as heater (flight experiment in orbit), for $\bar{\varepsilon}$

In this brief outline it is not feasible to analyze in full detail each of these methods. However, I shall point out which of the above mentioned methods we maintain are necessary for a complete knowledge of coating properties, and a short description of this equipment will be given.

Optical Methods

I. Solar Region (.3 to 2.5 microns) - The wavelength region .3 to 2.5 microns contains 95.3% of the sun's energy; 3.4% is above 2.5 microns. This wavelength (2.5 microns) is the limit for most reflectometers of this region since most of them

employ integrating spheres coated with MgO which absorbs significantly beyond 2.5 microns.

At Goddard, we use a Beckman DK-2 (Figure 1) and a Perkin-Elmer 350 Spectrophotometer which are basically the same, as well as being similar to the Cary 14. The Beckman DK-2 is a single quartz prism monochromator, while the P. E. 350 and the Cary 14 utilize double monochromators. However, they all employ an integrating sphere coated with MgO. The integrating sphere is most accurate when the test sample reflectance is near that of the reflectance standard used, and, furthermore, when the polar reflectance patterns are similar. Thus, a specular sample should be measured with a specular standard and a diffuse sample with a diffuse standard. If the test sample is neither perfectly diffuse nor perfectly specular, but falls somewhere in between, it may be difficult to obtain a reflectance standard having a similar polar reflectance pattern. In this case, the accuracy of the measurement may be questionable since the average number of reflections undergone by light reflected from the test sample before it reaches the detector, may not be equal to the average number of reflectances undergone by light reflected from the reflectance standard. If the interior coating

of the sphere possessed a reflectance of 100%, this difference in the average number of reflections would be unimportant, since it is the light absorbed at each reflection which produces a difference between measurements otherwise equal but having a different average number of reflections. The highest reflectance obtainable for a sphere coating at present is about 98% (in the visible) with a thick (several millimeters) coating of MgO, and so, there is a possibility of error in reflectance measurements with an integrating sphere on materials having both a diffuse and specular component of reflectance.

As of now, we have only sketched measurements for near normal incidence; however, since most spacecraft are spherical, cylindrical, or are constructed with flat surfaces on rotating spacecraft, the normal absorptance is no longer adequate and the reflectance or absorptance must be known as a function of angle of incidence. For this measurement we use an integrating sphere made by Gier-Dunkle Thermal Instruments, in conjunction with their source optics and a Perkin-Elmer 99 Monochromator (Figure 2). This instrument can also measure transmittance as a function of angle of incidence (10^{o} to 80^{o}) for transparent and practically opaque materials. It is also invaluable for solar cell

measurements where the areas are small and sometimes covered with thick quartz radiation shields which are difficult to measure on the other instruments. This measurement of a multi-layer surface can be accomplished since the samples are mounted on the interior of the integrating sphere (Figure 3) at the end of a rod which penetrates the sphere and rotates to change the angle of incidence of the sample. Note that the integrating sphere can be rotated about two axes thereby allowing the uniformity of the reflectance of the sphere to be checked in place.

A portable integrating sphere was developed at Goddard for field measurements. It consists of a six-inch integrating sphere coated with barium sulfate which is considerably more rugged than MgO, and uses a six volt tungsten lamp as a light source which was powered by a regulated power supply (Figure 4). The light tube was designed to accept 2 x 2 inch interference filter to provide the wavelength band desired for the measurement. The integrated portable package is seen in Figure 5. The detector system originally used was a Photovolt photometer and 1P28 P.M. tube. At the present, the instrument is undergoing redesign and modification. A Schoeffel monochromator is replacing the filters, and an Eldorado photometer (Figure 6)

which was found to be more stable replaces the Photovolt. Since the monochromator has a range of .23 to 2.5 microns, the detector system will be designed to include a lead sulfide detector for the near infrared. The instrument is a single beam point by point measurement and is meant only for field use or where the samples cannot be brought up to the laboratory instruments (DK-2 or P.E. 350). These alterations should make the instrument more versatile and faster to use, since changing filters was so time consuming. The complete instrument will also be fitted and contained in two suitcases to make it more portable. Reference 1 has a complete description of the portable integrating sphere.

II. 5 - 35 Micron Region ($300^{o}K$ Blackbody)

Normal emittance for $300^{o}K$ blackbody is calculated from reflectance data in the wavelength range of 5 to 35 microns. This interval contains 91.0% of the energy of $300^{o}K$ blackbody; 7.7% is at longer wavelengths.

Unless the sample is optically flat and totally specular, a reflectance attachment is needed to measure spectral total reflectance. In this region a hohlraum

(heated cavity) and the Coblentz hemisphere, are the attachments most used. At Goddard we have both, but at present only use the hohlraum because the Coblentz was found to be initially unsatisfactory. The Coblentz hemisphere, which is really an approximation of an ellipoidal mirror, is attached to a Beckman IR-7, and works on the principle of conjugate foci, one for the sample and the other for the detector. In order to include both the specular and the diffuse components of the radiant energy, the detector must have a large angle of view, ideally 2π steradians. The thermocouple used for this purpose views about a quarter of the total solid angle and thereby neglects a significant part of the diffuse component. This is no small problem and Beckman still has not resolved it.

The hohlraum attached to a Perkin-Elmer 13-U Spectrophotometer, has two openings, one of which allows the insertion of a water-cooled sample holder which keeps the sample at a reasonable temperature ($100^{o}F$) even though the oven may be as high as $1,100^{o}C$. The other opening allows the infrared spectrophotometer to view the oven, or sample. It thus acts as the radiation source for the spectrophotometer and illuminates the sample diffusely which is a necessary feature for diffuse reflectance measurements.

To facilitate data reduction, a Hoffman calibrator is employed. The Hoffman calibrator permits digital read-out and automatic accumulation. The entire system can be seen in Figure 7.

Now consider the optical emitted radiation type instrument (classification A2b). The Barnes Emissometer (Figure 8) is such an instrument. The emissometer consists of an eight-inch radiometer with an emissivity attachment. It is designed to measure total normal emittance in temperature range from ambient to 220°C. The emissivity attachment (Figure 9) contains a temperature controlled blackbody reference and a temperature controlled sample holder. The temperature controls are capable of ±1°C temperature regulation. Both the blackbody and the sample are kept at the sample temperature during a reading. A mirror rotates, thus selecting the source of radiation for the emissometer. The emissivity attachment and radiometer had have exactly the same optics, a Cassegrainian System which provide the sample, blackbody, and detector with the same field of view. This scheme should provide an absolute measurement, since presumably the ratio of the reading of the blackbody and the sample should give the $\bar{\epsilon}$ for the sample. This, however, is not the case. For high reflectors, the radiation from the surroundings

reflecting from the surface of the sample is sensed by the detector, which gives rise to the additional term in the equation, several times greater than the term containing the parameter to be measured. We are now attempting to eliminate this source of error by cooling and thus reduce the radiation from the surroundings.

Thermal Measurements

One of the thermal vacuum chambers used for the measurement of hemispherical emittance and solar absorptance consists of an 18" vacuum evaporator fitted with a liquid nitrogen cooled shroud (Figure 15) and maintains a pressure of 10^{-7} Torr in the belljar. The sample, as shown in Figures 16 and 17, hangs from cotton or dacron strings while the temperature is sensed by a copper-constantan thermocouple. A Dymec Data Acquisition System and a Joseph Kay reference junction are used together with the thermocouple to measure the temperature. The data is then punched and/or printed on paper tape and will be programmed for machine data reduction.

The carbon arc (Figure 18) serves as the source for heating the sample through a quartz port. When the monitor sample and test sample reach a temperature equilibrium (B1b classification), the arc is turned off allowing the sample to cool. This provides a temperature transient by which one may calculate the hemispherical emittance (B2a classification). Reference 2 contains a more complete description of the apparatus.

Presently, the mass of the sample substates are selected as to make the thermal mass of the coating material small compared to that of the copper substrate, the thermal capacitance of which is known very accurately. It is planned to use a specific heat apparatus which will hopefully yield accuracies of ±2%. The accuracy of the present thermal vacuum system is better than ±4% of hemispherical emittance and ±3% for $\alpha_s/\bar{\epsilon}$, not taking into account the error in spectral match to the sun.

Since not more than two samples can be measured in this chamber, another chamber (Figure 19) is being built in-house which will facilitate measurement of hemispherical emittance of four samples at one time. This instrument is similar to that reported by Butler and Inn*. It consists of a container which can be evacuated and in which a sample is mounted by the thermocouple wires. The exterior is heated, in our case, by an electrical mantle, and when the sample reaches some elevated temperature the container is immersed in liquid nitrogen. When the container walls achieve a temperature of $77^{o}K$, the sample rate of cooling is recorded (B2b). This chamber will maintain a pressure of 10^{-8} Torr or less. It is planned to study the variation of emittance

*Reference 3

measurements due to gas conduction losses by installing a calibrated leak in this chamber which will vary the pressure during the measurement.

To determine by a thermal technique the solar absorptance as a function of angle of incidence (B1b), a rotating frame has been designed and fabricated (Figure 20). This frame will position the sample at some angle θ, to the arc beam within $\pm 1/2^{\circ}$. The procedure is as follows: the $(\alpha_s/\bar{\varepsilon})$ is measured at zero degrees and at some angle θ. If the emittance is considered constant with temperature, the intensity is unimportant as long as the sample remains in this range. If this is not so, the arc intensity is altered as to maintain the same temperature for both angles. The ratio $\left(\alpha_{s\theta}/\bar{\varepsilon}_{\theta}\right)/\left(\alpha_{s0}/\bar{\varepsilon}_{0}\right)$ is then taken, resulting in a ratio of $\alpha_{s\theta}/\alpha_{s0}$, and when multiplied by the value of α_{s0} determined optically (e.g., by a Beckman DK-2) gives $\alpha_{s\theta}$. For more information see Reference 4 which is in publication.

III. Instruments under Development

The instruments which are now in development are as follows:

1. The absolute reflectometer (solar region)
2. The I.R. absolute reflectometer
3. The goniophotometer
4. A high intensity reflectometer
5. A vacuum UV reflectometer

The absolute reflectometer for the solar region is a Strong type reflectometer preceeded by the Perkin-Elmer 99 monochromator and source optics (Figure 10). The detector system consists of an integrating sphere from lead sulfide and photomultiplier detectors. The instrument is designed to yield absolute specular spectral reflectance near normal incidence to a precision of ±.001 absolute and will be used to check reference samples for instruments which yield relative measurements.

The I.R. reflectometer is being designed to measure the spectral specular reflectance near normal incidence in the region of four microns to twenty-eight microns, and to an accuracy of better than ±.005 absolute. This design is based on H. E. Bennett's reflectance (J.O.S.A., January 1960). This design had to be modified to accept a smaller sample, more specifically, to fit the sample disc diameter of the hohlraum, since this instrument will be used to measure the reference standards for the hohlraum. The mechanical design and fabrication will be initiated during this calendar year.

A high intensity reflectometer (Figure 11) designed to monitor the change in specular reflectance or polar reflectance

pattern of samples upon irradiation with high intensity light, has been fabricated. Signals from two Eppley thermopiles, monitoring the source and the sample reflectance are displayed on a dual channel recorder. Because of the high intensity (1/3 solar constant) the thermopiles are being calibrated for signal to light flux linearity, and preliminary measurements show agreement to ±1%. The high intensity light source consists of a Strong Peerless carbon arc which is used from the side by collimating the radiation from the arc gap with a five-inch quartz lens. This illuminates the sample which can be rotated through different angles of incidence. This was designed primarily for thermophototropic coatings and their evaluation at high temperature. An addition will be made whereby the sample temperature may be contolled by means of a heater or cooling system.

A goniophotometer (Figure 12) was designed to determine the proper reflectance standard which might be used to measure the reflectance of a material. The polar reflectance pattern would indicate how specular or diffuse a coating is. A 98 Perkin-Elmer monochromator and source optics are

used in conjunction with a modified spectroscope having an Eldorado detector mounted on it. The sample mount is located on the prism table of the spectroscope. Presently, A Bausch and Lomb grating monochromator is being used for preliminary measurements, until the 98 Perkin-Elmer is received. The angles of incidence and view range from 0^{o} to 80^{o} and 15^{o} to 180^{o}, respectively. The measurements on this instrument are currently in the visible region, but will be extended to the ultra-violet and near infrared regions.

In addition to this instrument, another instrument will be designed to cover the infrared which will have all reflecting optics.

The vacuum ultra-violet reflectometer uses a McPherson half meter grazing incidence vacuum ultra-violet monochromator (Figure 13). The reflectance attachment, based on the design of one in Dr. G. Hass' laboratory, will enable us to make specular spectral reflectance and spectral transmittance measurements as low as 500A and at angles of incidence from 10^{o} to 75^{o}. At present, helium is used in the source arc, to illuminate the sample. Reflectance measurements have been reproduced to within 1-1/2% absolute. It is hoped

that a suitable source for continuum measurements for the region from approximately 500 to 4000 can be obtained in order to measure reflectance in this region. These measurements are needed to determine whether laboratory simulated U-V degradation studies are valid.

Other instruments which will be in use in the next twelve months include: (1) A variable angle of incidence hohlraum which will be used to correlate optical and thermal measurements. The source optics of the IR-7 (Figure 14) will be modified to accept a Gier-Dunkle hohlraum. (2) A portable emissometer was ordered from Gier-Dunkle which will be capable of measuring coatings on spacecraft with a precision of better than 4%. (3) A Gaertner ellipsometer Model L119 with a Babinet-Soleil compensator and Tronstard-Nakamura bi-plate assembly will be used to measure n and k which, in turn, can be applied to calculate reflectance at various angles of incidence by means of Fresnel's equations. Band pass filters in conjunction with line sources will be used as the monochromatic light source for this instrument.

Conclusions

When choosing an optical method, one might have the choice of a relative or absolute instrument. In general, the relative instruments which operate by comparing the sample to a reference, are faster and lend themselves to digitalization for rapid data reduction. However, the accuracy of the measurement depends on the reference matching the sample reflectance pattern, a knowledge of the absolute reflectance of the reference and the type (surface characterization) sample to be measured. The absolute instruments are slow and, therefore, impracticable for use in screening measurements. Accordingly, the need exists for both absolute and relative instruments. This need would be eliminated if a dual beam absolute instrument was developed capable of measuring all types of samples

Optical measurements are important but limited in usefulness when considering low emittance materials, since the most accurate optical methods at room temperature measure reflectance. Optical methods are imperative for analytically

studying materials where spectral distribution is needed for a more complete understanding of the interaction of radiation with matter. However, thermal techniques are more accurate for thermal design values of emittance if the heat losses can be kept small.

References

1. Fussell, W. B., Triolo, J. J., Jerozal, F. A., "Portable Integrating Sphere for Monitoring Reflectance of Spacecraft Coatings," NASA TND-1714, April 1963.

2. Fussell, W. B., Triolo, J. J., Henninger, J. H., "A Dynamic Thermal Vacuum Technique for Measuring the Solar Absorptance and Thermal Emittance of Spacecraft Coatings," NASA TN D-1716, March 1963.

3. Butler, C. P., Inn, E. C. Y., "The Total Hemispherical Emissivity of Metals," Research and Development Technical Report USNRDL-TR-327, 28 May 1959.

4. Hoke, M. G., "A Thermal Vacuum Technique for Measuring the Solar Absorptance of Satellite Coatings as a Function of Angle of Incidence," in the Transactions of the 1964 Symposium on Thermal Radiation Properties of Solids, to be published.

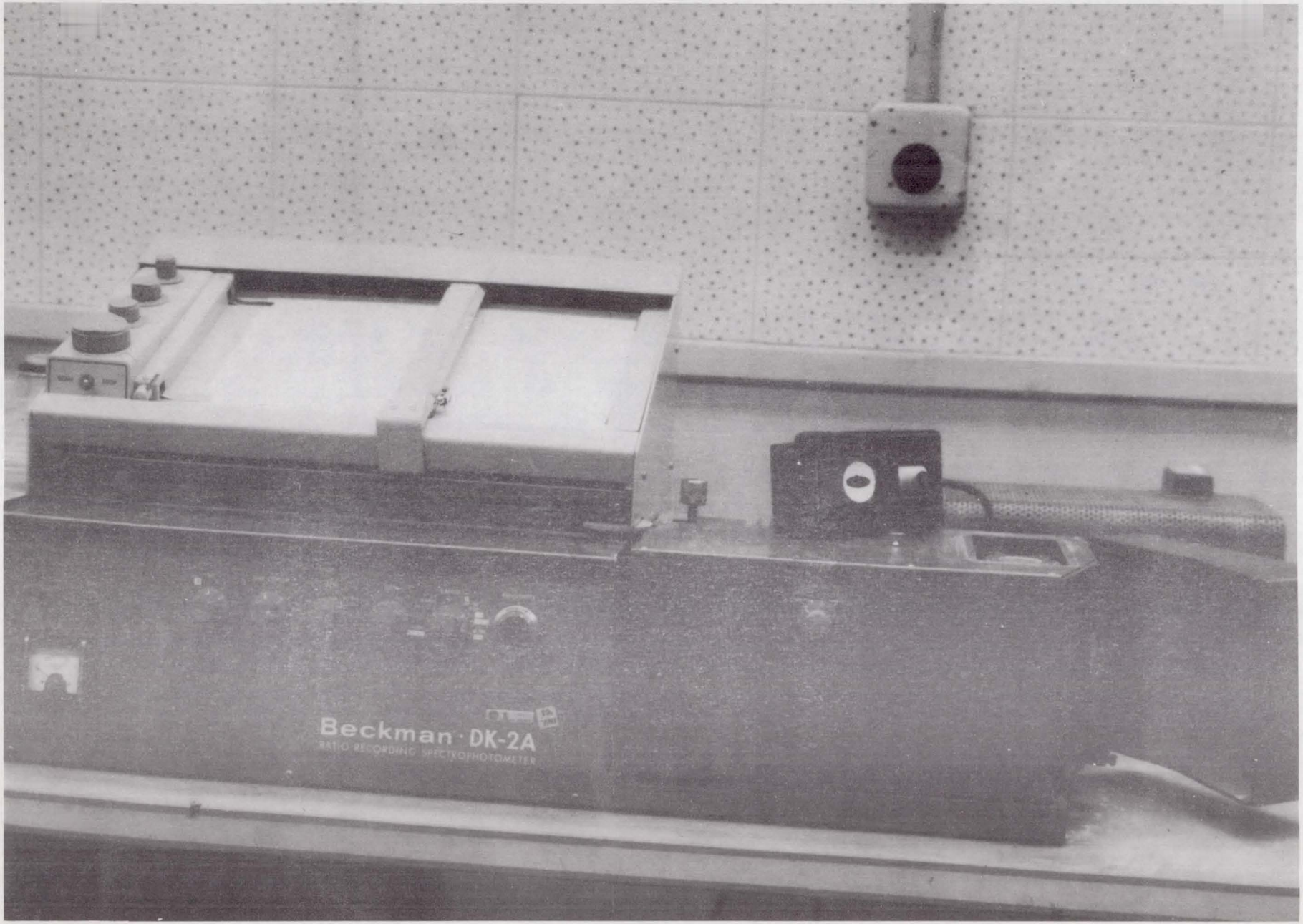

Figure 1. Beckman DK-2

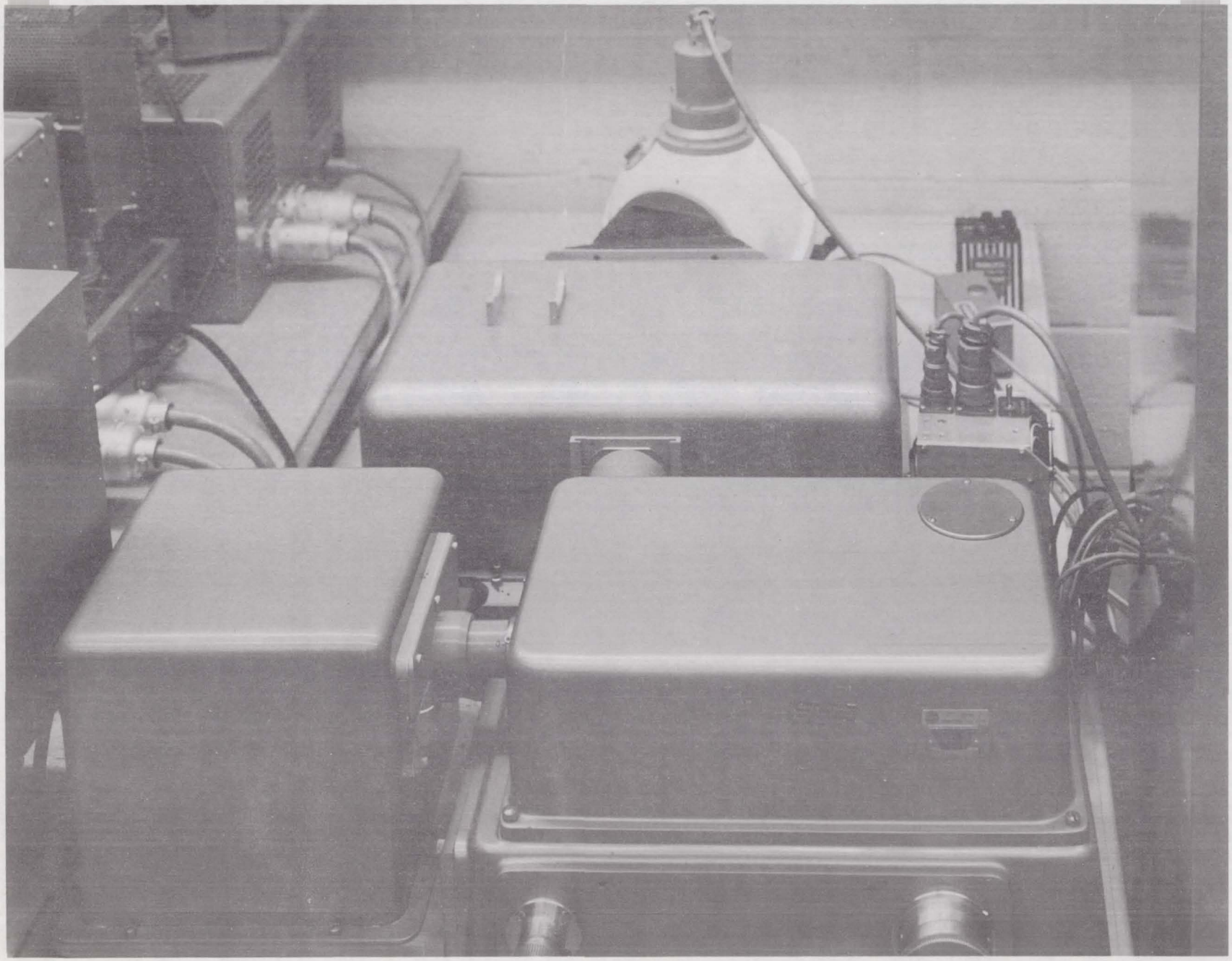

NASA G-65-1088

Figure 2. Perkin-Elmer 99 Monochromator

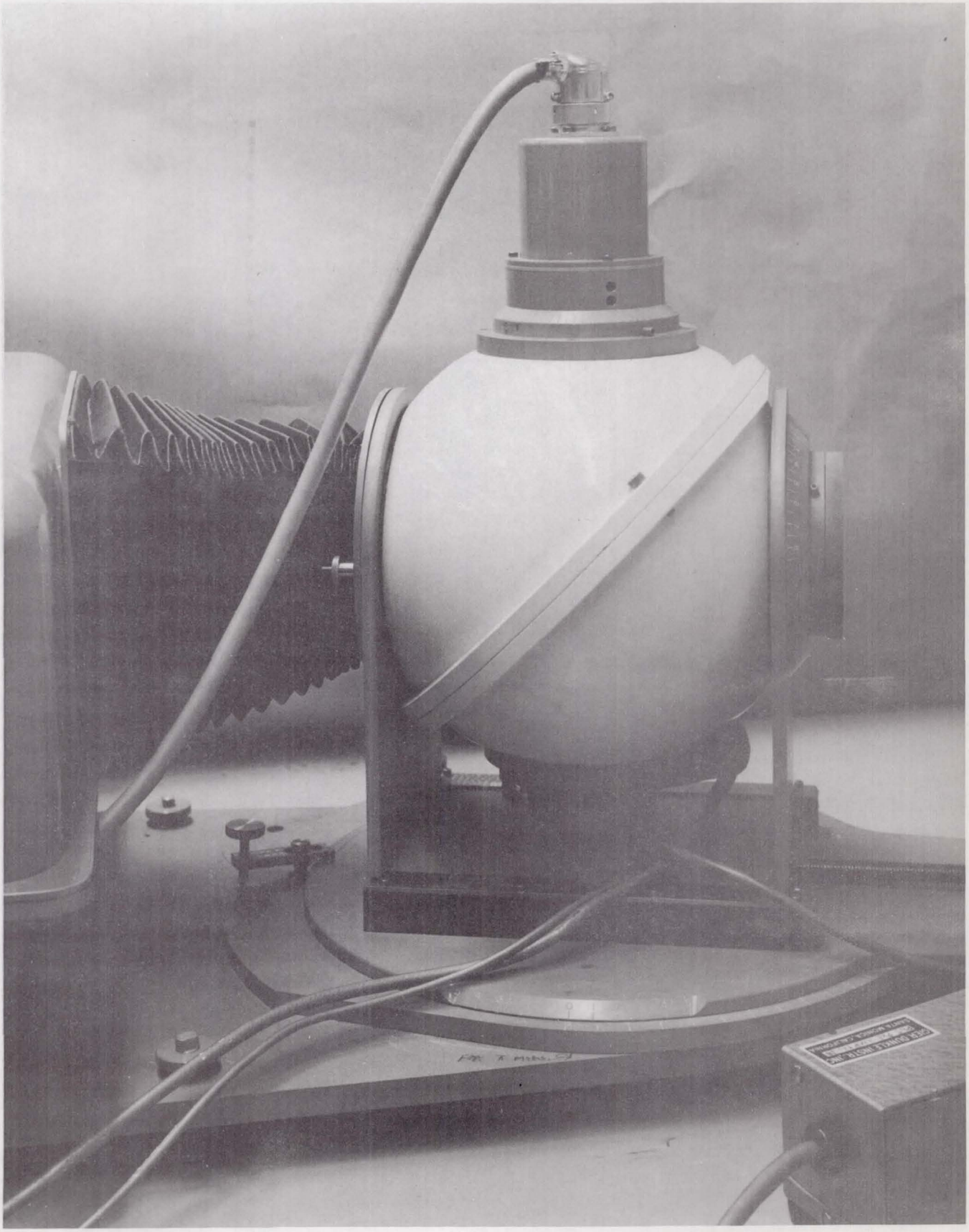

Figure 3. Integrating Sphere

NASA G-62-2571 Figure 4. Portable Integrating Sphere and Accessories

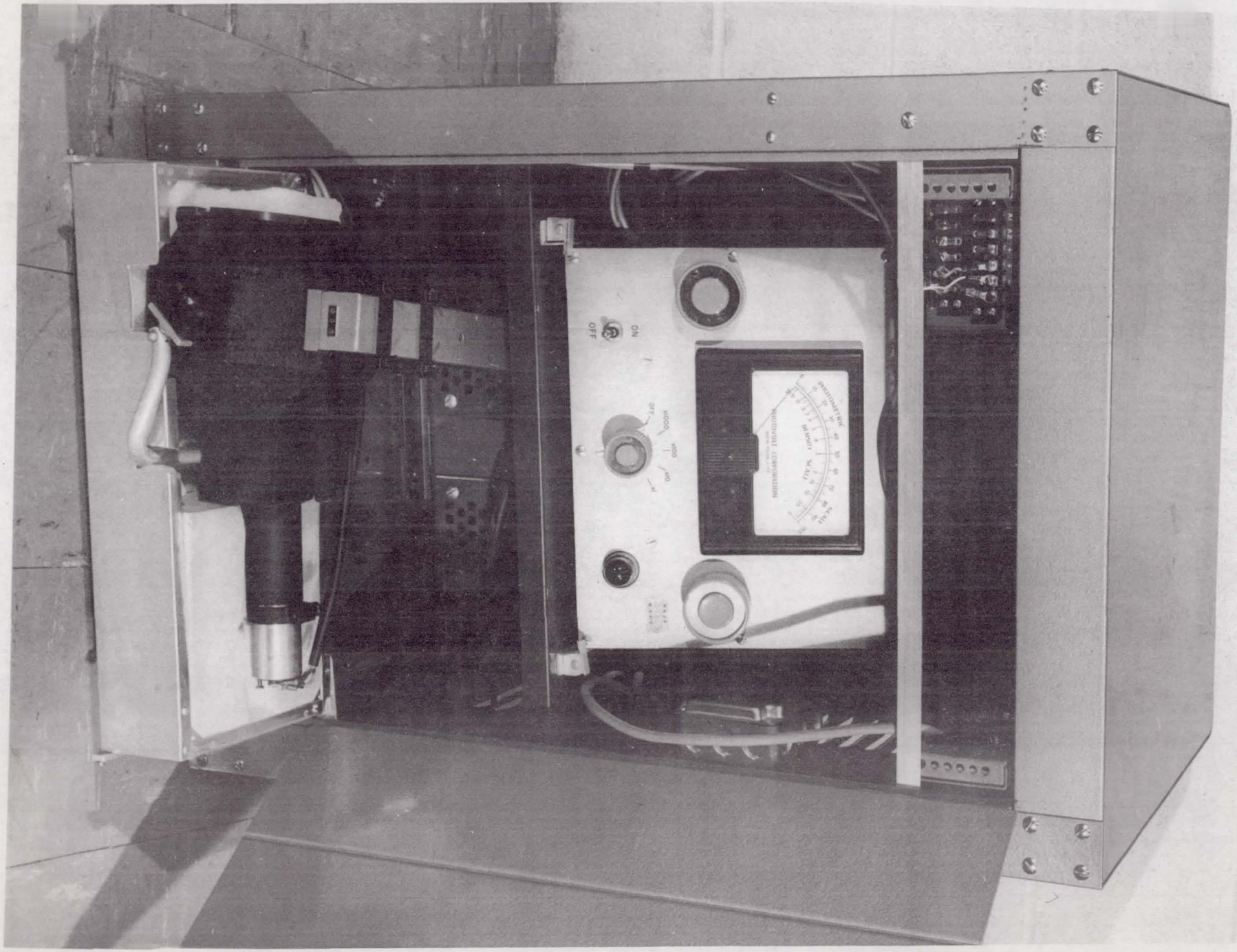

NASA G-62-2571 Figure 5. Integrated Portable Integrating Sphere Package

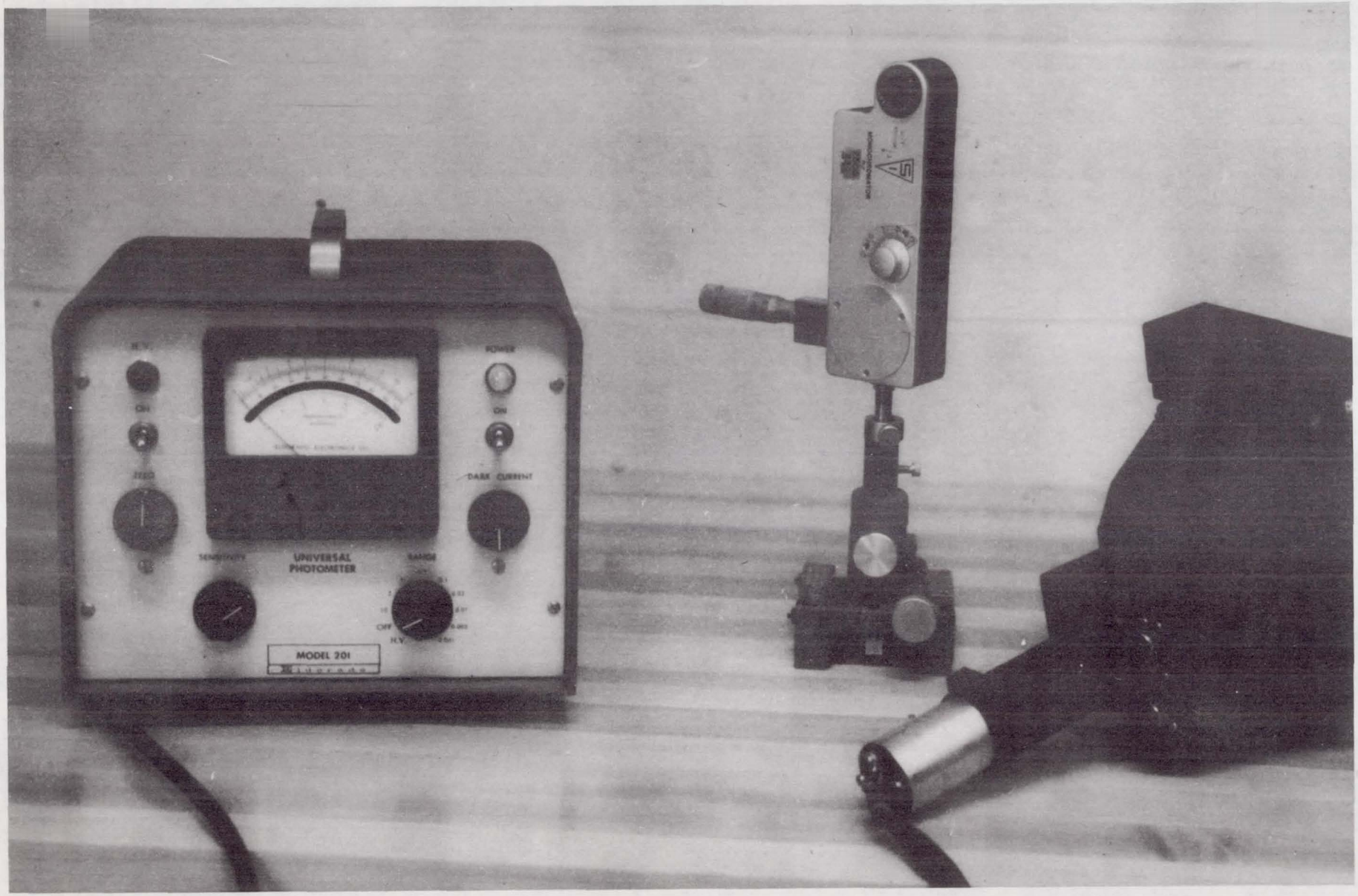

Figure 6. Eldorado Photometer

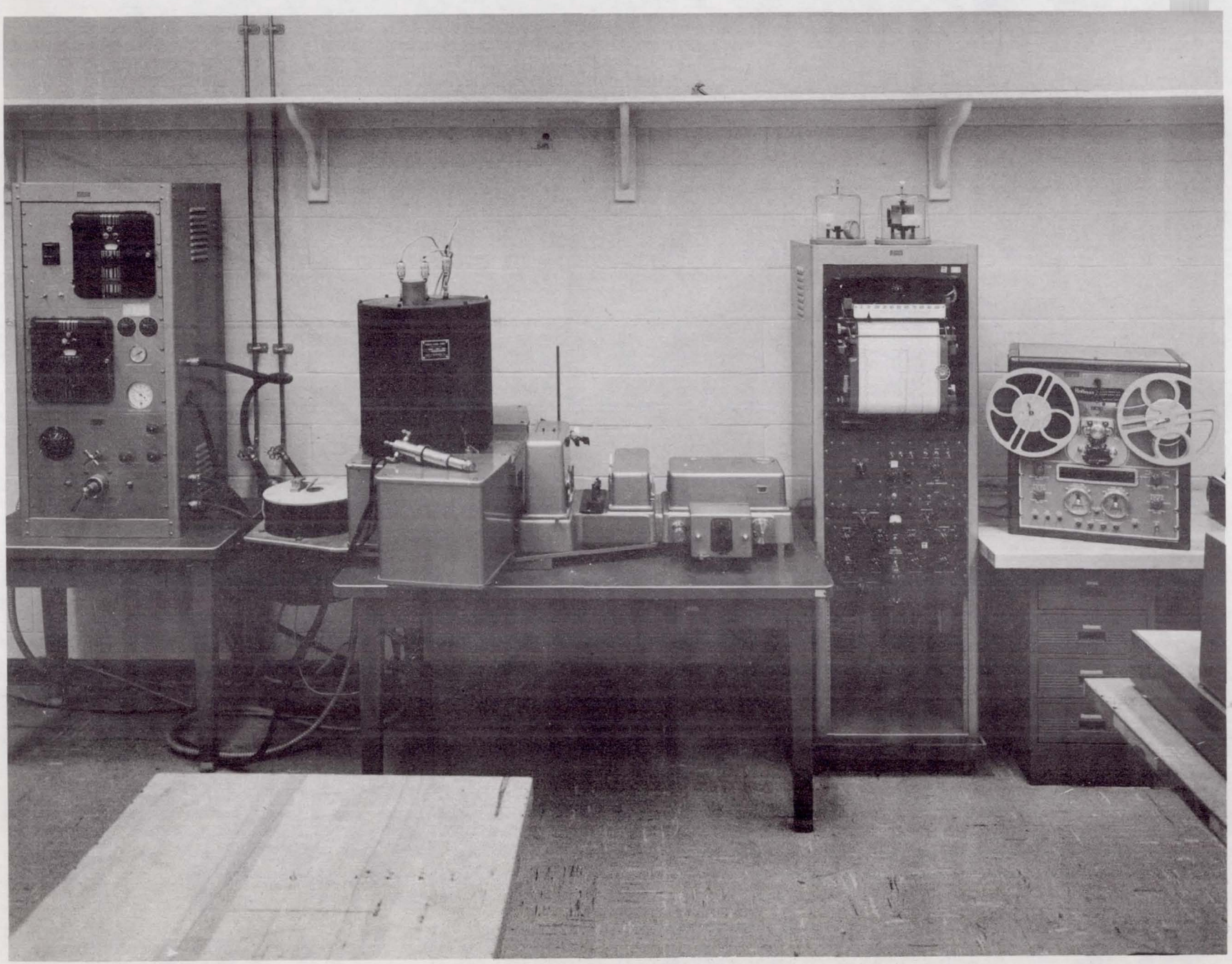

NASA G-65-1087

Figure 7. Reflectane Apparatus (5-35 microns)

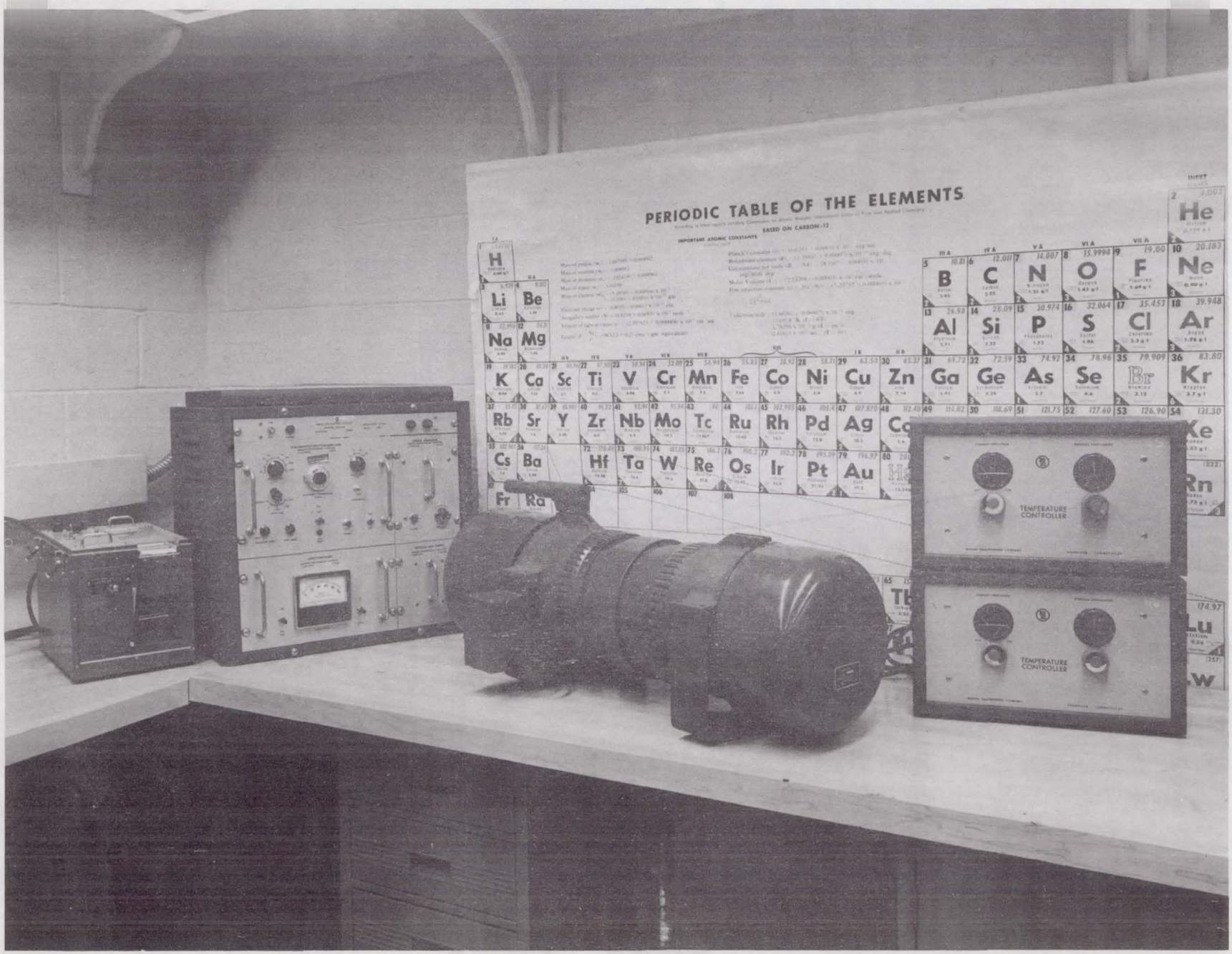

NASA G 65-1094

Figure 8. Barnes Emissometer

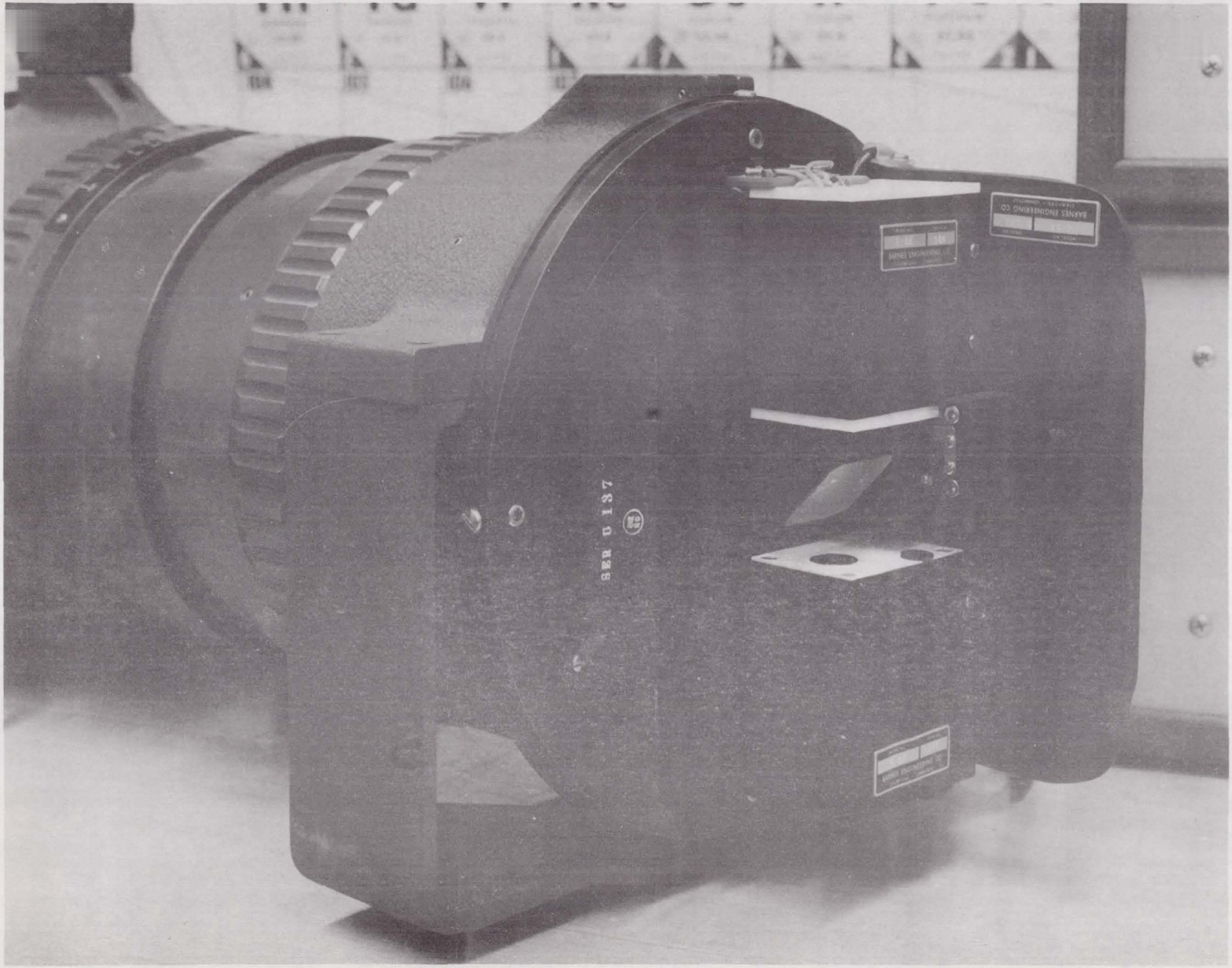

NASA G-65- 1090 Figure 9. Barnes Emissometer Emissivity Attachment

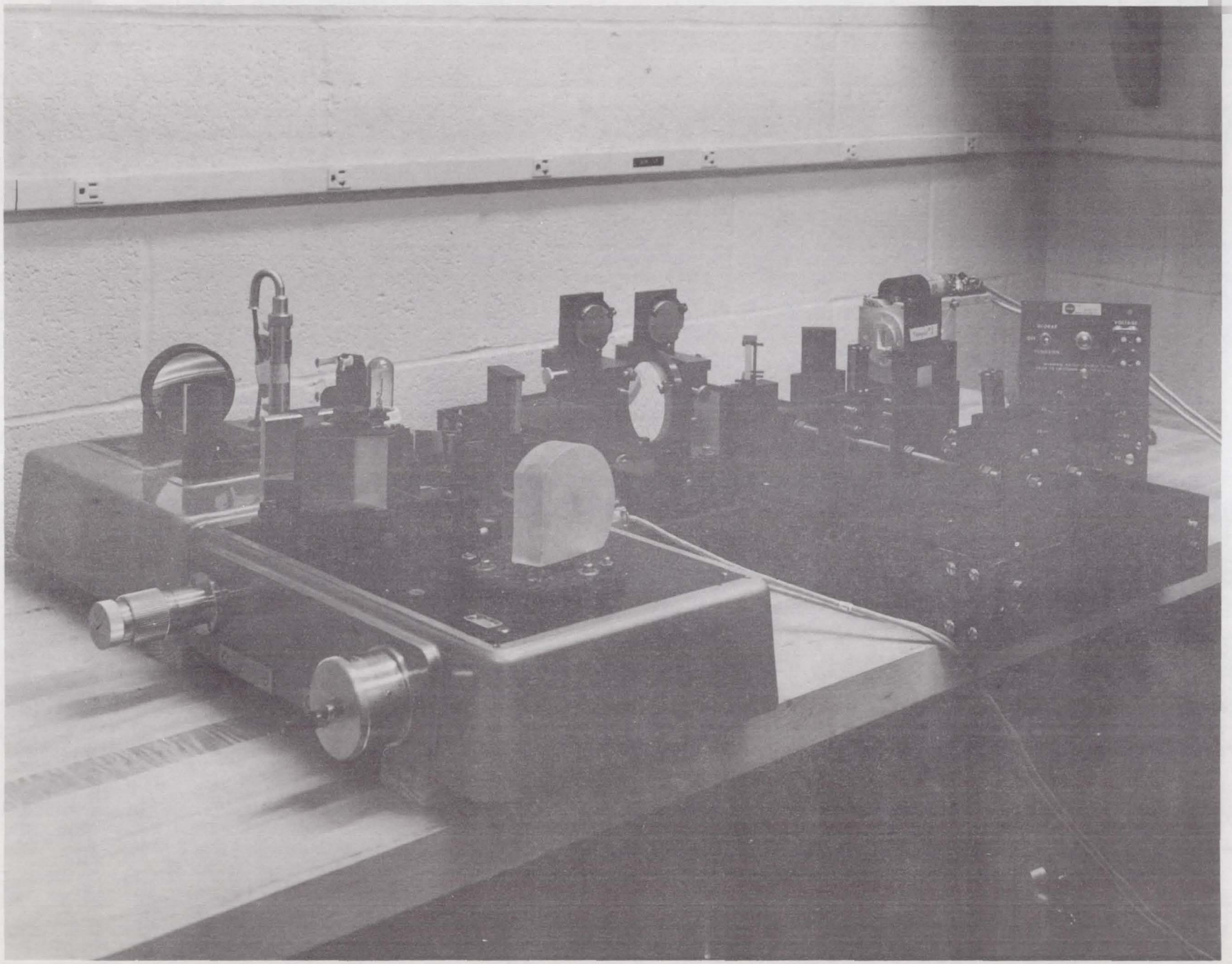

NASA G-65-1091 Figure 10. Perkin-Elmer 99 Monochromater and Source Optics

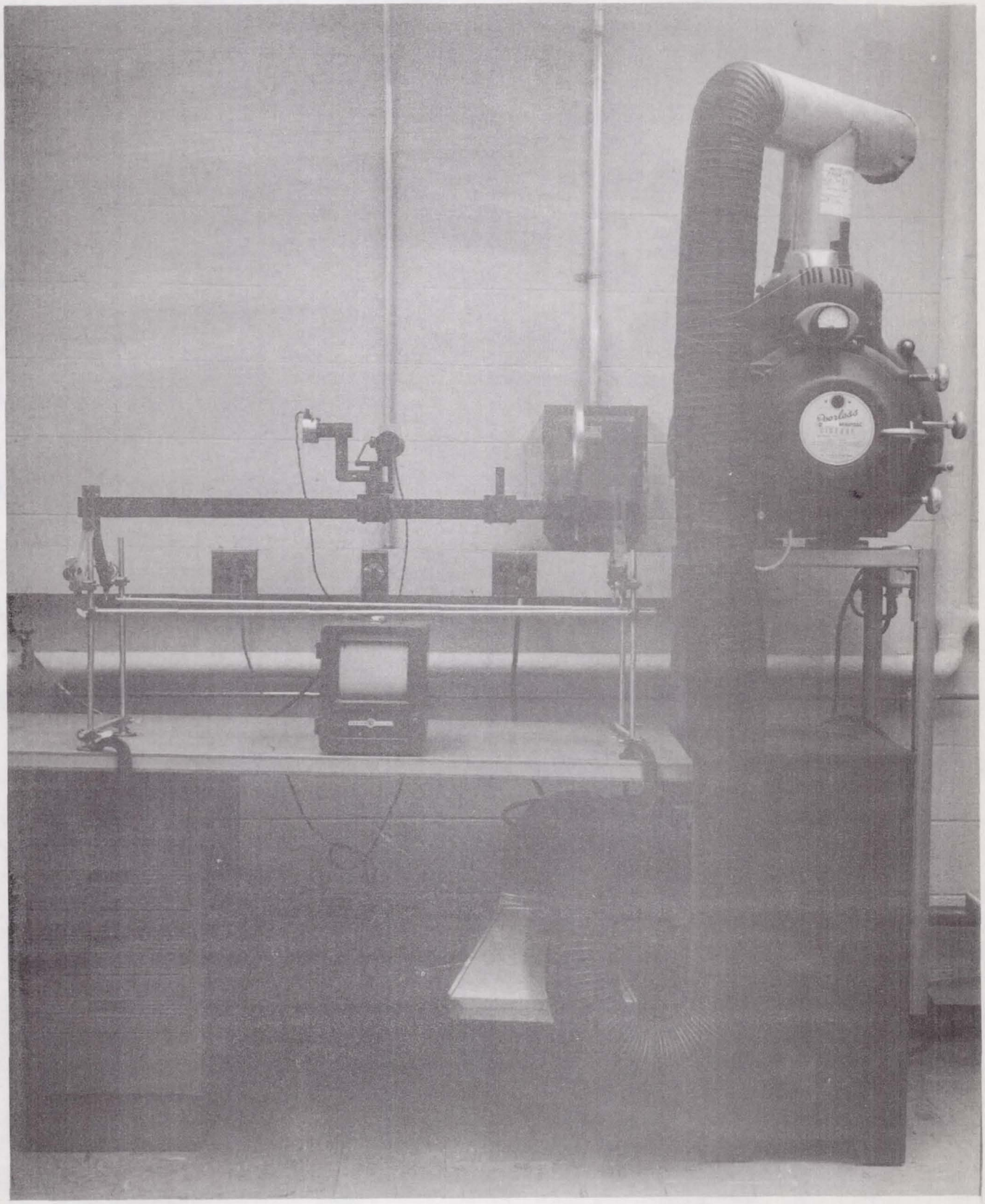

NASA G-65-1089

Figure 11. High Intensity Reflectometer

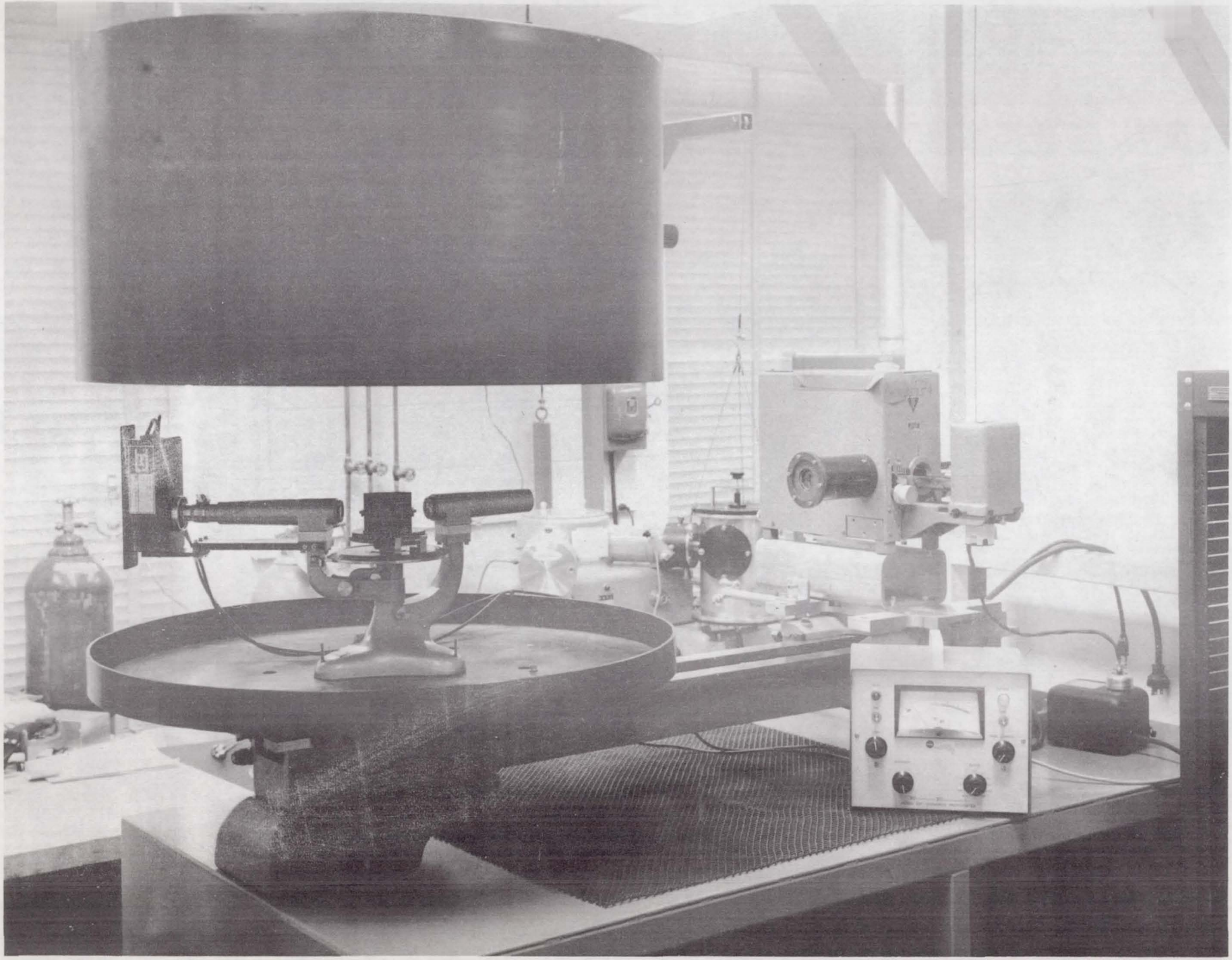

NASA G-65- 1086 Figure 12. Goniophotometer

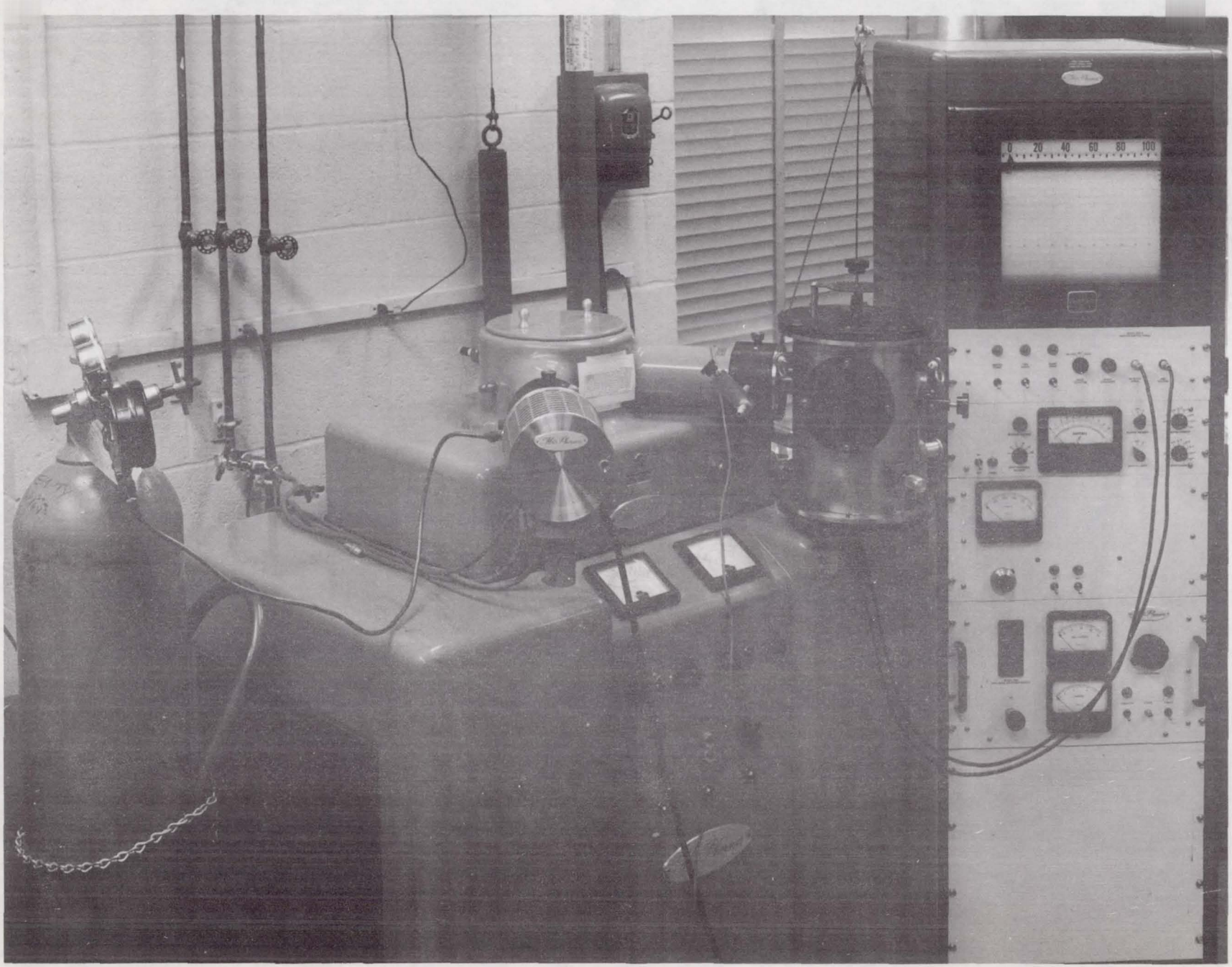

NASA G-65- 108

Figure 13. McPherson Monochromater

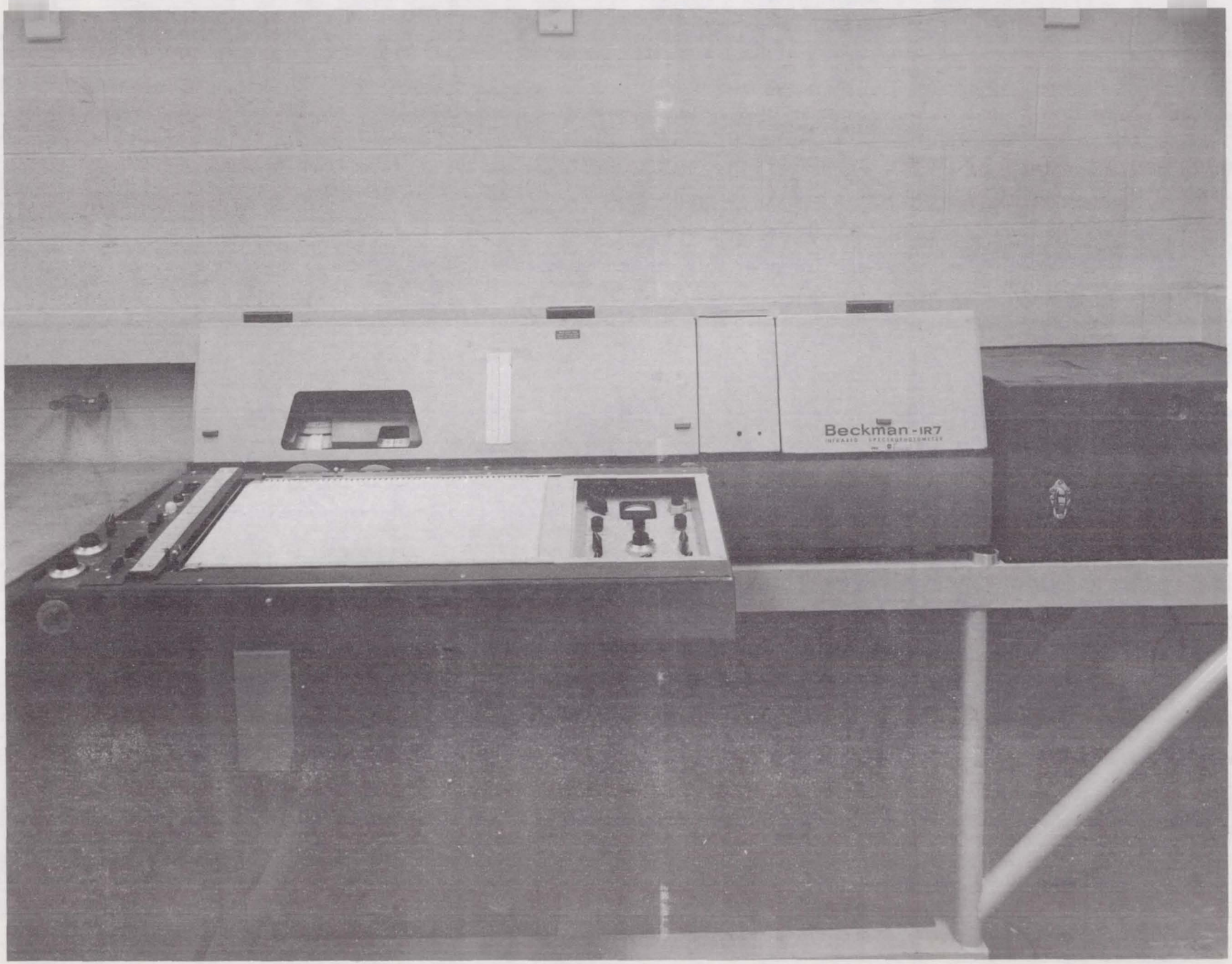

NASA G-65-1093

Figure 14. Beckman IR-7

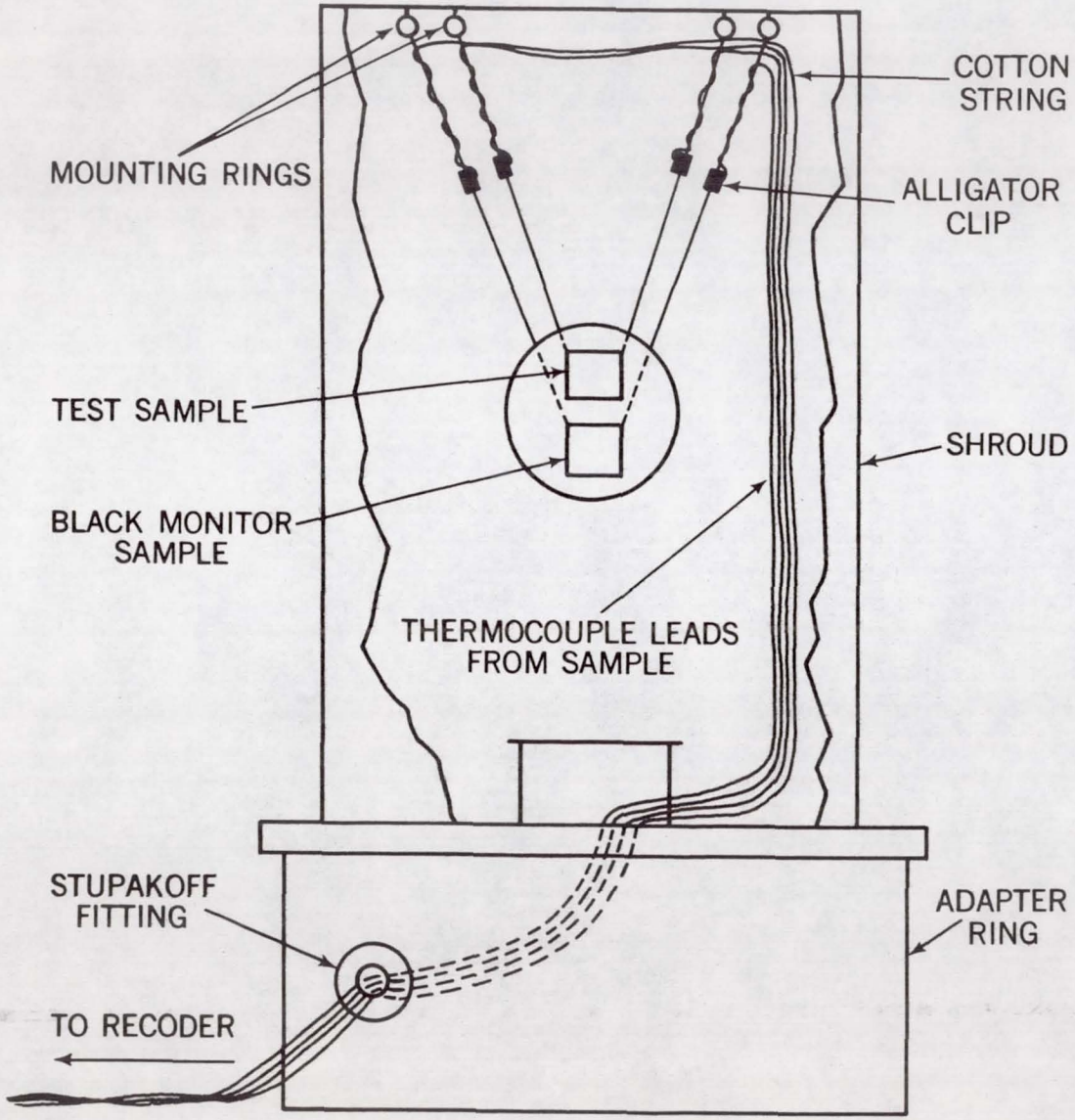

Figure 15. Thermal Vacuum Chamber

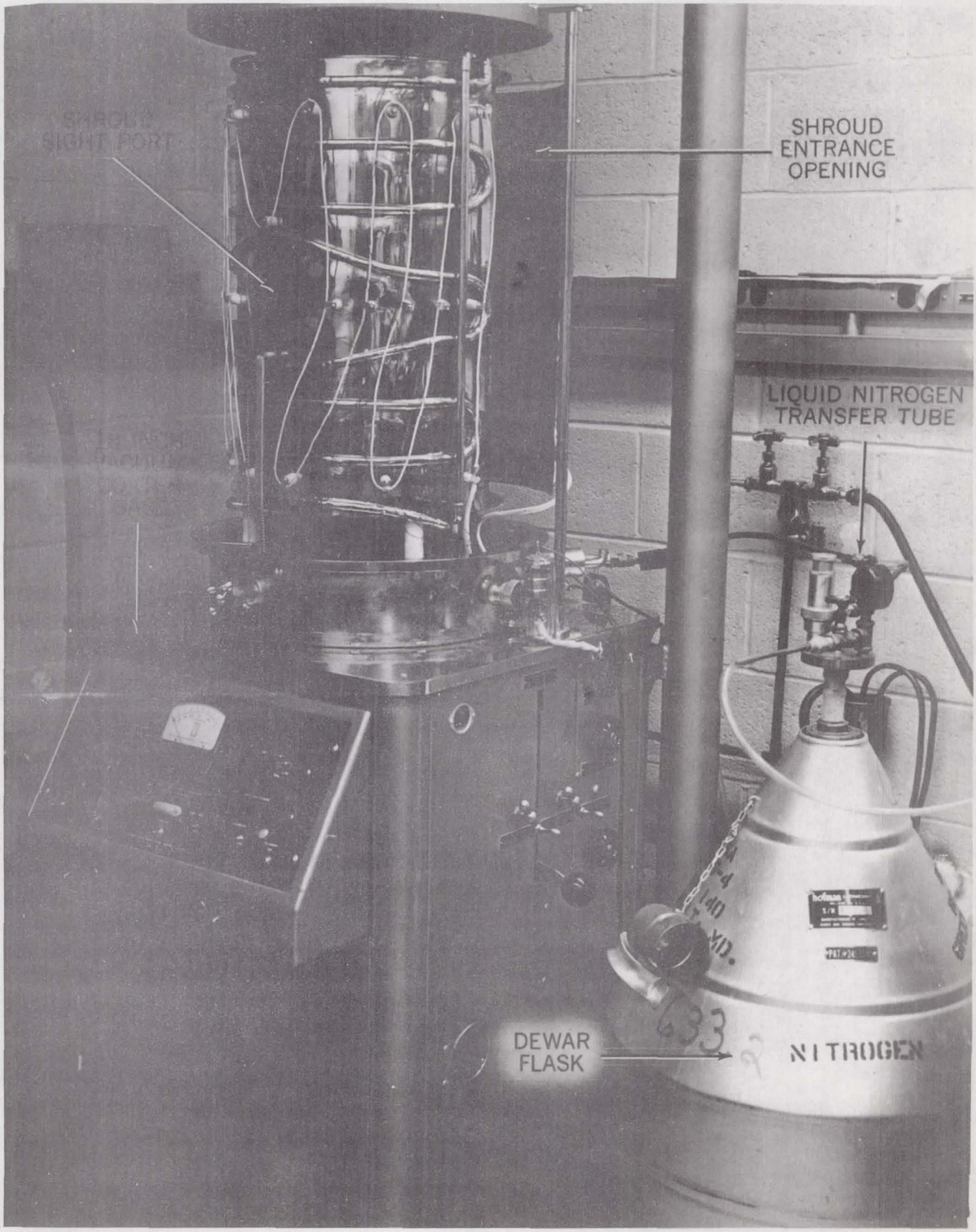

Figure 16. Thermal Vacuum Chamber

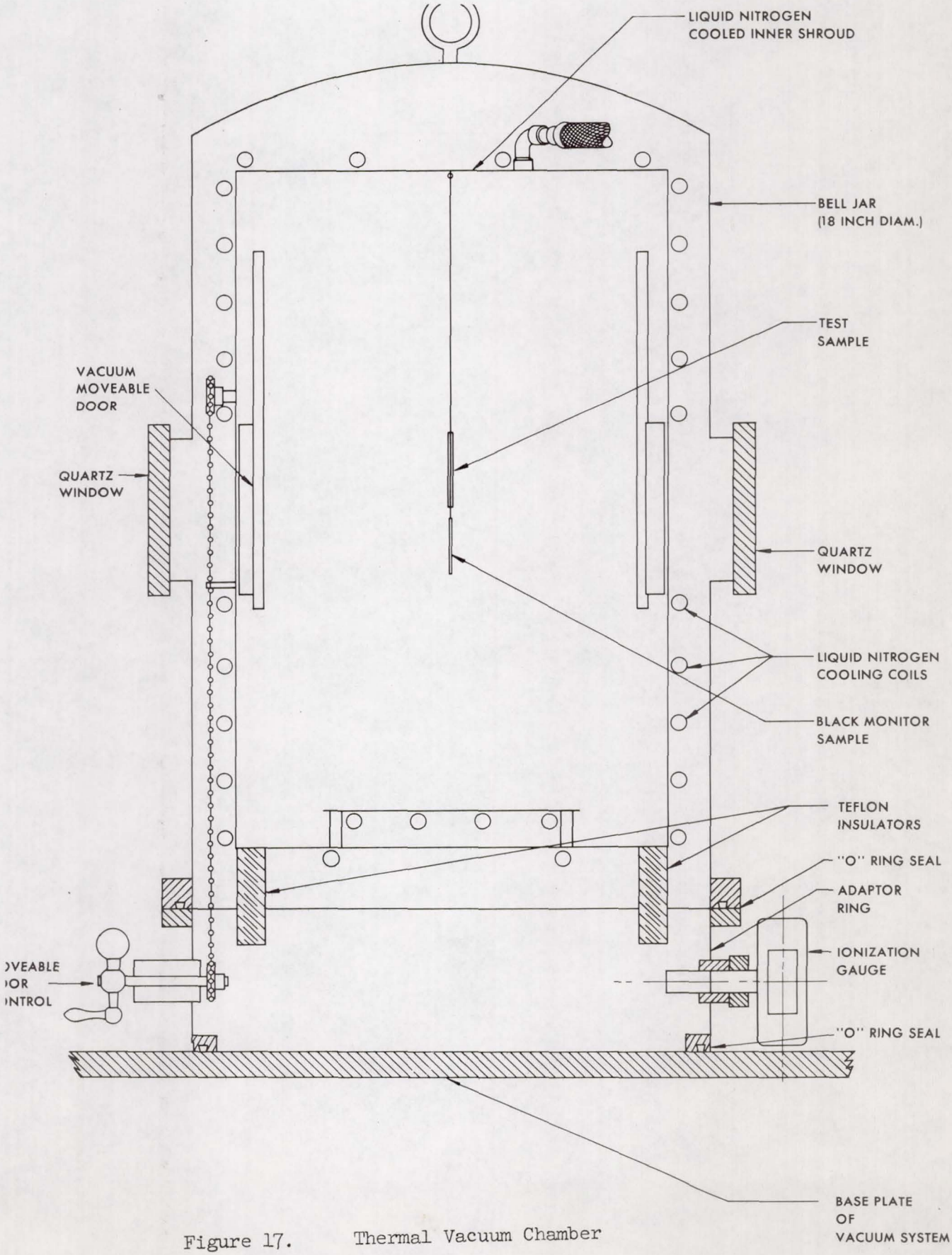

Figure 17. Thermal Vacuum Chamber

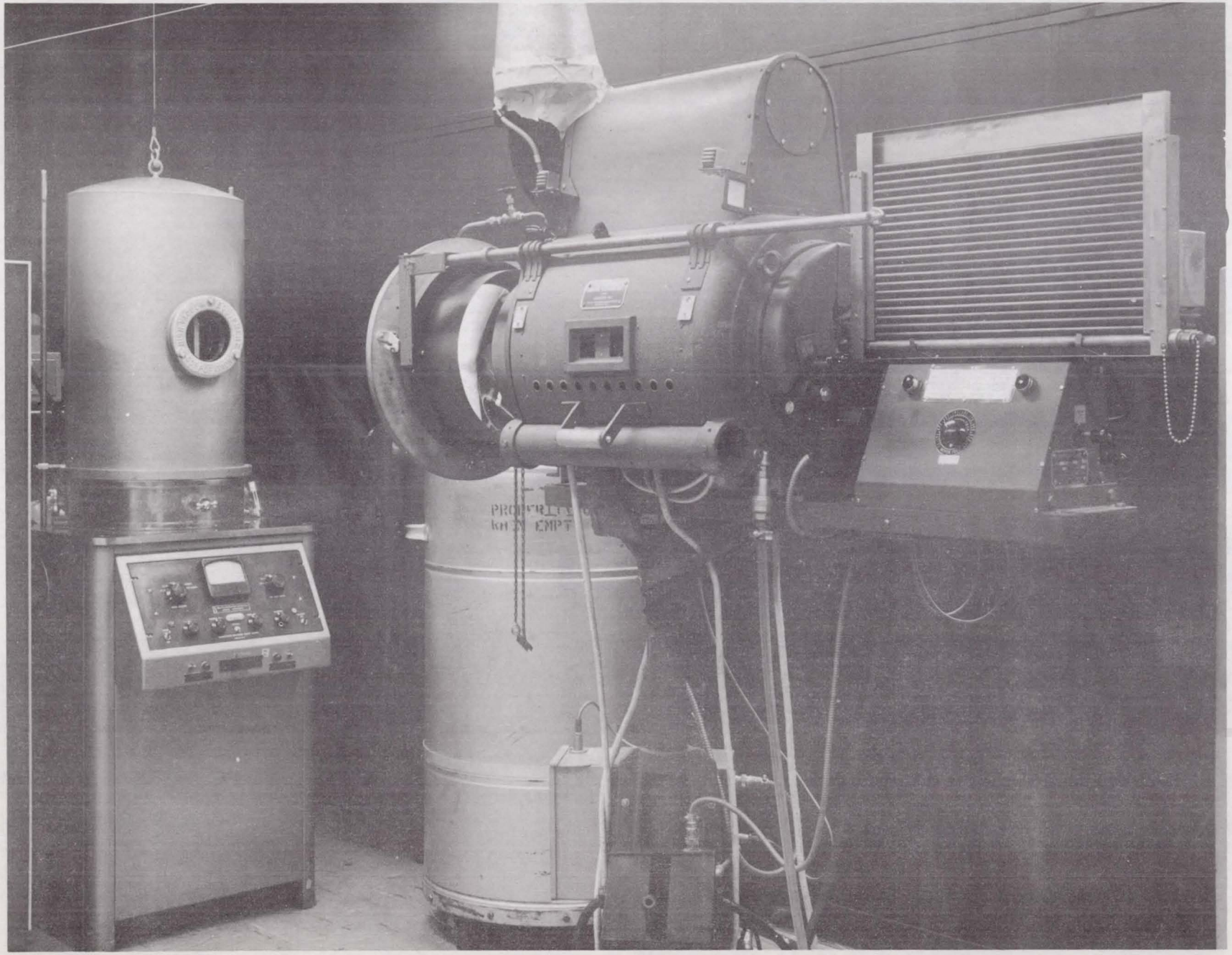

NASA G 65-1092

Figure 18. Carbon Arc

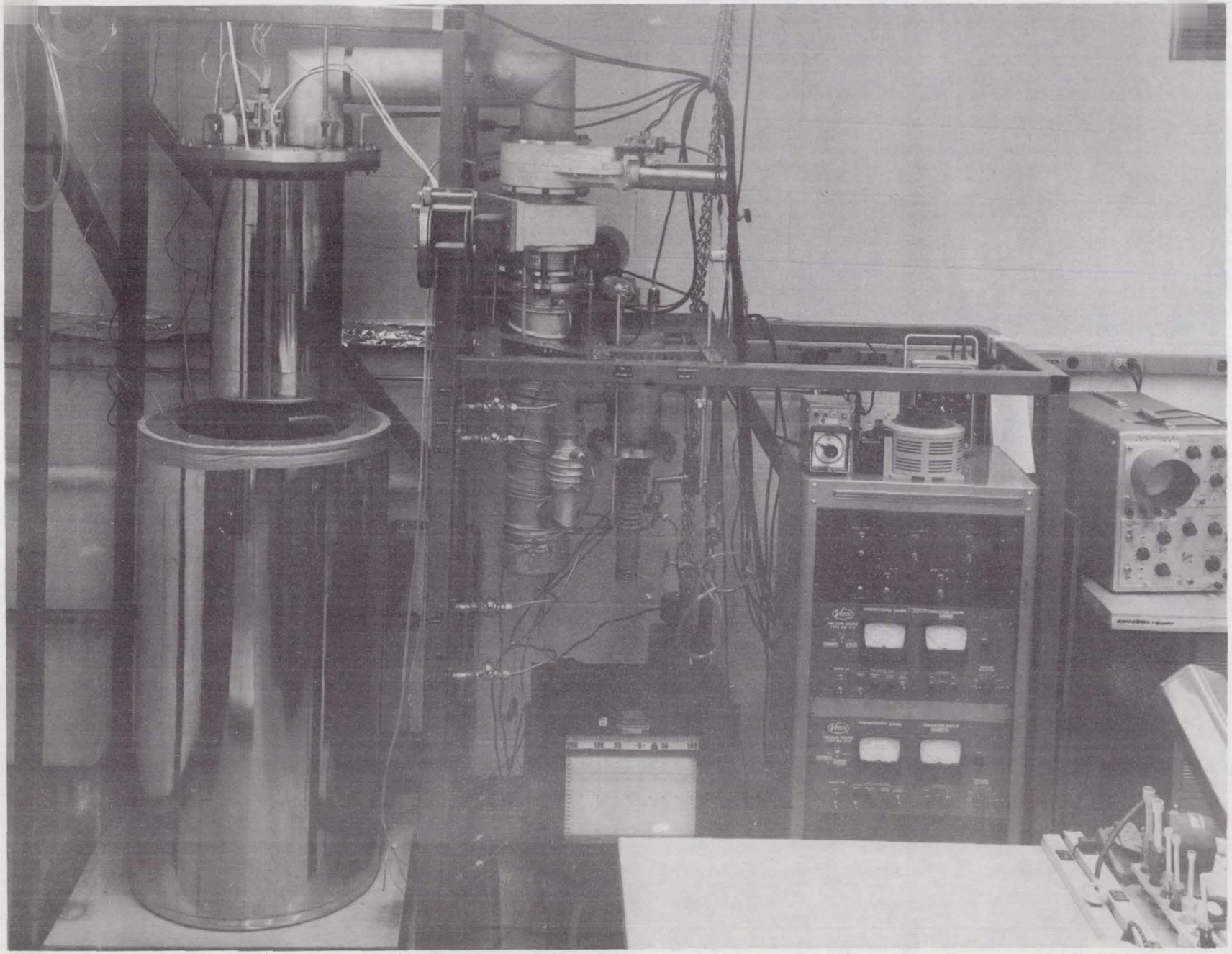

Figure 19. Four Sample Capacity Thermal Vacuum Chamber

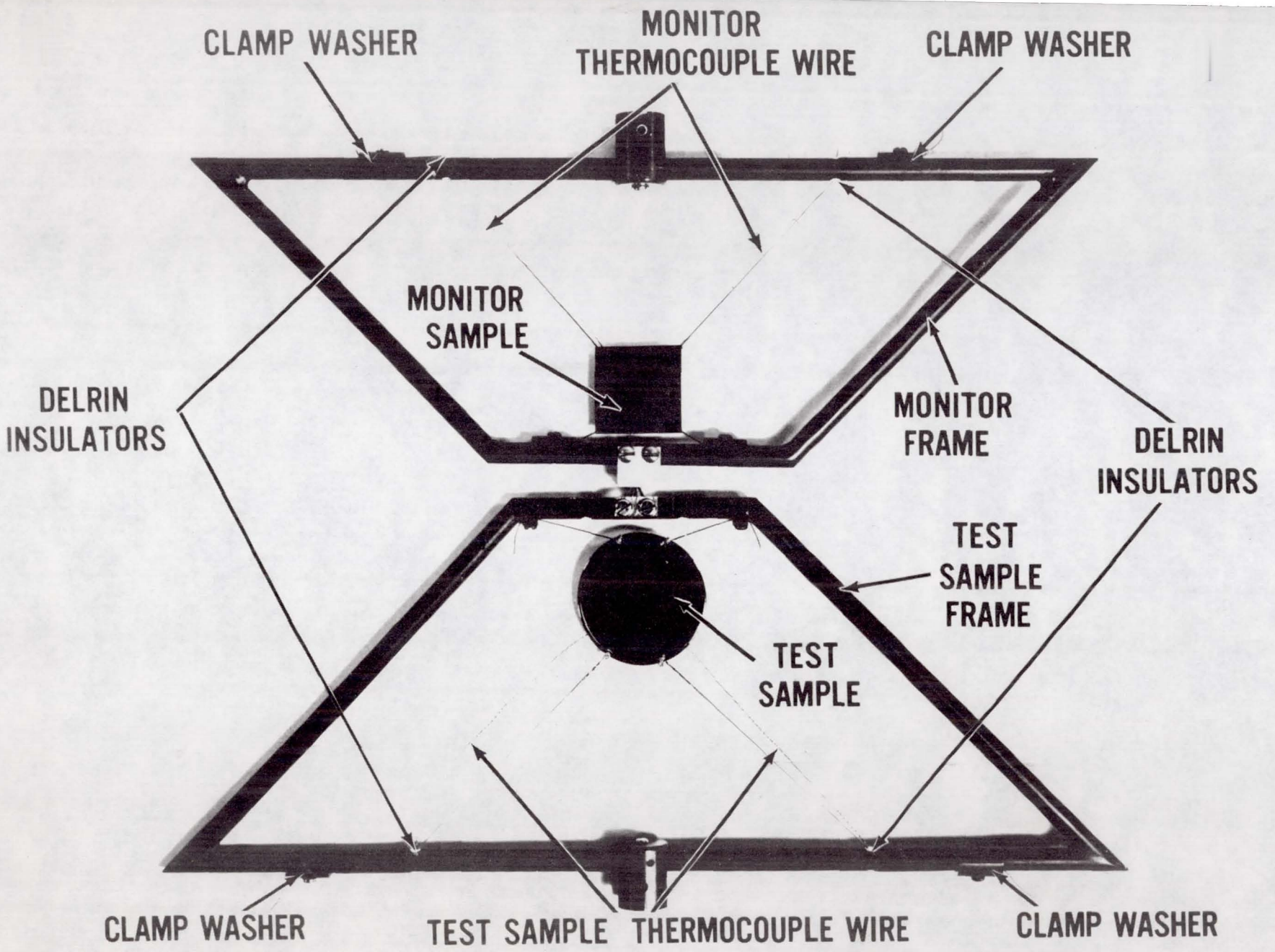

Figure 20. Rotating Frame

NASA G-64- 2599

SPACECRAFT COATINGS FROM A TEMPERATURE CONTROL STANDPOINT

W. A. Hagemeyer
Jet Propulsion Laboratory

Abstract

Interactions between basic spacecraft mission, temperature control philosophy, and coating development and measurement philosophy are discussed in relation to the various phases of spacecraft design. Present and future needs for coatings and/or their thermal radiation characteristics are given.

The basic spacecraft coatings requirements, as viewed from the temperature control area can be summarized as follows:

1. A group of standardized coatings should be developed which cover the range of radiation properties: low α-high ϵ, high α-high ϵ, and low ϵ. These standard surfaces must have the ability of being relatively easily applied, must withstand the normal handling associated with a spacecraft, have stable properties relative to both handling and flight environments, and in some cases be easily removeable without destroying the surface underneath.
2. Enough data must be acquired on the properties of the standard surfaces so that the maximum range of property values is known fairly definitely. This allows the temperature control engineer to have more confidence in his predicted temperature extremes and consequently, spend more time on the detail problem solutions.

3. There must exist the ability to rapidly evaluate the properties of a new or peculiar surface. On every new spacecraft there are surfaces dictated by other than thermal reasons. These must be rapidly evaluated by the materials engineer and the thermal engineer to insure that the thermal design will be adequate.

Temperature control philosophy both influences and is influenced by the choice of standard coatings. At the Jet Propulsion Laboratory the basic coatings are either a polished or plated metallic surface for the low ϵ, with paints used for both the low α - high ϵ and the high α - high ϵ. This choice is a very valuable combination for two reasons. First, the combination of these three types of surfaces allows an extremely wide range of effective properties by making a mosaic of the three coatings. Secondly, by its very nature a polished or plated surface requires a long lead time. Since the paints are short lead time, easily applied coatings, the low ϵ surfaces can be specified when the drawings are being made, deferring a decision on actual painted areas until the component is ready for testing, at which time the analysis can be more complete.

During the various phases of a spacecraft design, the temperature control engineer has differing requirements for surface coating properties. In the Study Phase, when temperature control concepts are being defined, only gross coating properties are required to adequately define the thermal environment.

In Preliminary Design the temperature control engineer is refining his analysis based on more definite sizes and power dissipations

of the components. At this stage he needs an estimate of the coating properties limits to be sure his design is feasible.

During the Hard Design Phase of the spacecraft, the temperature control engineer must call out the basic surface coatings he needs (i.e. long lead time low or high ϵ's) as the drawings are being made. In addition, he is beginning to finalize his design to the point that he can test the critical items as soon as possible. Thus he needs to have the nominal property values with their maximum extreme variations at this time to adequately define the flight temperature extremes.

As the testing program begins in earnest, the temperature control engineer refines his analysis on the basis of the test results. Many times he retests components after modifying the mosaic of surface coatings. This is the time when the ease of application and removal of these coatings is needed.

A spacecraft flight is really a proof test of the thermal design. The steps leading to the flight have been described above. One important aspect not yet mentioned is the importance all through the design process of the necessity of establishing the Quality Control and Inspection Procedures which will insure the coating properties at the time of flight. This important area is the joint responsibility of the temperature control engineer and the materials engineer.

In the future, the basic requirements for coating information will be the same as described above. However, the characteristics of the environments the coatings are subjected to may change drastically. There will probably be need for information on coatings at very high temperatures and very low temperatures. The spacecraft lifetime will

become radically longer necessitating a knowledge of coating reaction to space environments, including U.V., high energy solar particles, and nuclear source radiation, over much longer time periods. More information will undoubtably be needed on wavelength selective coatings for various special needs. A final future need will be directional surface properties to allow the thermal engineer to properly account for all the radiant energy entering and leaving his spacecraft.

A CONFIGURATION COORDINATE MODEL FOR THE THERMAL AND ULTRAVIOLET STABILITIES OF α-Al_2O_3

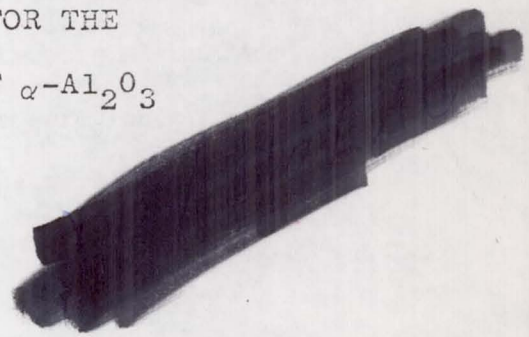

by

John B. Schutt & Buford A. Macklin
NASA Goddard Space Flight Center
Greenbelt, Maryland

TABLE OF CONTENTS

SUMMARY

This investigation was carried out to determine the thermal and ultraviolet stabilities of α-Al_2O_3 in a vacuum environment in order to gain some knowledge about the behavior of anodized aluminum in similar environments. α-Al_2O_3 was selected because of its reproducible responses to the formation of the characteristic brown coloration. It was found that α-Al_2O_3 could be browned significantly at 350°C at 10^{-4} torr, as well as in a 60°C thermal environment at 10^{-7} torr under one solar constant of ultraviolet energy. In all cases bleaching in air was observed to occur significantly at about 350°C. A wavelength of 360 mμ was found to give partial bleaching under ambient conditions. Using these observations, a configurational coordinate scheme was worked out to explain the behavior. In addition, a brief discussion of the surface chemistry is included.

author

INTRODUCTION

The structural advantages of aluminum for spacecraft use and the ease by which an in situ oxide coating can be electrolytically formed, need little introduction. An additional advantage is afforded by the wide range of (a/e) which the anodically deposited oxide layer can possess[1]. However, the interaction of ultraviolet radiation with anodized aluminum and the generation of a characteristic brown color has not been systematically investigated. Unfortunately, the molecular distillation of vacuum greases, or other organic contaminants, onto an aluminum oxide surface in the presence of ultraviolet irradiation can develop a brown color visually indistinguishable from the oxide brown. Careful investigations, however, do reveal that aluminum oxide is inherently capable of turning brown in an actinic vacuum environment.

In order to simplify a study of the variable absorptance property of aluminum oxide, anodized films were not investigated, but rather high purity α-aluminum oxide obtained from Linde Air Products.

---

1. Weaver, J. M., "Bright Anodized Coatings for Temperature Control of Space Vehicles," WPAFB(TM-MAN 63-53)

This approach seemed reasonable because unsupported anodized films were found to be unstable, i.e., with the instability localized in anodized layer of aluminum, because the anodizing process introduces impurities. For example, the sulfuric acid process will introduce sulfate ions into the oxide matrix which can at best be removed by careful calcining; to check the effect of sulfate, ν-aluminum oxide was slurried with sulfuric acid, dried, pressed into a pellet and subjected to the synergistic vacuum and ultraviolet environment. Samples contaminated with 0.02 mole per cent sulfuric acid were tested for 50 solar actinic hours using the Hanovia 673A high pressure mercury lamp in a vacion system and found to color significantly. Absorptance changes at selected wave lengths are given in Table 1. ν-aluminum oxide was selected as host for the sulfate ion because anodized films are purported to be dominately of the ν form[2].

The study described in subsequent sections was carried out on α-aluminum oxide because this form was most readily analyzed by the simple phenomenological configurational coordinate scheme used for unifying experimental observations with thermodynamics. For example, the ultraviolet degradation of high purity ν-aluminum oxide was less reproducible than that of α-aluminum oxide, and as a result a consistent instability

---

(2) Wernick, S., Pinner, R., Finishing of Aluminum, Robert Draper Ltd., Teddington, 1959 (p.221).

TABLE I

Absorptance comparisons of the U-V stabilities of ν-aluminum oxide with sulfuric acid treated high purity ν-aluminum oxide at selected wavelengths

λ, μ Treatment	0.3	0.5
ν-Al_2O_3 before	0.96	0.95
	Δa =0.21	Δa =0.05
ν-Al_2O_3 after	0.75	0.90
ν+H_2SO_4 before	0.76	0.92
	Δa =0.35	Δa =0.26
ν+H_2SO_4 after	0.41	0.66

pattern was not found. However, ν-aluminum oxide appears to behave, phenomenologically at least, quite similarly to the α-form.

The Experimental Observations and Their Configurational Coordinate Interpretation

When α-Al_2O_3 is subjected to the combined effects of heat and vacuum in a conventional diffusion pump system operating at 10^{-4} torr in a 350°C thermal environment, it turns to a brown color characterized by the experimental conditions. The resultant color is shown in Figure 1. This particular temperature turned out to be significant because at 10^{-4} torr, this was the minimum heat level for incipient browning. At 900°C, for example, a more intense coloration was found. Figure 2 shows the combined ultraviolet and vacuum effects on α-Al_2O_3. The experiment was carried out in a vac-ion system for 500 hours at 10^{-7} torr with the temperature maintaining itself between 50 and 60°C. The ultraviolet source was an Hanovia 673 A mercury lamp, adjusted to irradiate a given sample at one solar actinic constant. For purposes of comparison, an identical ultraviolet vacuum experiment was carried out on recrystallized α-Al_2O_3. Results of the reflectance measurements are shown in Figure 3. Apparently the recrystallized form is more stable even though the band edge occurs in the near ultraviolet and the maximum wavelength reflecting an absorptance change is nearly identical with that of α-Al_2O_3.

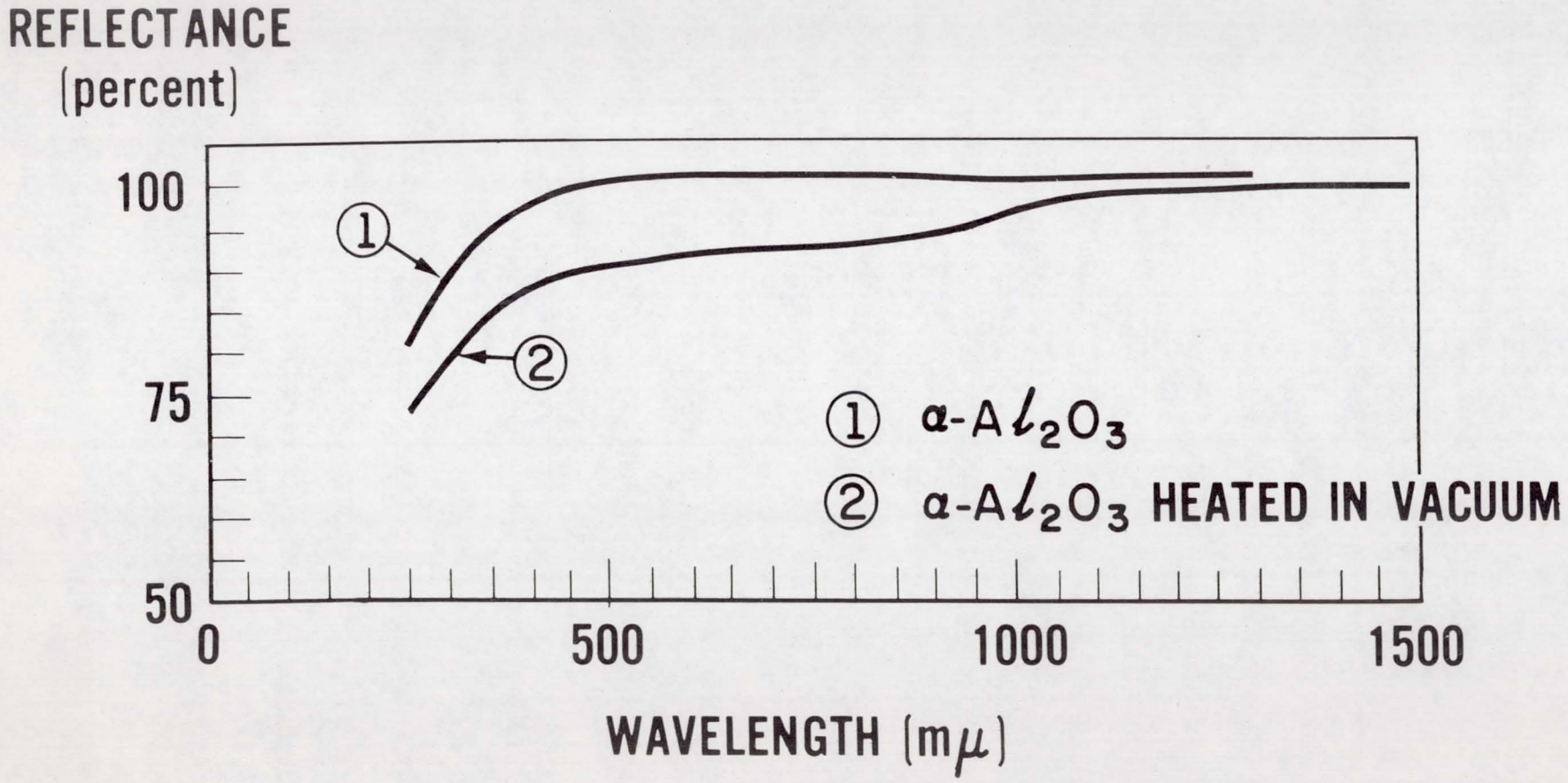

Figure 1. Combined Heat and Vacuum Effects on α-Al_2O_3 at 300°C and 10^{-4} Torr

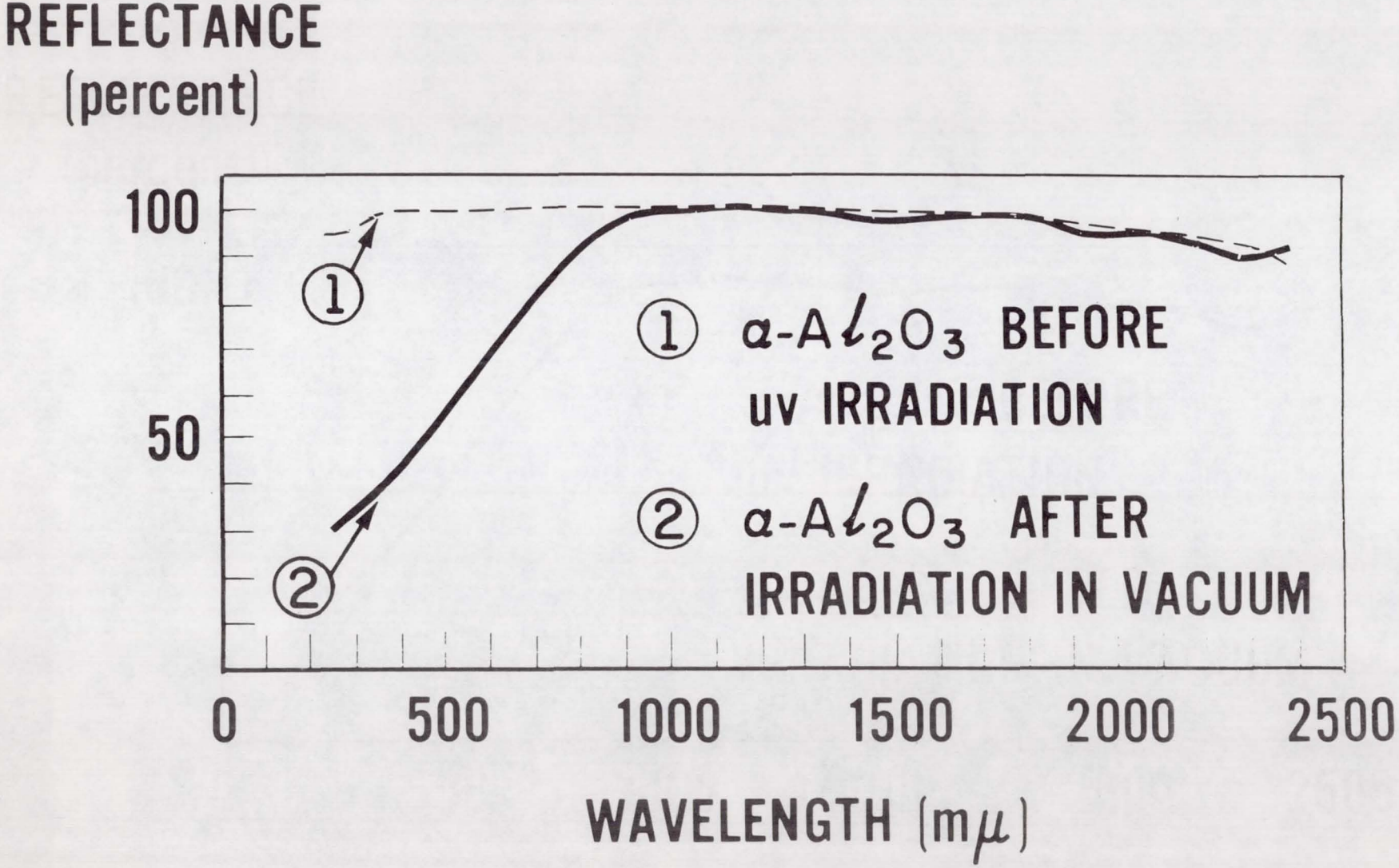

Figure 2. Combined u-v and Vacuum Effects on α-Al_2O_3 at 60°C and 10^{-7} Torr

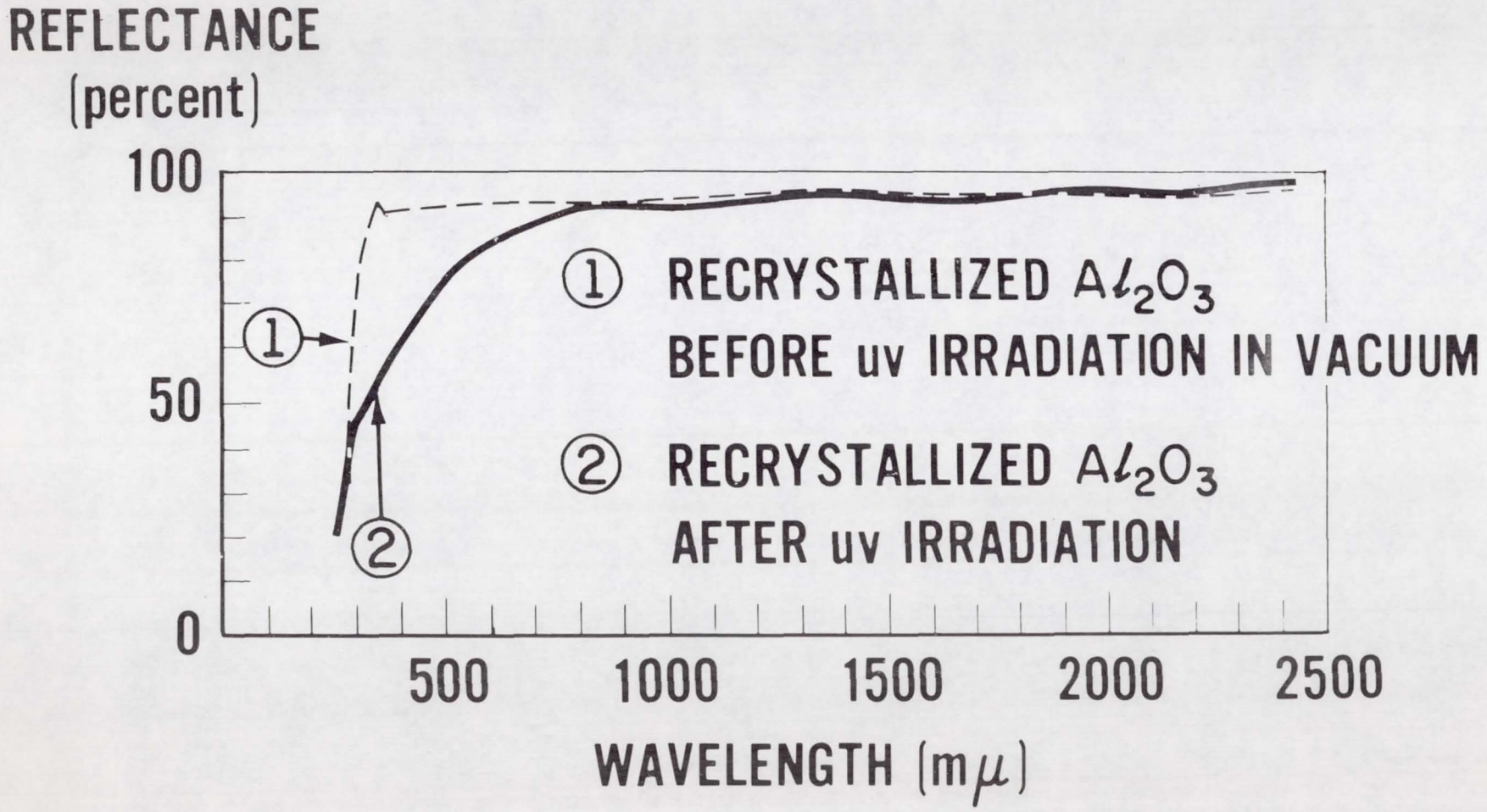

Figure 3. Combined u-v and Vacuum Effects on Reccrystallized $-Al_2O_3$ at 60°C and 10^{-7} Torr

Incipient to the degradation of α-Al_2O_3 in the ultraviolet and visible portions of the electromagnetic spectrum is the decrease in absorptance of α-Al_2O_3 in the near infrared part of the spectrum. This study is shown in Figure 4. A sample of α-Al_2O_3 was heated in air to about 300°C and its reflectance recorded before its initial reflectance was recovered by the reabsorption of water. In Figure 5 (Curve 3) is shown the reflectance curve for α-Al_2O_3 vacuum degraded under conditions previously described for 300 hours. An additional curve 2 has, however, been included. This reflectance curve not only represents one state among a continuous series obtainable by thermal bleaching in air, but also represents a metastable state resulting from irradiation with 360 mμ in the ambient environment.

Figures 1, 2, 4 and 5 can be interpreted in terms of the phenomenological configurational coordinate scheme. Such an interpretation is shown in Figure 6. When a sample is put into the vacuum-ultraviolet environment described above, it initially loses water and the surface energy rises by the amount ΔF_1 in the state A (Figure 3). Ultraviolet energy comparable to the short wavelength cutoff, λ_{cs}, then boosts the surface energy to the potential well designated by B.

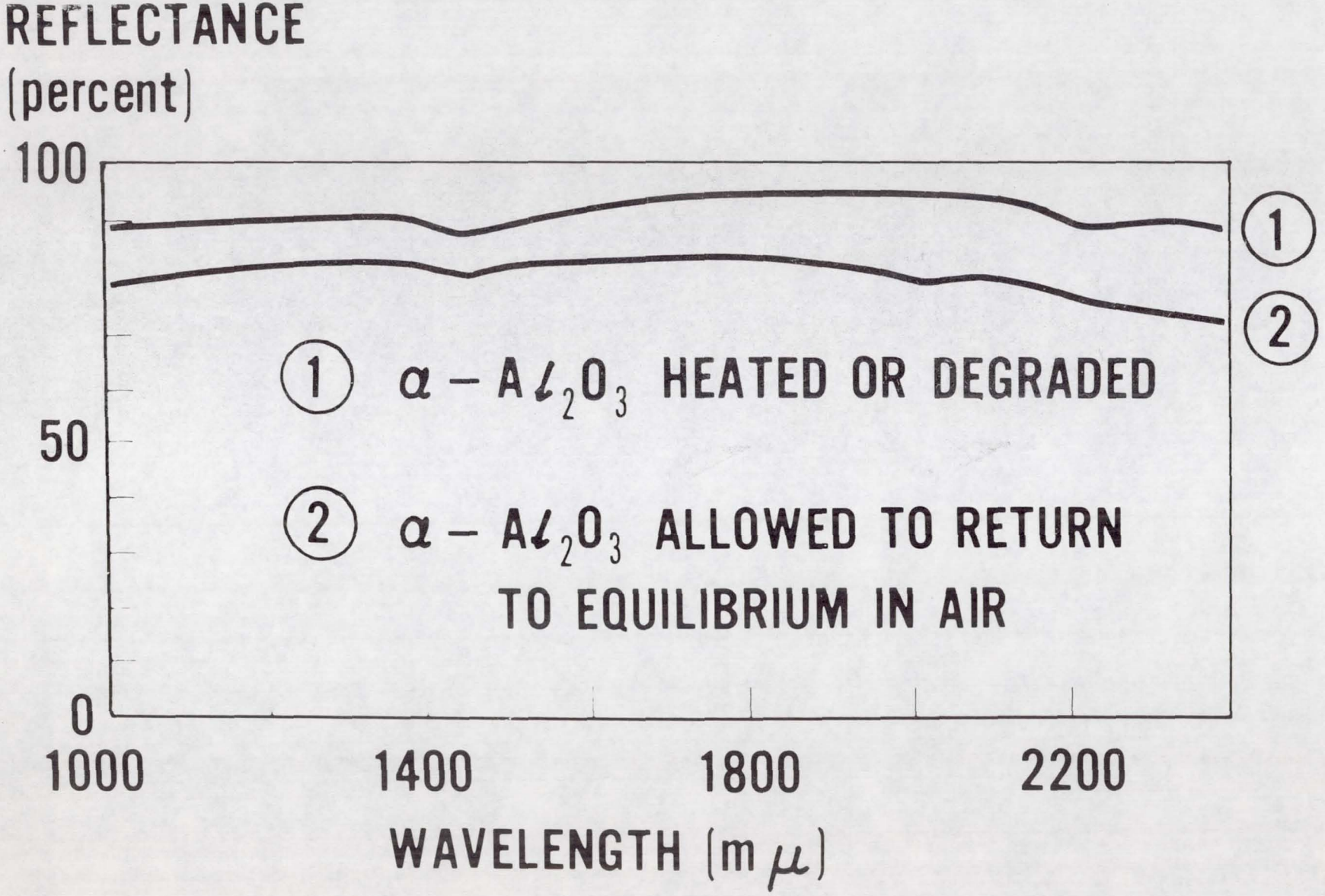

Figure 4. Effect of Dehydration on Infra-Red Spectra of $-Al_2O_3$

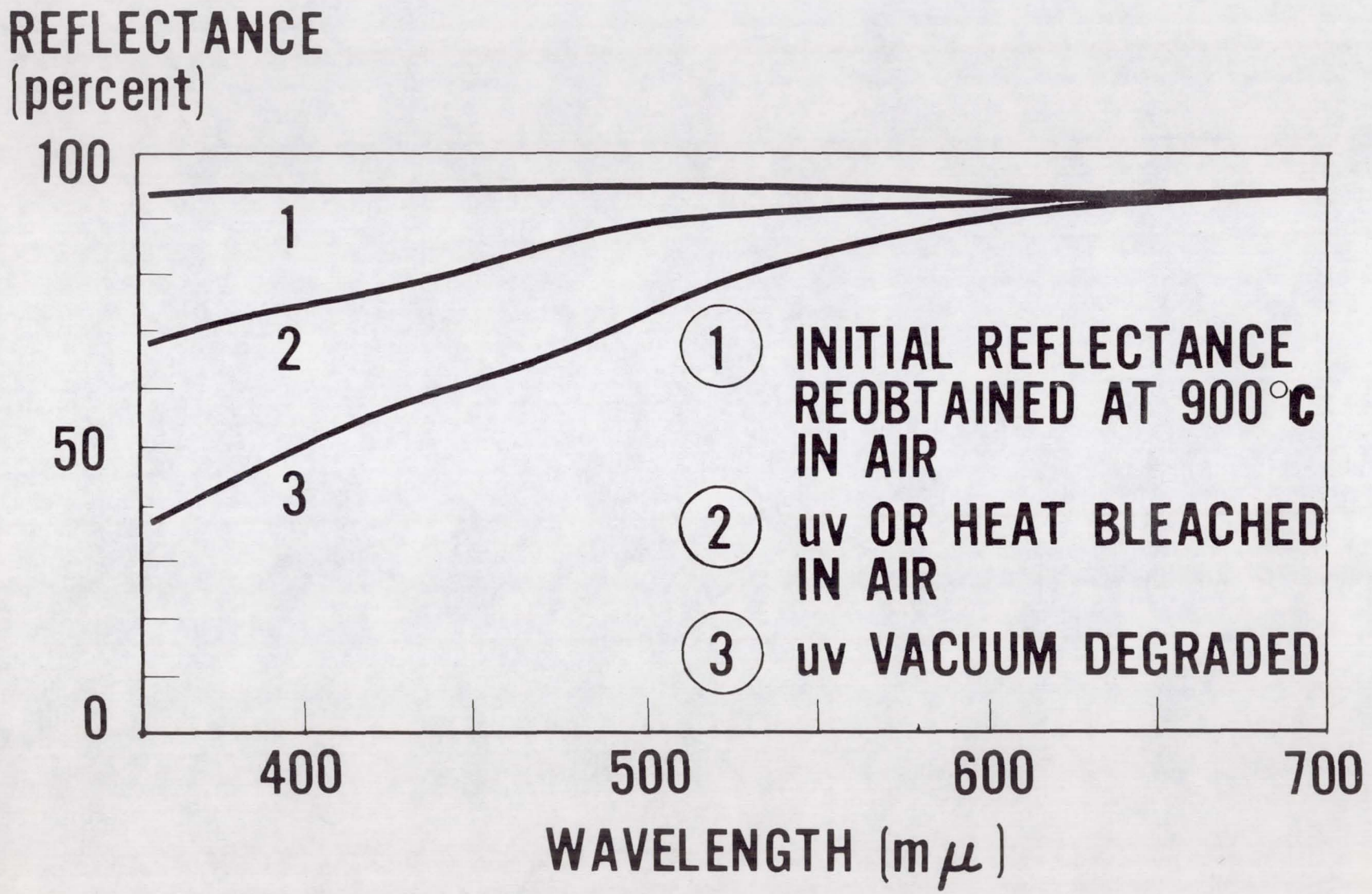

Figure 5. Representative Reflectance Spectra for Recrystallized $-Al_2O_3$ Showing Heat and u-v Effects

From B the surface energy becomes characterized by the state D (Curve 1, Figure 5 or Figure 2). Removing the sample from the vacuum-ultraviolet environment into the ambient environment then provides the driving force-ΔF, for the system represented by the state E. Subsequent irradiation by a wavelength greater than λ_{cs} and approximating the long wavelength cutoff, λ_{cl}, bleaches a sample to the metastable state C (Curve 2, Figure 3). Likewise, the state C can be derived from the state E by ambient heating of the sample to 300°C (Curve 2, Figure 3). In other words, the state C is arrived at by thermal tunneling and the state A derived from E by tunneling at 900°C (Curve 1, Figure 5). The state C can be derived from state A by heating in vacuum to 350°C (Figure 1); the system has tunneled to the state C. The metastable state C is somewhat artificial when considered in the light of states A and D with its existence being justified solely by the bleaching wavelength, λ_{cl} = 360 mμ.

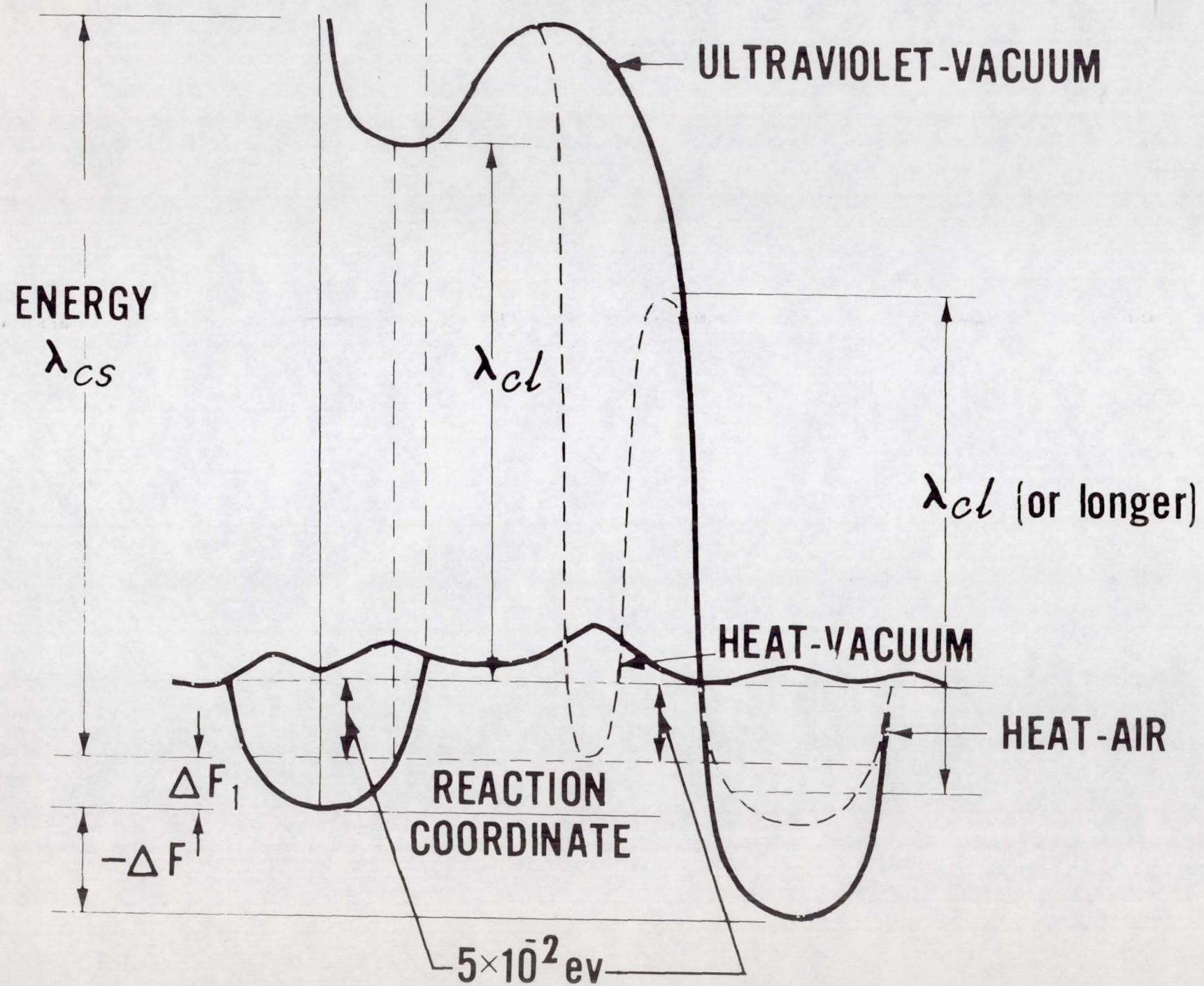

Figure 6. Configuration Coordinate Model for α-Al_2O_3

Chemical Thermodynamic Aspects

Since loss of water by α-Al_2O_3 is incipient to ultraviolet degradation (cf, Figure 4), this aspect of the problem may be represented by the following equilibrium:

$$n\,Al_2O_3]m\,H_2O \underset{H_2O}{\overset{\Delta/vac.}{\rightleftharpoons}} n\,Al_2O_3](m-x)\,H_2O + x(H_2O]) + x\,H_2O \qquad (R1)$$

Right brackets have been used to designate surface species, (H_2O]) to designate vacant water absorption sights and x the moles of water lost. Subjection of the material to a thermal vacuum environment, in which a temperature of at least 350°C has been attained, further promotes loss of surface water; continued dehydration will leave oxygen atoms free from hydration. These events can be represented by the following reaction scheme:

$$n\,Al_2O_3](m-x)H_2O \underset{\Delta, air}{\overset{\Delta, vac.}{\rightleftharpoons}} n\,Al_2O_{3-y/n}](m-x-z)H_2O + z_2(H_2O]) + y\,O]\left(\frac{z-z_2}{y}\right)(H_2O]) + z\,H_2O \qquad (R2)$$

For the above circumstances, simple dehydration leads to Z_2 active water absorption sites and Y dehydrated oxygen atoms covering $(Z-Z_2)$ water sites. Under the conditions of ultraviolet-vacuum, allowance must be made for the migration of oxygen ions; the complete representation can be written:

$$p\,Al_2O_3 + n\,Al_2O_{3-y/n}\,](m-x-z)\,H_2O \underset{\Delta,air}{\overset{UV,vac}{\rightleftharpoons}} p\,Al_2O_{3-y_p/p} +$$

$$n\,Al_2O_{3-y/n+y_p/n}\,](m-x-z-z_p)\,H_2O + y_p\,O^{-2+\delta+\xi/y_p}\,]\frac{(z_p-z_2)(H_2O])}{y_p} +$$

$$z_3\,(H_2O])\,\xi/z_3\,(e) + z_p\,H_2O + y_p\,(O^{2-\delta}\square) + y_p\,Al^{+3} + y_p\,(Al^{+3}O)$$

This reaction considers p moles of Al_2O_3 losing Y_p moles of oxygen to the surface with Z_p additional moles of water escaping from the surface. During the complete process, Y_p moles of oxygen vacancies are formed with charge $2-\delta$. The oxygen ions, which migrate to the surface, fill (Z_p-Z_3) vacant water sites and have a charge $(-2+\delta+\xi/Y_p)$ giving ξ hydrated electrons in the surface layer.

Each of the above reaction schemes involves the surfaces of any crystal of α-Al_2O_3. If the assumption is made that crystals in the micron range have the same fractional surface area with surface energy per unit area (A), $\nu_s \cdot i$, then the probability, P_i, of creating a surface of the i th type which can be formed n_i ways can be written:

$$P_i = \frac{n_i W_i^c}{\sum n_i W_i^c} \qquad (1)$$

W_i^c is the cohesion energy of ith face type. The average surface energy per unit area of a particle in vacuum is then given by

$$\bar{\gamma}_{s^0} = \frac{\sum n_i W_i^c \gamma_{s^0 i}}{\sum n_i W_i^c}$$

Letting $\bar{n}_{ij}$ and μ_{ij} represent the number of particles of species j on i th face and μ_{ij} the chemical potential of the j th species on the i th face, the Gibbs absorption equation is written

$$d\gamma = -\sum_{ij} \frac{\bar{n}_{ij}}{A} d\mu_{ij} = -RT \sum_{ij} \frac{\bar{n}_{ij}}{A} d \ln K_{ij}$$

where the usual substitution for the chemical potential has been made. Generalizing equation (2) for some arbitrary ambient pressure, p_A, and differentiating, the result is

$$d\gamma = \sum_{ij} \frac{n_i W_i^c d\gamma_{ij}}{n_i W_i^c}$$

Substituting equation (3) into (4) and integrating, the following expression is obtained,

$$\bar{\gamma}_{P_A} - \bar{\gamma}_{S^o} = -\frac{RT}{\sum n_i W_i^c}\left[\sum_{ij} \int_{P_{S^o}}^{P_A} n_i W_i^c \frac{\bar{n}_{ij}}{A} d\ln K_{ij} + \right.$$

$$\left. \frac{1}{2} \sum_{\substack{ijK \\ i \neq j}} \int_{P_{S^o}}^{P_A} n_i W_i^c \frac{\bar{n}_{ij}}{A} d\ln K_{Kj} \right]$$

where the K_{ij}'s refer to the equilibrium constants of the reactions E1 to E3, for example, K_{11} is the occurrence of the first reaction on a face of type 1, and the notation of species and reaction are now synonomous.

Briefly, equation (5) shows the following:

1) That surface energy decreases with pressure,

2) That the occurrence of any face type is not only dependent upon crystal plane particle density (as indicated by W_2^c) but also the number of conceivable ways the crystal plane can be created, and

3) That identical particle interactions need not be occurring on juxtaposed faces.

For reaction (R1),

$$K_{i1} \cong P_{H_2O}^{z_n/n} \; C_{(H_2O])}^{z_n/n} \qquad E1$$

Assuming unit activity for Al_2O_3, $C_{(H_2O])}$ is the concentration per unit area of water absorption sites. Similarly, for R2

$$K_{i2} \cong P_{H_2O}^{z_n/n} \; C_{(H_2O])}^{z_n/n} \; \bar{C}_{(H_2O])}^{(z-z_n)/n} \qquad E2$$

where, as before, unit activity has been assumed for Al_2O_3 an approximate equilibrium constant follows as readily for (R3):

$$K_{i3} \cong P_{H_2O}^{z_p/p} \; C_{(H_2O])}^{z/p} \; \bar{C}_{(H_2O])}^{(z_p-z_s)/p}$$

Each K_{ij} is, according to the above approximate equilibria, predominately dependent upon the partial pressure of water. Consequently, each type of surface active site must be related to the partial pressure of water in order to make equation (5) integrable. This end can be accomplished by determining the B.E.T. absorption isotherm as a function of the partial pressure of water. Once the fit has been carried, expressions for the K_{ij}'s can be substituted into equation (5). If then, one face type is assumed dominant, the equation can be summed and integrated for any combination of the reactions R1 and R3.

Discussion

Although the reaction system, R1 - R3, does not admit to the loss of oxygen as an unreacted entity, it does allow for the loss of chemisorbed oxygen in the form f water. Since aluminum compounds as a class habitually xist with considerable water coverage, the water must so over an individual crystal in liquid form that its surface area is a minimum. R1 then allows for the removal of water which only sees other water molecules. R2 allows not only for the removal of similar water molecules, but also for chemisorbed water. R3 considers chemisorbed water which is not only dependent upon the loss of oxygen, but also the atomic and electronic polarizations of lattice oxygens with an accompanying creation of oxygen vacancies. Aluminum oxide was used in the reaction series; however, impurities will enter in like manner. If, however, a given impurity can exist in multiple stoichiometries, the loss of oxygen as a separate entity can occur. Such a possibility gives rise to additional color center formation.

Due to the particular affinity of oxy-aluminum compounds for water, use of the B.E.T. absorption isotherms is particularly pertinent because its form allows for multi-layered absorbates. The Langmuir absorption isotherm would not be valid in this case, since it was derived on the basis

of monomolecular absorption. If, in addition to working out the B.E.T. absorption isotherm as a function of the partial pressure of water, it also must be established for selected thermal environments with and without ultraviolet illumination. The complete validity of the reaction system R1-R3 could be worked out on this basis and the surface free energies calculated from equation (5).

The ability of α-Al_2O_3 to exhibit ultraviolet and thermal instabilities is not an isolated phenomenon. Indeed, the variable absorptance property is impurity dependent and has been found in all white microcrystalline oxides investigated for ultraviolet stability in this laboratory. Generally speaking, the phenomenology is referred to as thermophototropism or the diffusion controlled temperature dependent variable absorptance of inorganic compounds.

SPECTRAL EMISSIVITY OF METALS AFTER DAMAGE BY PARTICLE IMPACT

by

Klaus Schocken
and
James A. Fountain
Space Thermodynamics Branch
Research Projects Laboratory
Marshall Space Flight Center

Presented at the conference,
"Spacecraft Coatings Development Including
UV Degradation and α/ϵ Measurement
Problems,"
May 6, 1964
NASA Headquarters
Washington D. C.

In order to evaluate the effects of micrometeoroids on the emittance of solids, information is required on the amount of damage which would be inflicted on a target on which impinges a particle between 1 to 10 microns in diameter moving with a velocity between 10 to 72 km sec^{-1} . The densities of the particles should range between 0.05 and 9.0 g cm^{-3} .

In the first stage of crater formation, immediately after impact, pressures of the order of 1 to 100 megabars arise in the neighborhood of the contact area. This process lasts only a very short time. In the second stage pressure waves are reflected from the free boundaries decreasing the pressure, and a flow of the projectile and the target material results. The extremely high pressure is attenuated rapidly before the crater has attained very large dimensions. After a few microseconds the pressure pluse has degenerated into an elastic wave. Also under low pressure conditions the crater continues to expand. The duration of the cratering process depends upon the physical characteristics of the target material. In very plastic materials, the expansion of the crater continues for long times; in more brittle materials, the crater expansion terminates comparatively early and is followed by crushing and fracture of the target material.

No agreement has been obtained on the dynamic relations between the crater formation and the impact parameters. Under these circumstances, consistent and reliable statistical data acquire great importance. The following results have been obtained for ductile target materials.

Craters produced by hypervelocity impact are approximately hemispherical. The depth of a crater is given by the formula:

$$P = \tfrac{1}{2} D + T$$

$$T = L \left(\frac{\rho_P}{\rho_t} \right)^{\frac{1}{2}}$$

where D denotes the diameter, T the depth of the penetrated layer, L the length of the projectile, ρ_P and ρ_t the densities of projectile and target material, respectively.

A linear correlation exists between the volume of the crater resulting from hypervelocity impact and the kinetic energy of the impacting projectile, which has been proved for a range of particle masses from 10^{-11} to 10 g and in velocity to 15 km sec^{-1}. In sufficiently thick skins a meteoroid having a kinetic energy E in a coordinate system fixed with respect to the space vehicle will produce a hemispherical crater of volume V, given by the expression:

$$V = 4 \cdot 10^{-9} \frac{E}{B} \cos \alpha \quad \text{(cgs-units)}$$

where B denotes the Brinell hardness number of the target material, representing the ratio of load in kg on a sphere used to indent material to the spherical area of indentation in mm^2, and α the angle of attack.

Since statistical correlations have been obtained between the crater and impact parameters, corresponding correlations can be expected between radiation and surface parameters.

The total amount of radiation absorbed by a specimen depends on its surface area projected on a plane perpendicular to the direction of propagation. The total amount of emitted radiation depends on the effective radiating area. Cavities will therefore affect the amounts of absorbed and emitted radiation.

Since neither physical relations nor statistical correlations involving radiation parameters have been established, the George C. Marshall Space Flight Center awarded a contract to the AVCO Corporation on June 5, 1961, for the investigation of the spectral emittance of selected metals and for the determination of the effect of simulated micrometeorite impact on the emittance of metal surfaces.

The samples used by AVCO were gold, aluminum, silver, stainless steel (types 304 and 316), tungsten, chromium plate on copper, and platinum. The samples were carefully polished and measured for reflectivity and for the ratio of solar absorptance to infrared emittance. The samples were then cratered with spherical particles of zircalloy at 1.5 km/sec and tungsten at 7 km/sec. The diameter of the particles in both cases was about 100 microns. An example of a gold sample is shown in Figure One. This sample was bombarded with tungsten particles at 7 km/sec. The total area of the crater openings is about 30 per cent of the total sample area. Figure 2 shows a cross section of a hemispherical crater in a copper sample. Notice the compacting of the material in the region around the crater. Notice also how the target material flowed upward and outward from the center of impact.

Because of the large number of craters involved in these tests, the bombarded sample area was divided up into nine 40° segments. The number of craters in three of the segments was counted. The average of the three segments was multiplied by nine to obtain the total number of craters over the whole sample. The diameter of each crater of the three segments was measured

with a micrometer eyepiece. The depth of the craters was measured by focusing a microscope on the sample surface and then on the crater bottom and recording the distance traveled by the microscope. From these numbers the depth-to-diameter ratio and the area of the crater openings were calculated. A tabulation of these data is given in Figure 3.

The large increase in the number of craters at 7 km/sec is caused by the fact that foreign particles of less than 50 μ in the system did not cause measurable craters at the lower velocity, but at 7km per second they did cause measurable craters. Tests showed that a large number of the foreign particles in the system were smaller than 20 microns. The apparent anomaly that the average dimensions to the craters produced by the 1.5 km/sec particles is greater than the craters produced by the 7 km/sec particles can be attributed to the fact that the large number of smaller craters at the higher velocity effectively reduced the dimension averages. Figure 4 shows the differences due to the velocity of the particles. This compares two samples of Stainless Steel 304 where side A was bombarded at 1.5 km/sec and side B was bombarded at 7 km/sec. There are many more large craters in side B and the particles that produced craters (appearing as small white specks on side A) produced many well-defined craters of a small to medium size in side B. In side B, much more of the material is pushed out into the rim, making the overall appearance very rough.

Since, for opaque materials, the emittance is equal to one minus the reflectance, the spectral reflectance of the cratered samples was measured from 2 to 26 microns. Figure 5 shows the reflectance curve for gold. The top curve is for the polished sample, the center curve is for the sample bombarded at 1.5 km/sec, and the lower curve is the reflectance for the sample bombarded at 5.2 km/sec.

Figure 6 shows the same three curves for aluminum, but in this case the change from the lower to the higher velocity is much greater. The reflectance curves for all the samples were integrated in order to compute the fractional change in reflectance per area and per particle impact. For the 1.5 km/second tests this data is shown in Figure 7. The same parameters for the 7 km/sec experiments are shown in Figure 8 . The last two columns in each of the two preceding slides are shown together for comparison in Figure 9.

The other thermal properties measured were the solar absorptance and the infrared emittance. A spacecraft absorbs solar radiation at short wavelengths and emits thermal radiation at long wavelengths. In the laboratory, this situation was simulated by irradiating one side of the sample with a xenon-filled mercury arc lamp to simulate the solar radiation. The opposite side radiated to a blackened chamber whose walls were cooled by liquid nitrogen. The rate of change of temperature of the sample was monitored. The solar absorptance, α , and the infrared emittance, ϵ , were calculated. A typical change in the α/ϵ ratio as a function of temperature is shown in Figure 10 which is for a chromium plated copper sample. A tabulation of the data (Figure 11) shows some interesting results. In this Figure, the subscript o denotes the original condition, and i the impacted condition. In the first two columns, note that α was increased by the cratering in every case; this was expected. Similarly in the ϵ_o and ϵ_i columns, ϵ is also increased in each case, but in the first four samples at a much greater percentage than α , causing an overall reduction in the value of the α/ϵ ratio. However, in the case of Stainless Steel 304, notice from the columns for percent change of $\Delta\alpha/\alpha_o$ and $\Delta\epsilon/\epsilon_o$ that the increase is very nearly at the same rate . This results in an

almost negligible change in the value of the α/ϵ ratio. This can be seen in Figure 12 which shows the ratio for Stainless Steel 304 plotted for the polished and cratered sample for two separate tests. This effect is, as of yet, unexplained, and it is clear that further study is needed to substantiate these findings, to find the reason for it, and to determine if other alloys act similarly.

In summarizing, we can conclude that (1) cratering by micro-particles at velocities of 1.5 km/sec causes a decrease in reflectance from 1 to 10 per cent, (2) cratering by particles at 7 km/sec causes a decrease in the reflectance by 10 to 26 per cent, (3) cratering by particles at 7 km/sec caused marked decreases in the solar absorption to thermal emittance ratio of the four metals: gold, platinum, aluminum, and chromium-plated copper, but did not substantially affect the ratio for Stainless Steel 304. In the four metals in which the ratio changed, ϵ increased much more than α. In the Stainless Steel 304, α and ϵ increased at approximately the same rate.

Work in this area should continue. A study is to be made by Space Technology Laboratories to determine the effect on thermal control surfaces of very small particles of the size order of 0.1 to 3 microns and at velocities up to 25 km/sec. According to present measurements and theories, particles of this size should be very numerous in space.

REFERENCES

1. Eichelberger, R. J., and Gehring, J. W., "Effects of Meteoroid Impacts on Space Vehicles," ARS J., p. 1583-1591 , 1962.

2. Eichelberger, R. J., "Summary: Theoretical and Experimental Studies of Crater Formation," Proc. Sixth Symp. on Hypervelocity Impact, Contract No. DA-31-124-ARO(D)-16, The Firestone Tire and Rubber Co., 1963.

3. Leigh, C., and Wolnik, S., "Emissivity of Metals After Damage by Particle Impact," AVCO RAD-SR-61-68, 1961.

4. Leigh, C. H., "Spectral Emissivity of Metals After Damage by Particle Impact," AVCO RAD-TR-62-33, 1962.

5. Laszlo, T. S., and Gannon, R. E., "Spectral Emissivity of Metals after Damage by Particle Impact," AVCO RAD-TR-63-39, 1963.

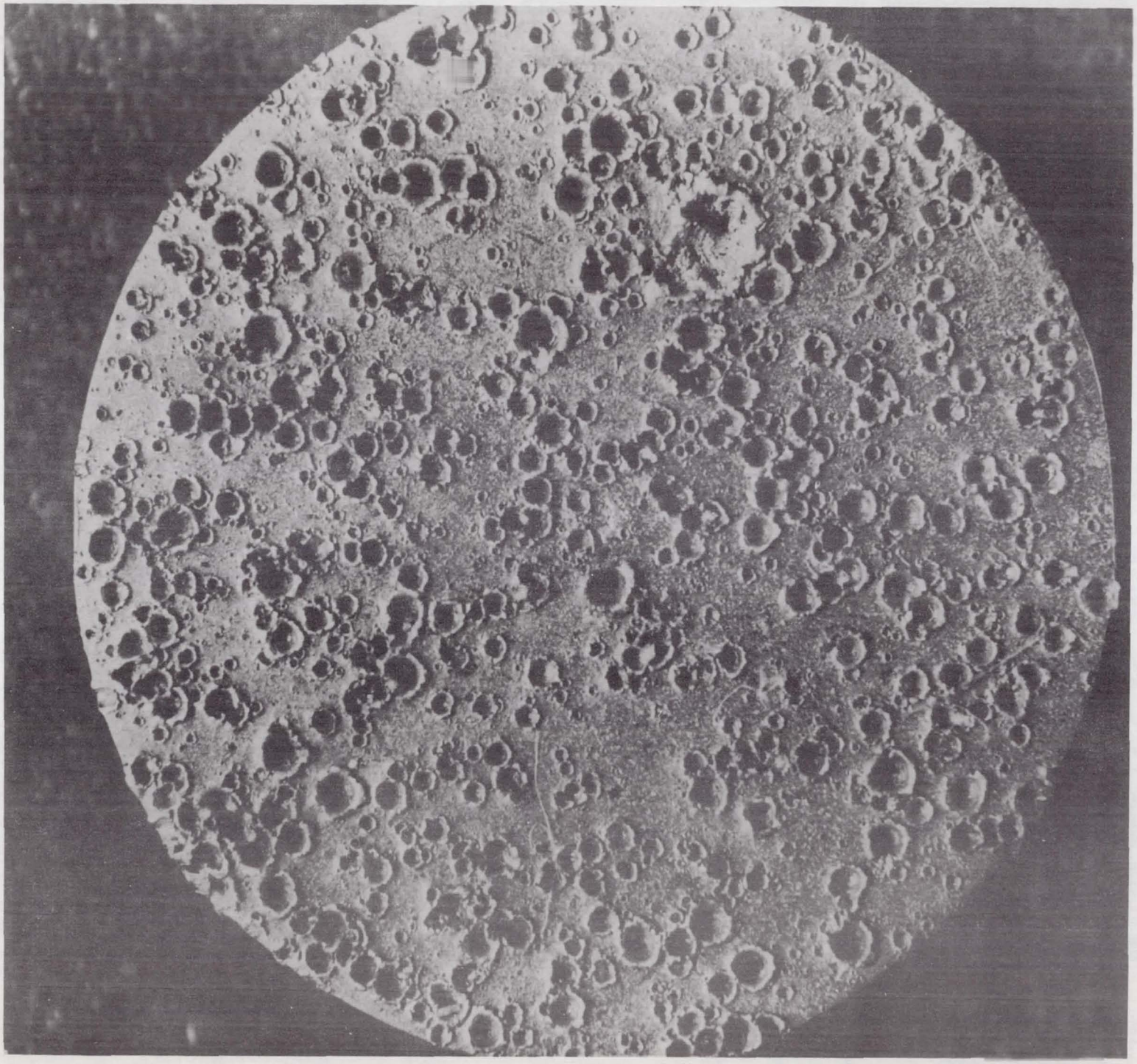

FIGURE 1

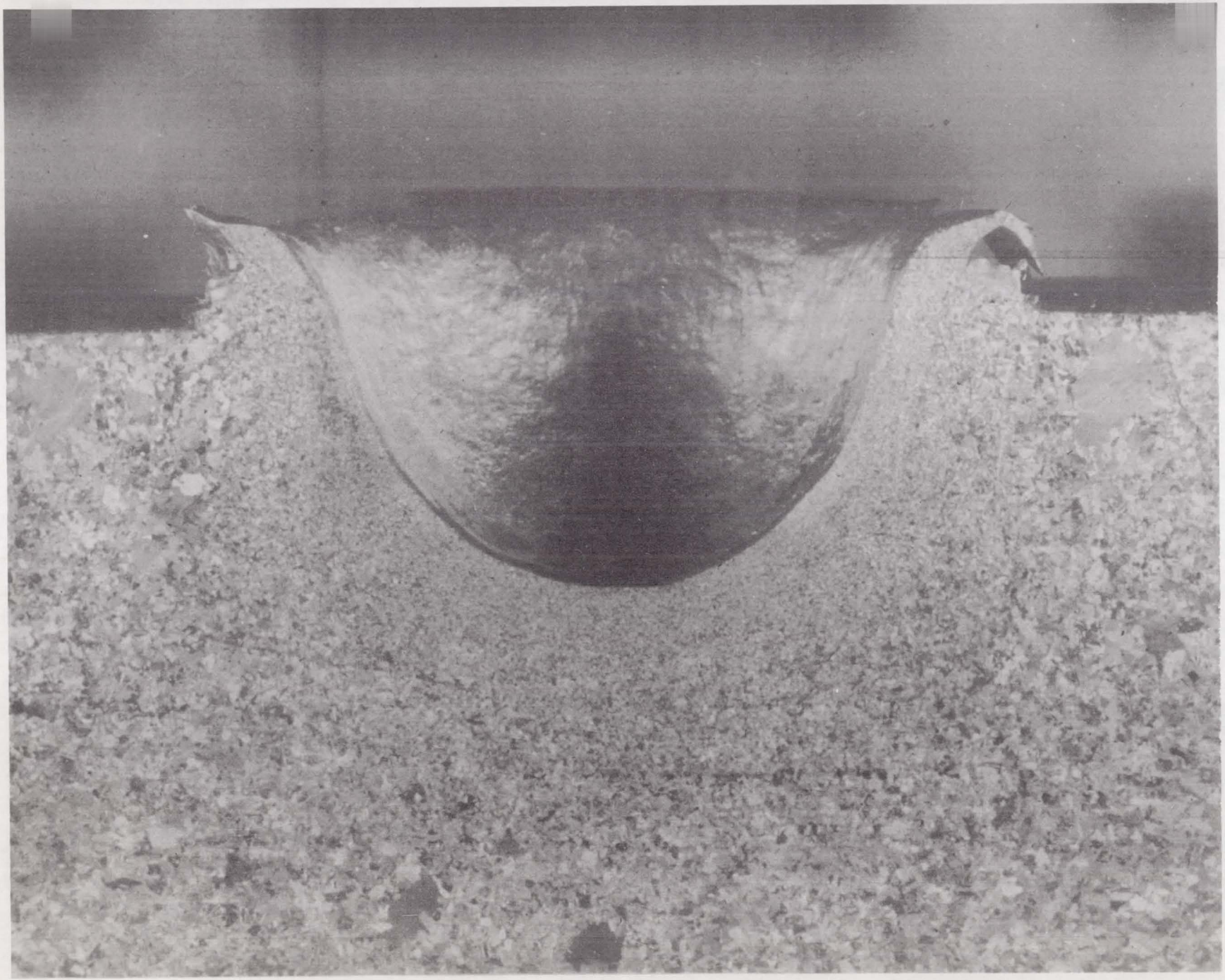

HEMISPHERICAL MICROMETEOROID CRATER

FIGURE 2

DESCRIPTION OF DAMAGE TO SPECIMENS

Material		Projectile Velocity (ft/sec)	Projectile Velocity (m/sec)	Number of Craters	Average Diameter (microns)	Average Depth (microns)	Depth Diameter (microns)	Area Damage (percent)	Knoop Hardness 100-g load
Al	R	5,000	1500	549	123	289	2.35	3.41	22
Al	R	20,000	7000	7,830	54	183	3.39	18.9	
Al	a/ϵ	20,000	7000	19,467	27	78	2.87	17.6	
Au	R	5,000	1500	630	213	241	1.13	9.99	40
Au	R	17,000	5200	5,526	63	61	0.97	21.47	
Au	a/ϵ	20,000	7000	8,380*	53	60	1.13	29.68	
SS 304	R	5,000	1500	327	111	172	1.55	1.42	219
SS 304	R	20,000	7000	3,672	106	179	1.69	17.44	
SS 304	a/ϵ	20,000	7000	6,012	74	124	1.68	19.04	
Cr	R	5,000	1500	663	130	196	1.51	3.88	697
Cr	R	20,000	7000	3,321	125	239	1.91	21.10	
Cr	a/ϵ	20,000	7000	1,764*	112	237	2.12	11.40	
Pt	R	20,000	7000	2,844	182	189	1.04	38.20	120
Pt	a/ϵ	20,000	7000	4,099*	122	127	1.04	34.24	
SS 316	R	5,000	1500	438	205	186	0.91	6.43	
W	R	5,000	1500	456	120			2.27	
Ag	R	5,000	1500	710	175	306	1.75	7.61	

*Total number of craters on both sides of $a\epsilon$ specimens.

FIGURE 3

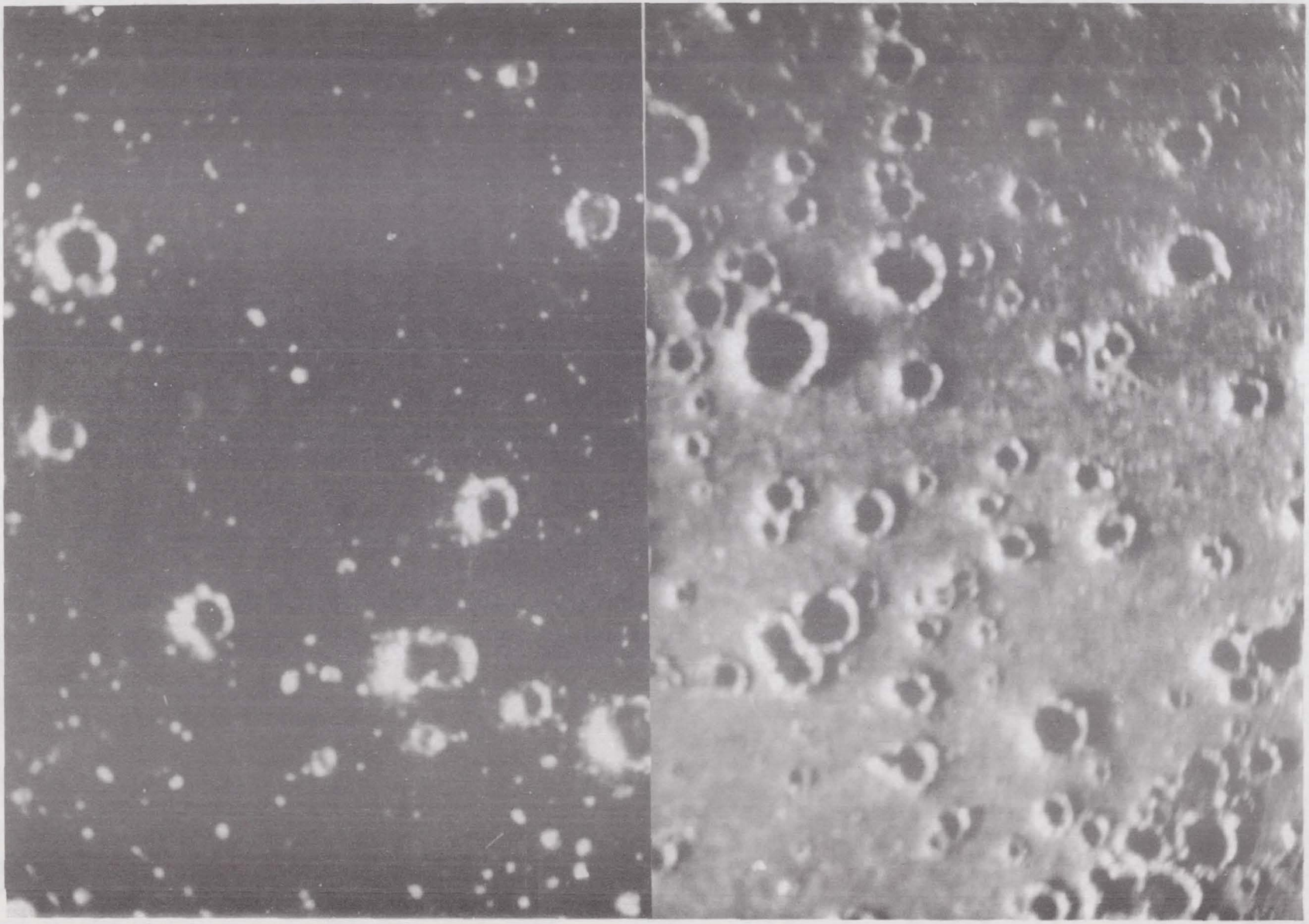

A

B

FIGURE 4

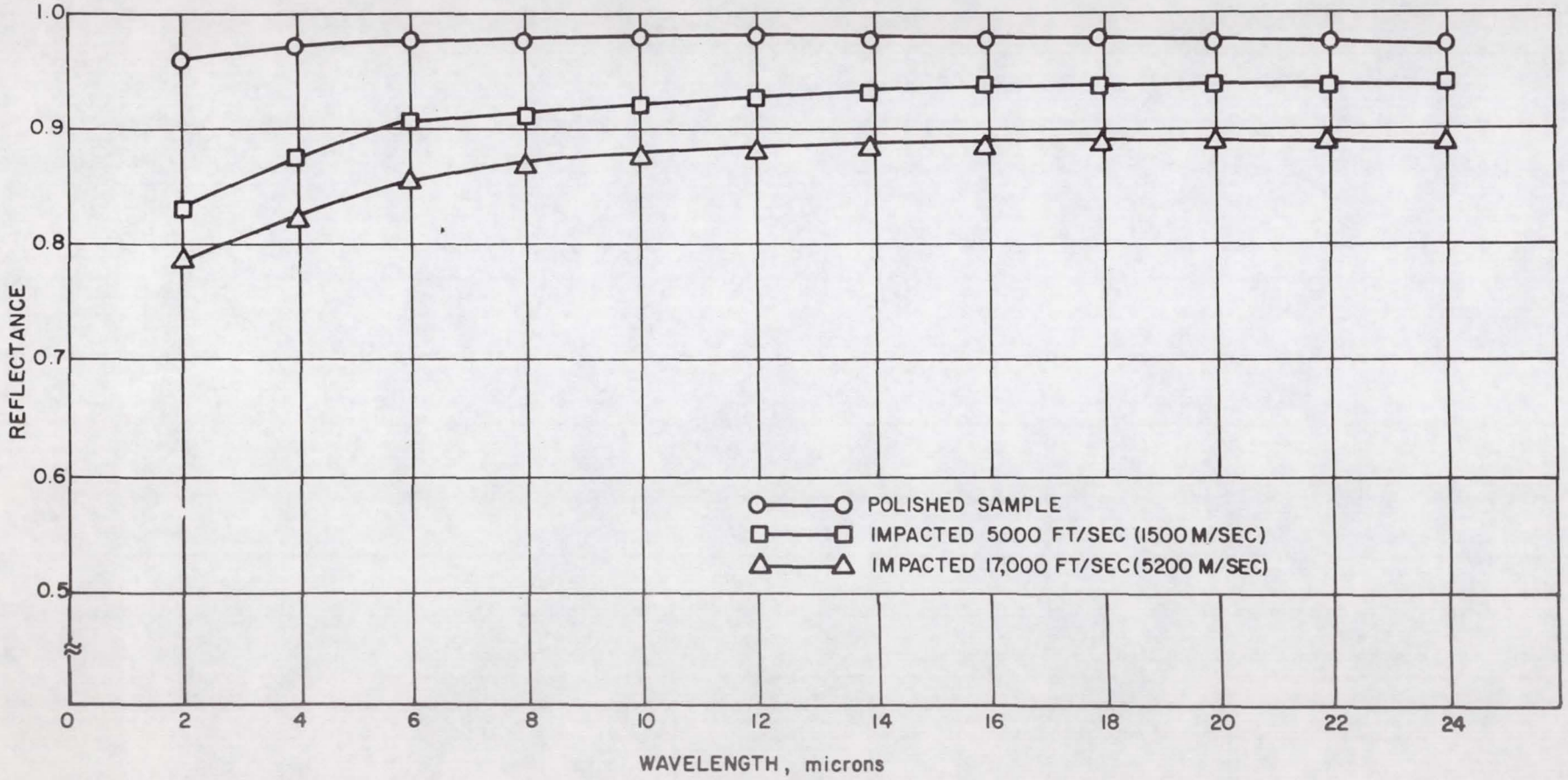

SPECTRAL REFLECTANCE OF GOLD

FIGURE 5

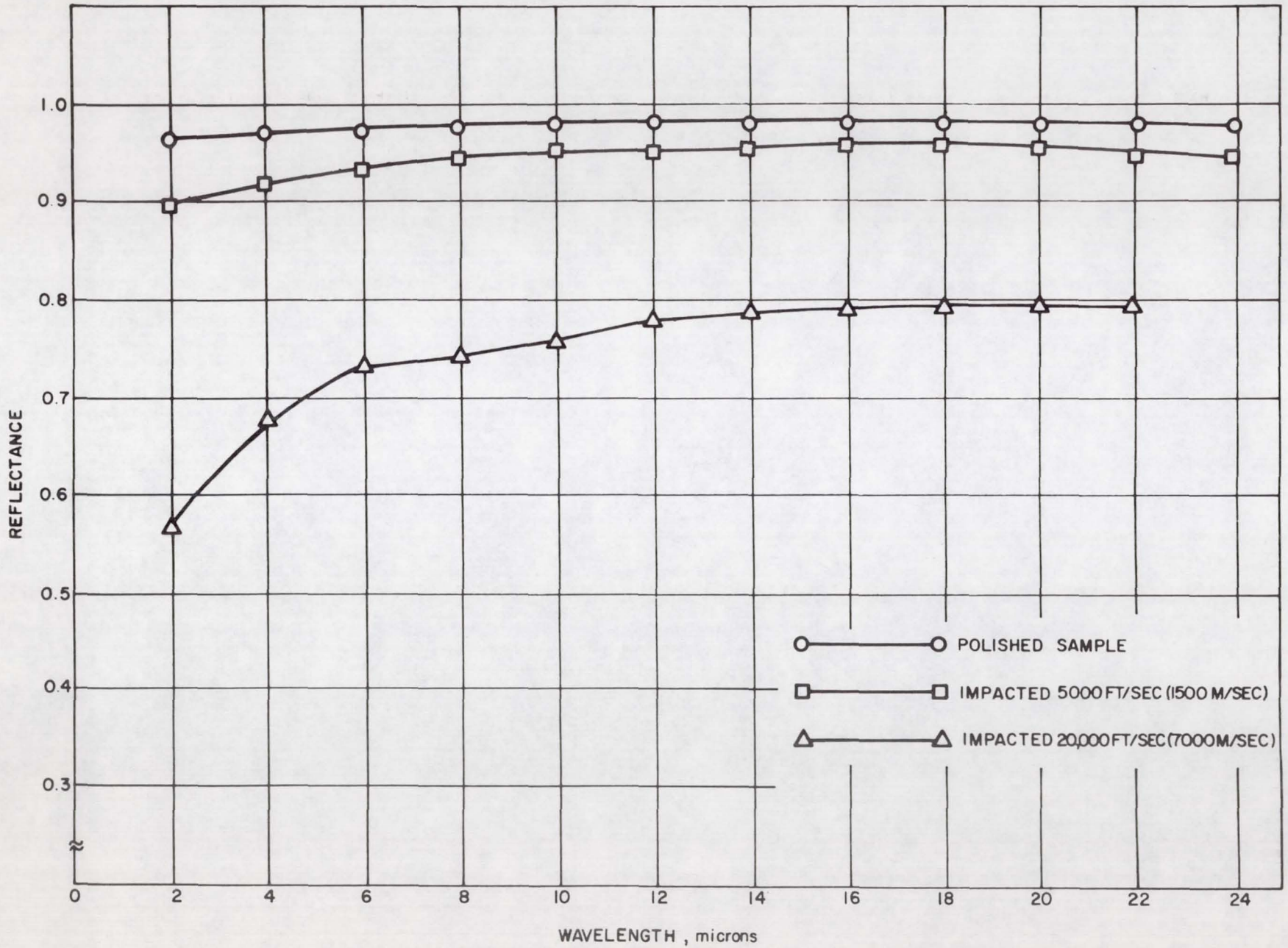

SPECTRAL REFLECTANCE OF ALUMINUM

FIGURE 6

REFLECTANCE BEFORE AND AFTER IMPACT BY 5000 FT/SEC
(1500 M/SEC) ZIRCALOY PARTICLES

Material	Number of Craters	Area Damaged (percent)	** R_o 2 to 24μ (percent)	** R_i 2 to 24μ (percent)	ΔR (percent)	$\Delta R/R_o$	$\frac{\Delta R/R_o}{A}$	$\frac{\Delta R/R_o}{N}$
Al	549	3.41	97.66	95.81	1.85	1.90	0.557	0.0035
Au	630	9.99	97.58	91.49	6.09	6.24	0.625	0.0099
SS 304	327	1.42	87.84	86.11	1.73	1.97	1.387	0.006
Cr *	663	3.88	92.55	89.11	3.44	3.72	0.957	0.0056
SS 316	438	6.43	88.39	85.55	2.84	3.21	0.533	0.0078
W	456	2.27	96.50	92.95	3.55	3.67	1.335	0.0066
Ag	710	7.61	97.93	89.73	6.20	8.37	1.226	0.013

* Chromium-plated copper

**Percent reflectance values obtained by integrating spectral reflectance curves between 2 and 24 μ

FIGURE 7

REFLECTANCE BEFORE AND AFTER IMPACT
BY 20,000 FT/SEC (7000 M/SEC ZIRCALOY PARTICLES

Material	Number of Craters	Area Damaged (percent)	** R_o 2 to 24 μ (percent)	** R_i 2 to 24 μ (percent)	ΔR (percent)	$\Delta R/R_o$	$\frac{\Delta R/R_o}{A}$	$\frac{\Delta R/R_o}{N}$
Al	7830	18.88	97.66	76.17	21.49	22.00	1.17	.0028
Au	5474	21.79	97.58	96.97	10.61	10.87	0.50	.0020
SS 304	3672	17.45	87.84	75.17	12.67	14.42	0.83	.0039
Pt	2844	38.28	94.37	70.10	24.27	25.71	0.67	.0090
*CR	3321	21.08	92.55	76.28	16.27	17.57	0.83	.0053

*Chromium plated Copper
**Percent reflectance values obtained by integrating spectral reflectance curve between 2 and 24 μ.

FIGURE 8

CHANGE IN REFLECTANCE PER CRATER AND PER AREA DAMAGED
FOR TWO IMPACT VELOCITIES

Material	$\Delta R/R_o$ A	$\Delta R/R_o$ N	$\Delta R/R_o$ A	$\Delta R/R_o$ N
	1.5 km/sec		7 km/sec	
Al	0.557	0.0035	1.17	0.0028
Cr	0.957	0.0056	0.83	0.0053
SS 304	1.387	0.006	0.83	0.0039
SS 316	0.533	0.0078	--	--
Ag	1.226	0.013	--	--
W	1.335	0.006	--	--
Pt	--	--	0.67	0.0090
Au	0.625	0.0099	0.50	0.0020

FIGURE 9

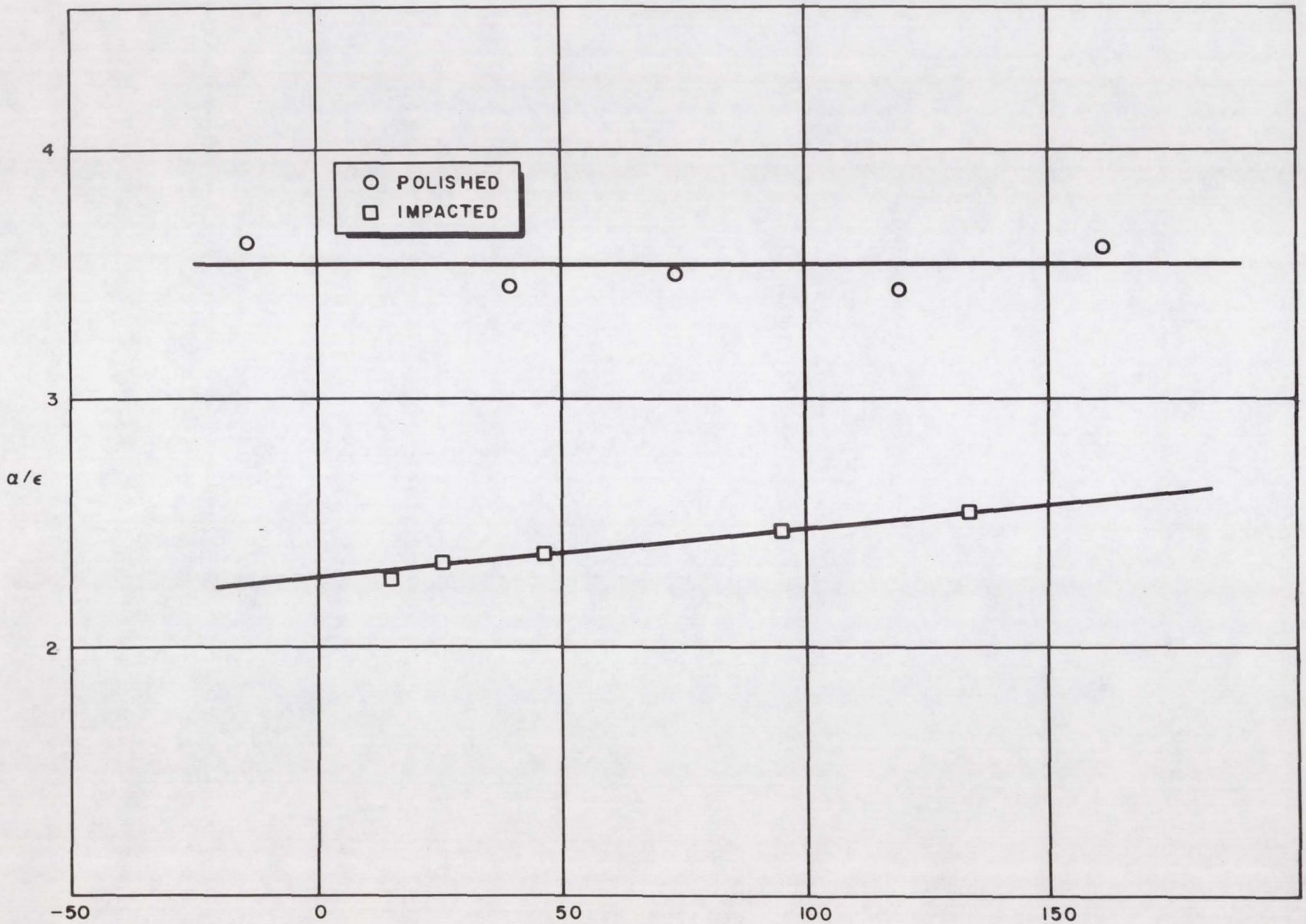

α/ϵ OF CHROMIUM-PLATED COPPER

FIGURE 10

EFFECT OF MICROMETEORITE IMPACTS ON OPTICAL PROPERTIES

Material	a_o^*	a_i^*	Δa	$\Delta a/a_o$ x 100 (percent)	ϵ_o^*	ϵ_i^*	$\Delta\epsilon$	$\Delta\epsilon/\epsilon_o$ x 100 (percent)	a_o/ϵ_o	a_i/ϵ_i	$\Delta a/\epsilon$	$\Delta a/\epsilon \Big/ a_o/\epsilon_o$ x 100 (percent)
Aluminum	0.18	0.74	0.56	311	0.044	0.367	0.323	735	4.0	2.0	2.0	-50
Gold	0.27	0.63	0.36	133	0.047	0.250	0.203	440	6.0	2.5	3.5	-58
Platinum	0.24	0.68	0.44	183	0.059	0.336	0.277	470	4.0	2.0	2.0	-50
Chromium plated Copper	0.41	0.58	0.17	41	0.106	0.222	0.116	109	3.8	2.6	1.2	-32
Stainless Steel 304	0.23	0.42	0.19	83	0.084	0.167	0.083	98	2.8	2.5	0.3	-11

* a_o and ϵ_o refer to the measured a and ϵ values of the polished specimen and a_i and ϵ_i refer to the properties of the impacted specimens.

FIGURE 11

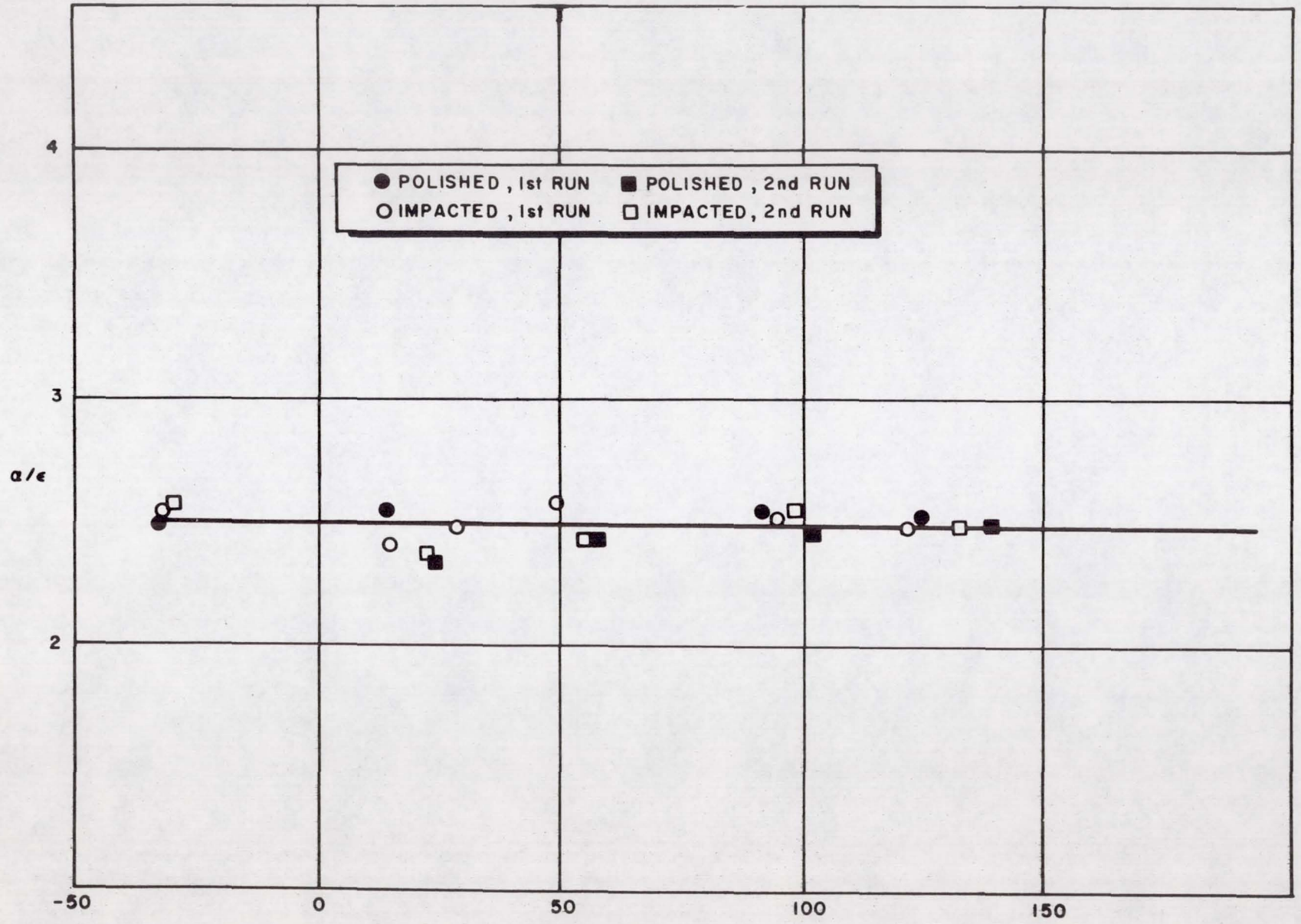

α/ε OF STAINLESS STEEL, TYPE 304

FIGURE 12

SOME POLY-BASIC PHOSPHATE CONVERSION COATINGS FOR THERMAL CONTROL

Noel T. Wakelyn and George F. Pezdirtz

INTRODUCTION

As a result of an increasing number of orbital missions extending over long periods, there has been considerable need for thermal-control surfaces which are "stable" to the space environment, that is, surfaces which retain their original optical properties after extended exposure to the space environment. A considerable amount of work has recently been directed toward developing and testing such coatings (ref. 1-4). In some instances, such as the Echo passive communications satellite program, the thermal-control coatings must meet further stringent requirements. The thermal-control surface of the Echo II is approximately 57,000 square feet. The total structural shell of the Echo II is only 0.75 mil thick and is composed of two outer layers of 0.18 mil aluminum foil glued to a 0.35-mil Mylar plastic film as shown in figure 1. As a result of the very large surface and the very thin substrate, it was necessary to use a thermal-control surface with a minimum weight and thickness.

Chemical conversion coatings have proved to be the most practical approach to this problem. A mixture of chromium phosphate and aluminum phosphate deposited by a dip process on the thin outer aluminum foil was successful. This coating was a commercial product, Alodine 401-45[1].

---

[1]Trade mark of Amchem Products, Inc., Ambler, Pennsylvania.

It was necessary to investigate the ultraviolet stability of its optical properties over extended times since Alodine had previously been used primarily as a paint primer and weather protectant for aluminum, and virtually nothing was known of its use for thermal-control purposes.

Determination of Solar Absorptance and Thermal Emittance

The total hemispherical reflectance from 0.2 to 2.1 microns was measured with a Cary-14 Spectrophotometer equipped with an integrating sphere coated with barium sulfate. Freshly smoked magnesium oxide plates were used as reflectance standards. Calculations of solar absorptance were made by determining the reflectance of the specimen for each wavelength increment corresponding to a 1-percent energy increment under the solar-energy curve. These weighted reflectance increments were then summed over the 0.295-to-2.02-micron range and the total reflectance subtracted from unity.

The "total hemispherical reflectance" from 4 to 15 microns, NaCl region, was measured with a Perkin-Elmer 13-U spectrophotometer equipped with a hohlraum attachment. The emittance values were calculated by determining the reflectance of the specimen for each wavelength increment corresponding to a 1-percent energy increment under a 295°K blackbody curve. These weighted reflectance increments were then summed over the 4-to-15-micron range and subtracted from unity. The resultant value, based upon 55% of the blackbody energy, is referred to in this paper as thermal emittance. Preliminary data recently obtained by a calorimetric technique indicates that the spectrophotometric method, for the phosphate

coating in the 4-to-15-micron range, is systematically high in ε by about 0.02.

Chemical Conversion Coatings

The chemical conversion coating, Alodine 401-45, is produced by reacting an aluminum surface with an aqueous solution of chromic, phosphoric, and hydrofluoric acid. Clemmons and Camp (ref. 4) have reported that the ratio of solar absorptance to thermal emittance (α_s/ε) varies from 7.0 to 0.80 as a function of the surface densities, which varied from 30.4 milligrams per square foot to 426 milligrams per square foot, respectively. They also found that the solar absorptance increases initially and then remains virtually constant over a wide range of surface densities (thickness). In contrast, the thermal emittance was found to increase almost linearly over the same range of surface densities. This variation of thermal emittance with surface density permits a wide range of equilibrium temperatures for an Alodine 401-45 coated satellite simply by selecting the appropriate surface density with the desired α_s/ε ratio. Since the thermal emittance of this type of surface is the controlling factor in its useful optical properties, attention was focused on the infrared spectra of these coatings (ref. 5).

A typical infrared absorptance spectrum for Alodine 401-45 is shown in figure 2 along with a plot of the spectral-energy distribution for a 300°K blackbody. There are two prominent peaks in this infrared spectrum. The peak in the 3.8-micron region, which has been attributed to the acidic hydroxyl group (ref. 6), is of much less significance to the thermal emittance than the broad peak in the 7.5-to-11-micron region, which is

which is due to the phosphate group (refs. 6 and 7). The reason is that over 25 percent of the total energy of a 300° blackbody falls within the 8-to-12-micron region whereas less than 1 percent of the total energy for a 300°K blackbody is found at wavelengths shorter than 4 microns. If the chemical nature of the phosphate group could be sufficiently changed to alter the intensity of the broad peak at 7.5 to 11 microns, it would be possible to increase the thermal emittance of the Alodine 401-45 surface without resorting to an increase in surface density. Alteration of this group is possible by varying the acidic nature of the phosphate group as shown in figure 3.

By removing protons, stepwise with base, a shifting from the mono-basic, through the di-basic, to the tri-basic orthophosphate would be accomplished and thus the vibrations of the P-O bond should be changed. The subsequent decrease in the hydroxyl content should reduce the possibility of hydrogen bonding involving the OH group and thus permit increased P-O vibrations. Increased P-O vibrations would result in an increase in the intensity at the 7.5-to-11-micron band and hence a surface with a higher emittance.

A series of experiments were carried out to test this hypothesis. Samples of Alodine 401-45 on the Echo II laminate were reacted with dilute sodium and potassium hydroxide solutions for times ranging from 10 to 60 seconds. After washing in water and drying in air, the infrared-absorption spectra were again determined. The band at 7.5 to 11 microns was found to increase whereas the acidic OH band at 3.8 microns was found to decrease with reaction time in the basic solution, as shown in figure 4. The resultant increase in the thermal emittance was found to be linear with reaction time from an ε of 0.2 to 0.4.

In addition to increasing the thermal emittance of the Alodine 401-45 surface, it was found that the solar absorptance decreased with reaction time as illustrated in figure 5. The overall effect of this treatment is to decrease the ratio of α_s/ε. This approach to modifying the surface of Alodine 401 now makes it possible to obtain lower α_s/ε ratios without the necessity of increasing surface densities, as previously described (ref. 4).

Results and Discussion of the Stability to Ultraviolet, Thermal, and Vacuum Environments

Exposure to ultraviolet and thermal environments are known to produce changes in the optical properties of thermal-control surfaces and coatings (refs. 1, 8, and 9). Most of the reported investigations of the stability of thermal-control surfaces have been concerned with the effects of ultraviolet radiation in a vacuum on the solar absorptance of the surfaces. In the case of thermal coatings which contain small molecular species of moderate volatility, it is reasonable to expect some effect from long-term exposure to elevated temperatures in a vacuum as well as ultraviolet effects. Very little has been reported on thermal effects alone, though in some cases the temperature of the specimen during exposure to ultraviolet can have a significant effect, even to the extent of obscuring the effects of the ultraviolet exposure.

The conditions and environments used for studying the stability of the chromium phosphate coatings are summarized below.

ENVIRONMENTAL CONDITIONS

[1]Intensity, approximately 3 to 4 suns. (BH-6 lamp.)

Radiation	Pressure, torr	Temperature °C
Thermal	1	100
Ultraviolet[1]	10^{-6}	70
Ultraviolet[1]	10^{-7}	25

In studying the effects of ultraviolet radiation on the optical properties of thermal-control surfaces, it is essential that the specimen temperature be well known and maintained as constant as possible so as not to obscure the ultraviolet effect with thermal effects. When the ultraviolet intensity is considerably higher than solar intensity, the high thermal output of the source increases the difficulty in maintaining the desired sample temperature. It has been found for the Alodine coating, for example, that the thermal test (100°C, 1 torr) was comparable in severity with the ultraviolet - slightly greater, in fact. The emittance tended to decrease from about 0.20 to about 0.17 with very little change after the first twenty hours of testing for both the ultraviolet and thermal exposures. The absorptance tended to increase from about 0.24 to about 0.27 after 100 hours of ultraviolet exposure while exhibiting a fairly linear increase to about 0.28 in about 600 hours at 100°C and 1 torr. In general, the thermal and ultraviolet effects on the emittance were very similar, while the thermal test was a bit more severe on the absorptance than the ultraviolet test.

The type of vacuum system used can be a variable in the measurement of the ratio of solar absorptance to emittance as is shown in figure 6. The specimens maintained at 0°C and 25°C while being irradiated with ultraviolet in an ion pump vacuum system exhibited virtually the same increase in α_s/ε for 100 hour exposure time while ultraviolet irradiated specimens maintained at 0°C in an oil diffusion pump system showed no change in α_s/ε for 100 hours and an actual decreasing trend (below the original value) with time out to about 500 hours. The possibility of obtaining spurious results due to oil contamination from improperly used diffusion pumps should not be overlooked.

Thus far only the effects on Alodine 401 have been discussed. Figure 7 compares the thermal and ultraviolet effect of Alodine with the ultraviolet effect on a typical alkali-modified chromium phosphate. The modified coating is seen to be at least as stable to simulated space environments as the Alodine for approximately 400 equivalent sun hours.

CONCLUSIONS

1. The optical properties of chemical conversion coatings can be altered by controlled post-treatments of the surface to provide a wider range of α_s/ε values without increasing surfaces thickness.

2. Temperatures of test specimens can be as important, or more important, than the degree of vacuum or ultraviolet flux in ascertaining the stability of optical properties optical properties for thermal-control surfaces.

3. More attention should be devoted to the basic spectrophotometric techniques for determining the cause of changes in optical properties as well as development of new thermal-control surfaces.

4. Spurious results can be obtained from improperly used oil diffusion pumps. Optical surface contamination can not only mask trends but can even produce trends of the opposite direction.

REFERENCES

1. Robert M. Van Vliet, Editor: Coatings for the Aerospace Environment. WADD Technical Report 60-773 (July 1961).

2. Robert E. Gaumer and Louis A. McKellar: Thermal Radiative Control Surfaces for Spacecraft. Technical Report LMSD-704014, Lockheed Missiles and Space Division (March 1961).

3. H. H. Hormann, J. H. Weaver, and James J. Mattice: Improved Organic Coatings for Temperature Control in a Space Environment. In Proceedings of Society of Aerospace Materials and Process Engineers "Symposium on Effects of Space Environment on Materials" (May 6-9, 1962) St. Louis, Missouri.

4. Dewey L. Clemmons and John D. Camp: Amorphous Phosphate Coatings for Thermal Control of Echo II. Presented at the Multilayer Systems Symposium of the Electrochemical Society, Los Angeles, California (May 6-10, 1962).

5. George F. Pezdirtz: Nonmetallic Materials for Spacecraft. Presented at the Materials for Space Operations Session of the NASA-Universities Conference (November 1-3, 1962), NASA SP-27.

6. E. Z. Arledge, et al.: Infrared, X-Ray, and Thermal Analysis of Some Aluminum and Ferric Phosphates. J. Applied Chem. 13, 17-26 (1963).

7. Foil A. Miller and Charles H. Wilkins: Infrared Spectra and Characteristic Frequencies of Inorganic Ions. Analytical Chemistry 24, 1253 (1952).

8. D. E. Field, J. E. Cowling, and F. M. Noonan: The Properties of Paints as Affected by Ultraviolet Radiation in a Vacuum. Part 2, U. S. Naval Research Laboratory Report 5737 (1962).

9. Carr B. Neal: Measurement of Thermal-Radiation Characteristics of Temperature-Control Surfaces During Flight in Space. Presented at 9th National Aerospace Instrumentation Symposium, San Francisco, California (May 8, 1963).

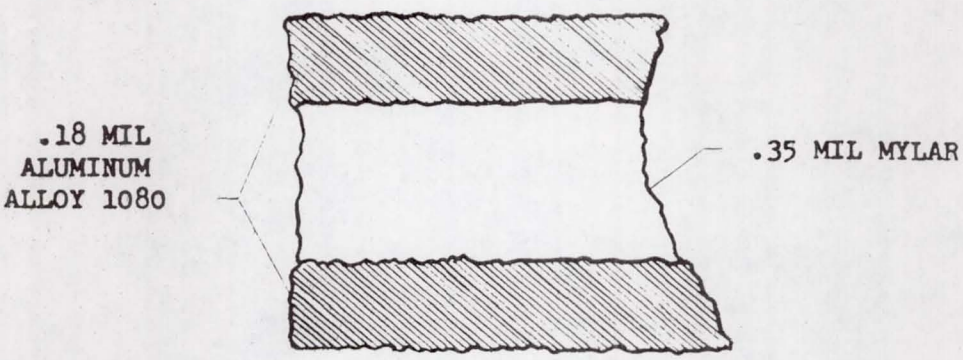

Figure 1. - Cross Section of Echo II Laminate

Fig. 1

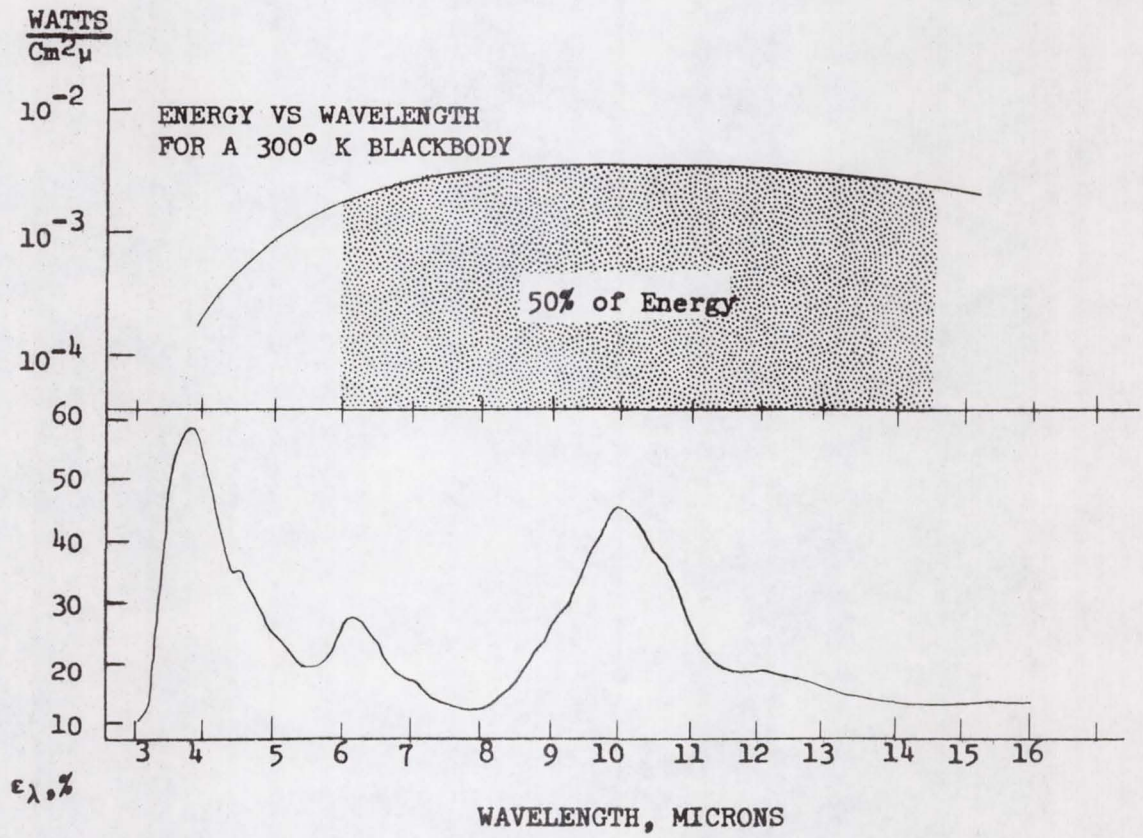

Figure 2. - Comparison of Blackbody Spectra with Emittance Spectra of Alodine 401.

Fig. 2

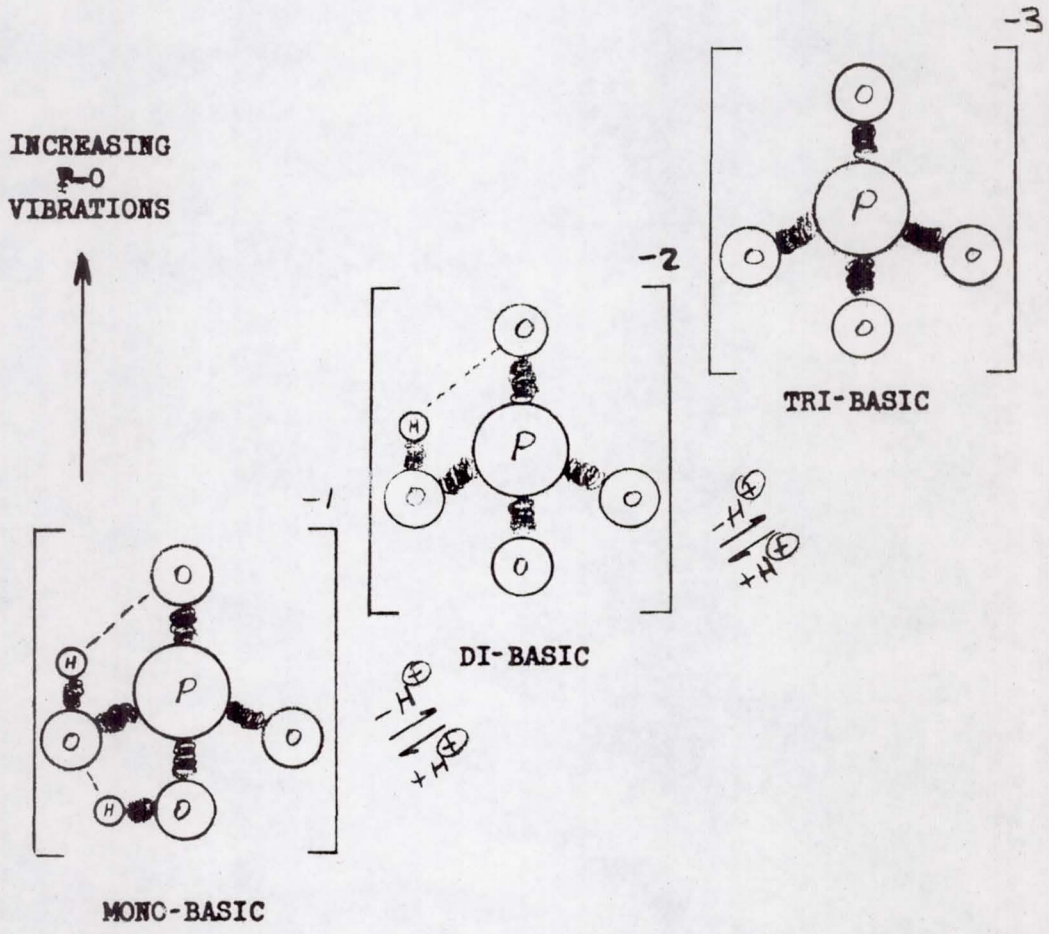

Figure 3. - Simplified Model of Orthophosphates

Fig. 3

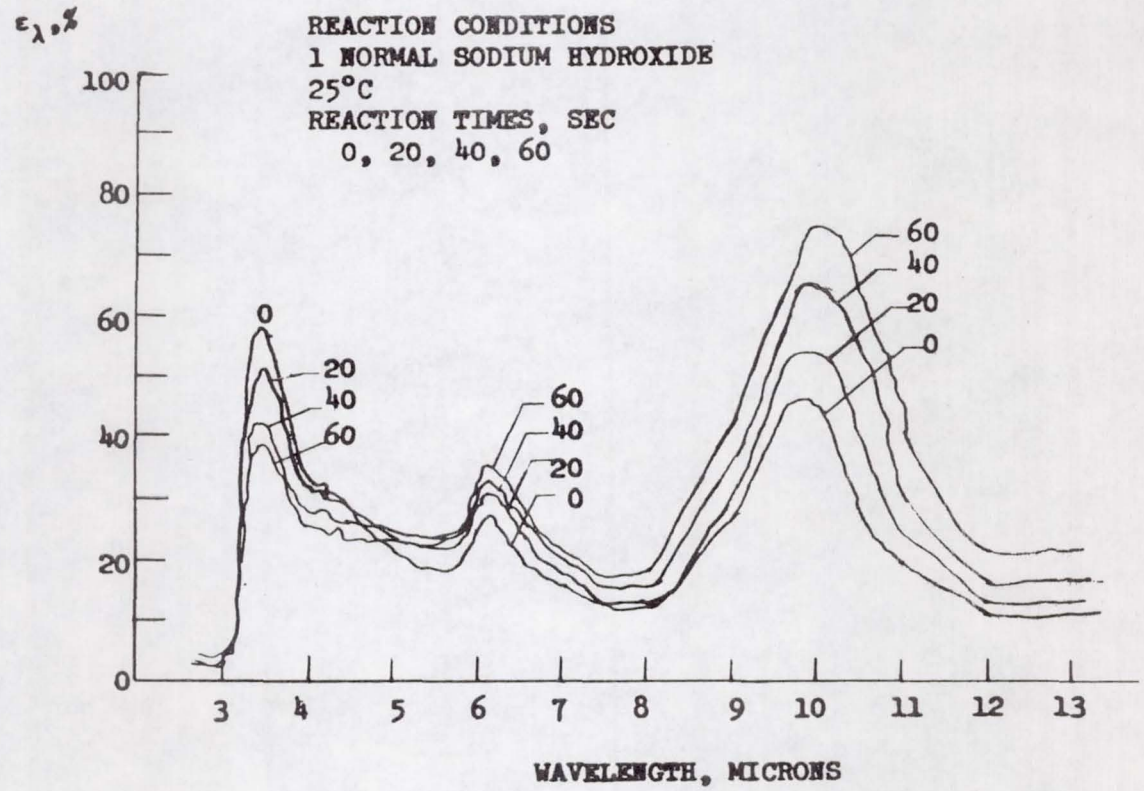

Figure 4. - Influence of Hydroxide Treatment on Infrared Spectra of Alodine 401.

Fig. 4

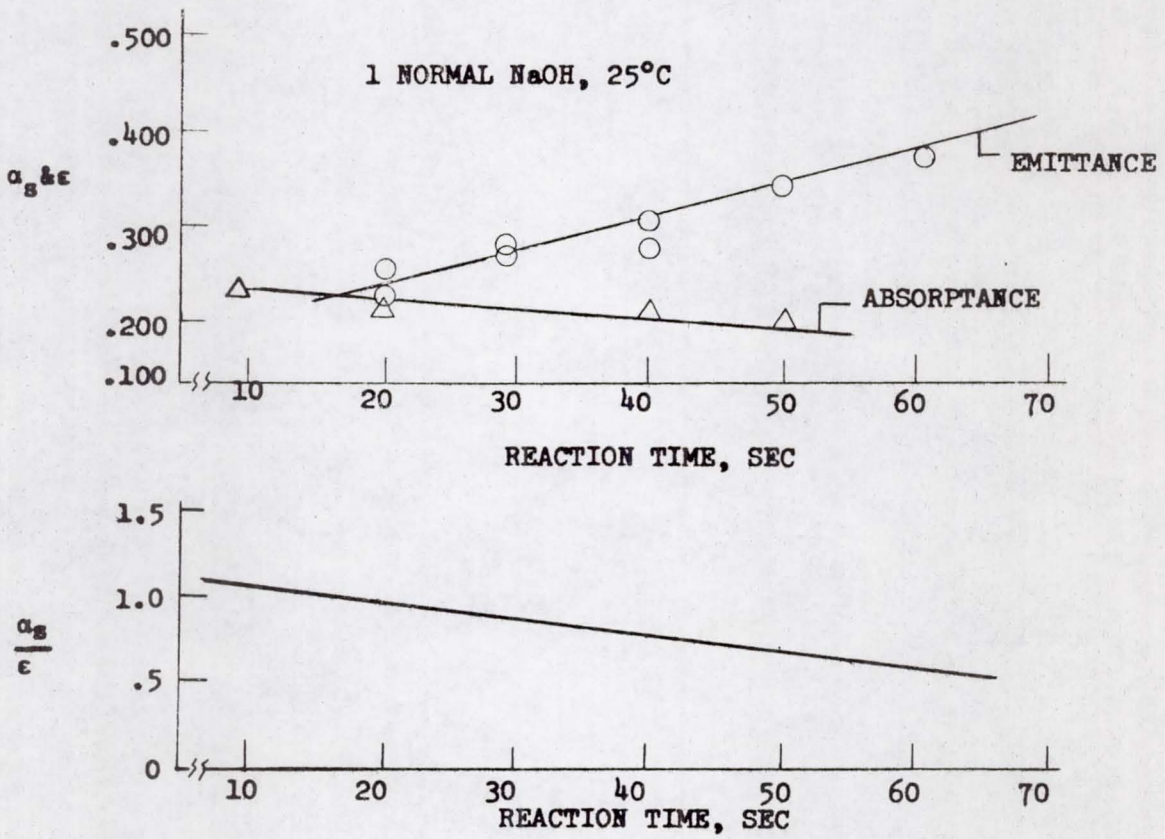

Figure 5. - Influence of Hydroxide Treatment on Solar Absorptance and Thermal Emittance of Alodine 401.

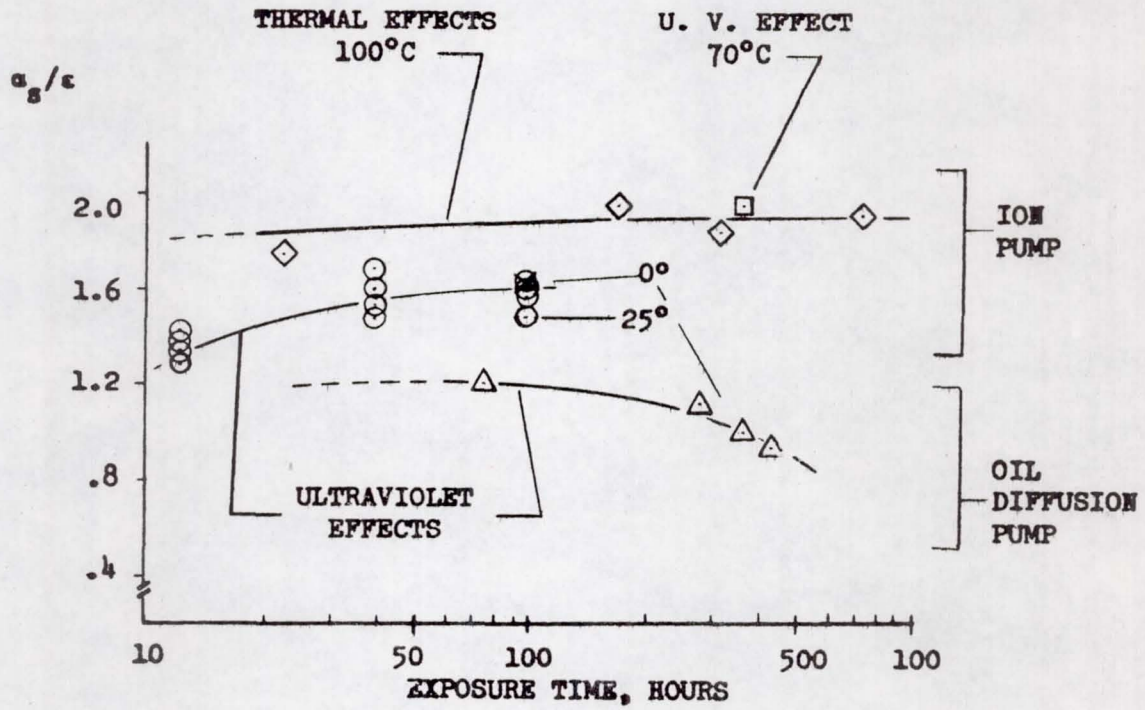

Figure 6. - Comparison of Thermal and Ultraviolet Effects on α_s/ε.

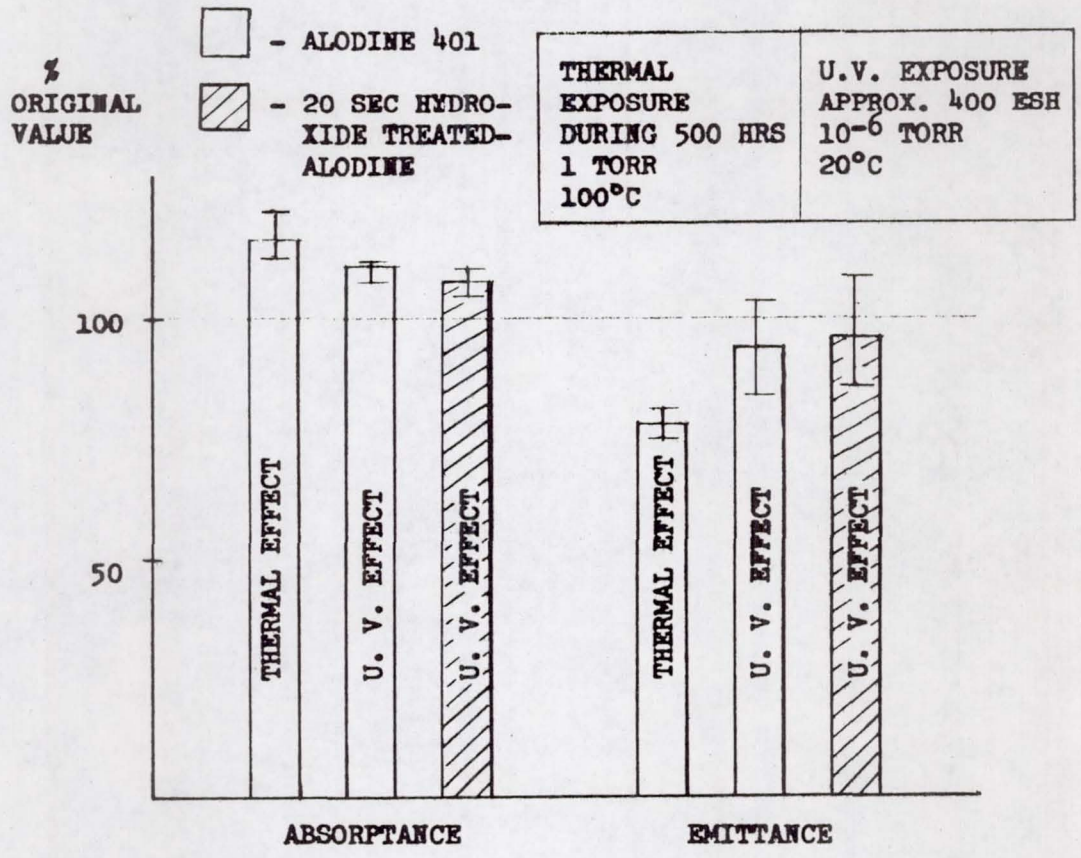

Figure 7. - Thermal and Ultraviolet Effects on Phosphate Coatings.

THE INFLUENCE OF TEMPERATURE ON THE STABILITY OF LOW α_s/ϵ COATINGS

By E. R. Streed*
Systems Engineering Division

Ames Research Center
Moffett Field, California

SUMMARY

A summary of available information is presented pertinent to the selection, application and performance of thermal control coatings for use on a perihelion flight to 0.3 A.U. Coatings with a solar absorptance of 0.30 or less and a total hemispherical emittance of 0.85 or greater at temperatures up to 500°F are desired. The results of an experimental program to measure the optical properties and to perform simultaneous exposure to simulated solar radiation, temperature and high vacuum are described.

INTRODUCTION

Reliable thermal design of spacecraft requires intimate knowledge of the initial optical properties of surface materials and their stability in the total space environment. The prelaunch environment is also considered as a source of contamination and resultant change in surface properties. The peculiar environment of temperature, vacuum, ultraviolet radiation and penetrating radiation has a degrading effect upon the optical and adhesive characteristics of thermal control coatings. Coatings with a low solar absorptance (α_s) to infrared emittance (ϵ) ratio have been developed with relatively predictable performance in the space environment for temperatures up to 150° F.

Emittance

Space environmental effects generally do not change emittance values of inorganic coatings except at high temperatures (above 1,000° F). However, the decrease in emittance with temperature for the white coatings can become important at temperatures above 500°F.

*This report is a summary of a paper to be published in the Proceedings of the Fourth Thermal Radiation Symposium held at San Francisco, California on March 4, 5 and 6, 1964. The work was performed while the author was employed at WDL, Philco Corporation, Palo Alto, California.

The emittance of white silicone type coatings generally decrease about 10 percent and white silicate pigmented coatings only 2 or 3 percent between 70° F and 500° F. The elevated temperature total normal emittance was calculated from spectral reflectance data.

Flight Experiment Data

Probably the best source of data on synergistic effects is obtained through actual space flight. A 1.25 microns (50 μin.) thick SiO coating has performed satisfactorily on a polished metal substrate on Vanguard II for about four years at altitudes varying from 350 to 2,065 nm. A more recent experiment on the S-16, Orbiting Solar Observatory, has indicated no serious deterioration of a 500 Å (Approximately 20 μin.) coating of SiO in fourteen months' exposure at an altitude of about 350 nm. Although deterioration of some coatings has occurred in the complete space environment, the extent of degradation to the optical properties has been conservatively predicted by the ultraviolet, vacuum and temperature simulation tests such as described herein.

EXPERIMENTAL STUDIES

A survey of the literature and of past experience with low α_s/ϵ coatings provided several coatings with simulated space exposure data at nominal room temperatures but no information at elevated temperatures. Therefore, an experimental program was initiated to determine the degradation of five promising coatings when exposed to the intensity equivalent of 10 suns in the 0.2 to 0.4 micron spectral region for 30 days. The samples were maintained at 500° F $\pm$ 25° F in a vacuum of 5×10^{-6} torr, or better. Additional studies of a ZnO system were performed as a function of temperature and exposure time. Measurements of room temperature α_s and ϵ were made before and after exposure.

Specimen Selection

The promising coating types were selected on the basis of resistance to high temperature, ultraviolet radiation, high-energy particles, and high vacuum. Organic vehicles were immediately excluded on the basis of temperature sensitivity. One silicone vehicle was selected because of its exceptional resistance to ultraviolet radiation. The other coating contained a silicone varnish binder which supposedly evaporated on heating. The three completely

inorganic systems were chosen to represent a cross-section of crystalline structure solids available as ultraviolet stable oxides with initially low α_s values. The coatings, source and comments on past performance are listed in Table 1. In addition to the ZnO coating, inorganic formulations of $CaSiO_3$, $ZrSiO_4$, $ZrSiO_4$-Al_2O_3 and silicone coatings were applied and exposed to ultraviolet radiation for short periods of time.

Specimen Preparation

All coatings were applied to 6061 T6 aluminum sheet. The substrates prepared at Western Development Laboratories (WDL) received a hot alkaline etch with a hot sulphuric acid-sodium dichromate cleaning solution and a 110° C oven drying. Inorganic ZnO-K_2SiO_3 coatings were prepared at WDL in a ball mill. Various ball-to-pigment charge ratios and mixing times were tried, with a 3:2 ratio for 5 hours providing the lowest α_s values.

The coatings were applied with an air brush in a fume hood. The inorganic coatings required from 6 to 10 coats to achieve an opaque coating with a total average thickness of 4 mils. The coatings were dried at 110° C for 2 hours and then fired in a muffle furnace for an additional hour at 500° F.

Detailed sample preparation for specimens supplied by other sources are proprietary or are described in the respective references.

Space Simulation Exposure Apparatus

The apparatus simultaneously permits exposure of materials to radiant energy in the 0.25 to 1.4 micron region, a vacuum of at least 1×10^{-6} torr and temperatures to 500° F. The complete apparatus is shown in Figure 5. The radiant energy is furnished by a high-pressure, mercury-arc lamp (PEK Labs, type C, which is equivalent to General Electric A-H6) mounted inside a water-cooled quartz finger. The specimens are mounted on individual holders in a radial fashion about the source. The units are mounted inside a stainless steel, water-cooled bell jar having walls coated with a black diffuse coating to reduce reflections. Vacuum is provided with a 4-inch oil diffusion pump trapped with a liquid nitrogen thimble trap and backed with a 5-cfm mechanical pump. An ionization guage is mounted in the chamber for pressure measurement.

Extensive measurements of the total and spectral radiation emitted by the A-H6 lamps and the B-H6 air-cooled lamps have been

reported. At sample distances of 5 inches, the average measured new lamp intensity was 11.8 ultraviolet suns. Variations of ± 15 percent were found for new lamps. Decreases in total ultraviolet radiation intensity in the 0.25 to 0.40 micron range of up to 75 percent were measured during the useful life of the lamps. Essentially, the same type apparatus was used for studies at Lockheed Missiles and Space Company (LMSC) and at WDL.

Exposure Results

The inexperience with low α_s coatings at elevated temperatures made it desirable to make some preliminary exposures of 50 hours. These tests served to provide additional screening information and to verify that the temperature of the specimen would stabilize at about 500° F with no supplemental heating. Specimens of Rokide "A" (Al_2O3) and pigmented silicone film material showed serious degradation and were eliminated from further study. Although the multiform, high-purity fused silica was significantly discolored after 50 hours, it was included in the final test to determine if a saturation point would be reached.

The results of a 700 hour exposure at an average ultraviolet intensity of 10.3 suns is shown in Table 2. The specimen temperature was measured with a chromel/alumel thermocouple attached to the specimen holder. A temperature gradient of 15° F was measured through the coating with fine wire thermocouples. Although the sample temperatures varied with lamp intensity and decreased to near room temperature during lamp changes, the temperature values indicated were maintained within ± 25° F for about 80% of the time. The average pressure during the complete exposure time was 4×10^{-7} torr.

The ZnO in methyl silicone showed the least degradation in α_s; however, the coating was checked and spalling was commencing at the end of the exposure. The SiO_2 pigmented silicone varnish coating turned dark brown as substantiated by the α_s value of 0.72. Of the three inorganic systems, the ZnO in K_2SiO_3 and the Li-Al-SiO_2 in K_2SiO_3 exposed α_s values were nearly identical at .33 and .32, respectively. However, the lower initial value of Li-Al-SiO_2 indicates a faster degradation rate occurred for this coating system. The $ZrSiO_4$ in K_2SiO_3 coating suffered the second greatest degradation as evidenced by the exposed α_s value of .42. Measurements of the total normal emittance indicated decreases of about 3 percent for four of the coatings and a 10 percent decrease for the badly degraded SiO_2-silicone varnish system.

The over-all performance of the ZnO in K_2SiO_3 coating system appeared to be superior to the other coatings but greater degradation in α_s had occurred than was previously reported for similar exposure times. Therefore, further investigation of the influence of temperature was conducted. Specimens prepared from the same coating batch, used for the 700 hour 10.3 sun exposure, were mounted in individual temperature controlled sample holders. Duplicate specimens were mounted on the back side of the holder to permit exposure to identical temperature and vacuum conditions but no ultraviolet. Different sets of specimens were exposed to 235 equivalent sun hours and 2,300 equivalent sun hours. The α_s values, determined from reflectance measurements, are shown in Figure 7 as a function of temperature and exposure time. The general trend of increasing α_s with temperature is clearly evident. Specimens exposed to temperature and vacuum only, for 2,300 equivalent sun hours, increased from .01 to .02 absorptance units irrespective of specimen temperatures between 60 and 350° F. However, under certain conditions, coatings can achieve temperatures as high as 700° F and still require the low α_s/ϵ ratio to minimize the heat load.

A comparison of these exposures with data reported by Armour Research Foundation (ARF) at about 70° F and the 495° F exposures (LMSC) can also be made in Figure 1. Although the performance of ARF was not matched for the 2,300 hour exposure, sufficiently good agreement for engineering purposes was achieved.

The spectral reflectance of the ZnO in K_2SiO_3 as a function of exposure time and temperature is shown in Figure 2. The initial degradation begins in the 0.4 to 0.6 micron region and as the temperature and exposure time increases the absorption increases in magnitude and wavelength. The surface becomes tan and for badly degraded materials will eventually turn a dark brown similar to a thermal scorching of a white material.

Measurement Techniques

The measurement apparatus used at LMSC included an integrating sphere reflectance attachment for a Model 14 Cary Ratio Recording Spectrophotometer and a heated cavity reflectometer used in conjunction with a Model 13 Perkin-Elmer Ratio Recording Spectrophotometer. The ARF apparatus consists of a General Electric Recording Spectrophotometer with associated integrating sphere and a total emittance device employing a blackbody reference. The WDL apparatus consists of a Model 350 Perkin-Elmer Spectrophotometer equipped with MgO-coated integrating spheres, tungsten and hydrogen lamp sources and photomultiplier and PbS detectors. Measurements are performed by directional illumination of the specimen and a reflectance standard. The ratio of the reflected radiation is recorded as a function of wavelength.

Pertinent data points are picked off of the recording and are computer-integrated with the extraterrestrial solar spectrum to give total solar absorptance.

CONCLUSIONS

The influence of elevated temperature in increasing the degradation of low α_s/ϵ coatings has illustrated the need for simultaneous simulation of as many environmental factors as possible. Of the three coatings exhibiting the lowest values of α_s/ϵ after exposure, the zinc oxide pigmented potassium silicate is considered the best coating system. The greatest uncertainty in degradation prediction results from the lack of theoretical models or experimental data on the effects of high-energy particle radiation. However, the ultraviolet radiation effects are considered to cause the greatest potential damage.

	Coating System	Source	Comments
1.	180 g ZnO 90 ml K_2SiO_3 180 ml H_2O cured for 2 hours at 500° F	SP500 New Jersey Zinc Co. PS7 Sylvania Electric Products, Inc.	Prepared at WDL and based upon formulations of ARF (ref. 3)
2.	ZnO in methyl silicone 40% PVC (ARF TC-46-20)	SP500 New Jersey Zinc Co. silicone-ARF prepared	Samples obtained from ARF. Easy to handle and good ultraviolet resistance (ref. 3)
3.	SiO_2 in silicone varnish	Corning #7941 multi-form fused silica Experimental silicone varnish, Dow-Corning	Obtained from Corning Glass Works. No prior ultraviolet or vacuum exposure data available. Coating described as potentially having good stability (ref. 13)
4.	Li-Al-SiO_2 in K_2SiO_3	Trade names of Lithafrax and Kasil 88 - obtained by LMSC	Coating prepared and applied by LMSC. Coating has consistently the lowest initial α_s and good adhesion
5.	$ZrSiO_4$ in K_2SiO_3	Trade names of zircon and Kasil 88 - obtained by LMSC	Coating prepared and applied by LMSC. Coating has shown good neutron radiation resistance

Table 1 - Description, source and pertinent comments on the coatings exposed to ultraviolet radiation at elevated temperature.

FIGURE 1 - THE SOLAR ABSORPTANCE OF ZINC OXIDE PIGMENTED POTASSIUM SILICATE AS A FUNCTION OF TEMPERATURE AND EXPOSURE TIME

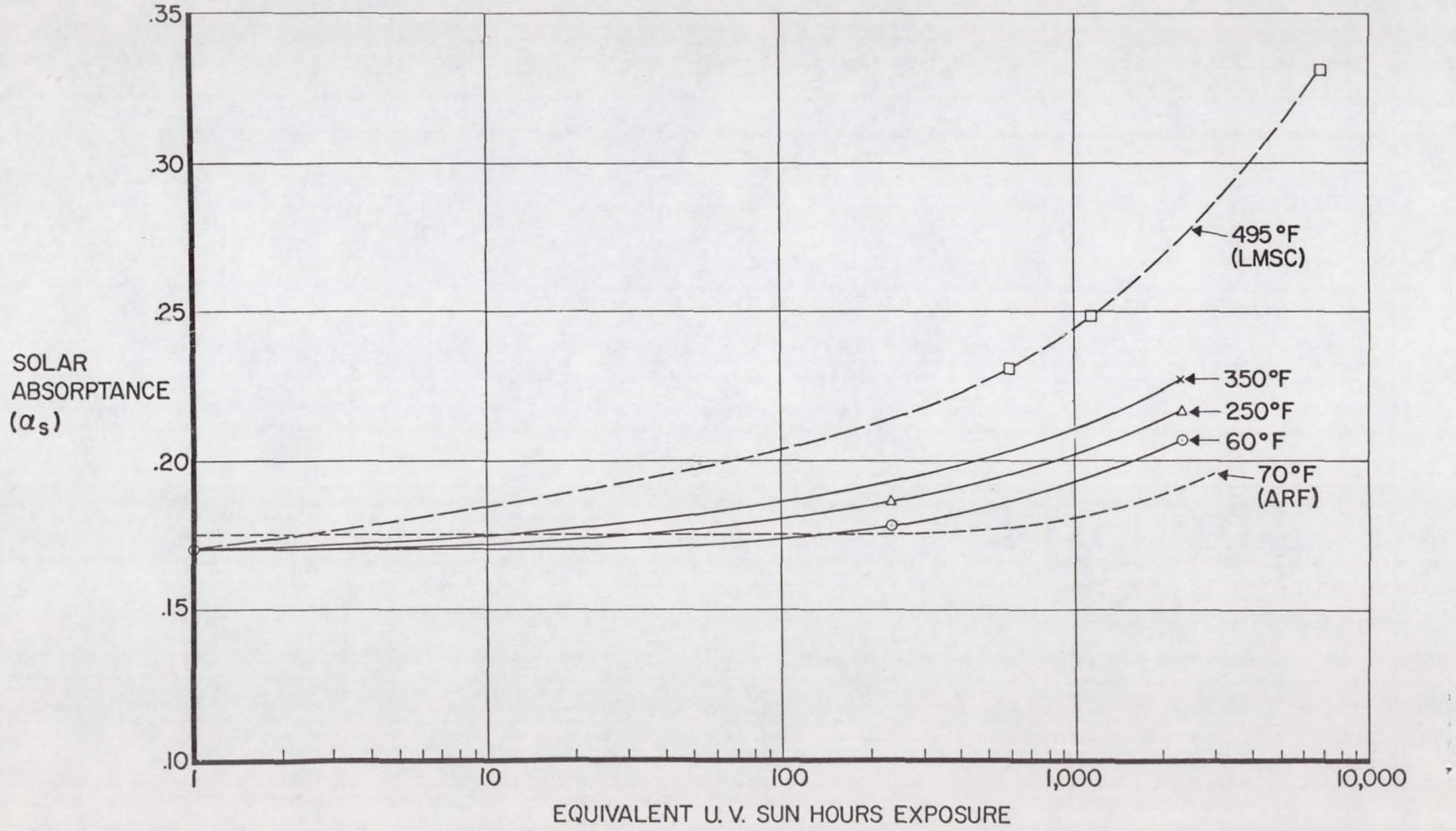

NATIONAL AERONAUTICS AND SPACE ADMINISTRATION
AMES RESEARCH CENTER, MOFFETT FIELD, CALIFORNIA

Material	Property	Hours at Approximately 10 Sun Ultraviolet Intensity		Avg. Temp. (°F)
		0	700	
ZnO in K_2SiO_3	α_s	0.17	0.33	495
	ϵ	.95	.93	
Zircon in K_2SiO_3	α_s	.13	.42	490
	ϵ	.95	.93	
Lithafrax in K_2SiO_3	α_s	.12	.32	495
	ϵ	.93	.89	
SiO_2 in silicone	α_s	.14	.72	510
	ϵ	.92	.83	
ZnO in methyl silicone (ARF TC-46-20)	α_s	.18	.27	505
	ϵ	.91	.88	

Table 2 - Solar absorptance and emittance of several coatings before and after ultraviolet exposure. Exposure and optical property measurements were performed by LMSC.

NATIONAL AERONAUTICS AND SPACE ADMINISTRATION
AMES RESEARCH CENTER, MOFFETT FIELD, CALIFORNIA

FIGURE 2 -SPECTRAL REFLECTANCE OF THE ZINC OXIDE-POTASSIUM SILICATE SYSTEMS AFTER EXPOSURE

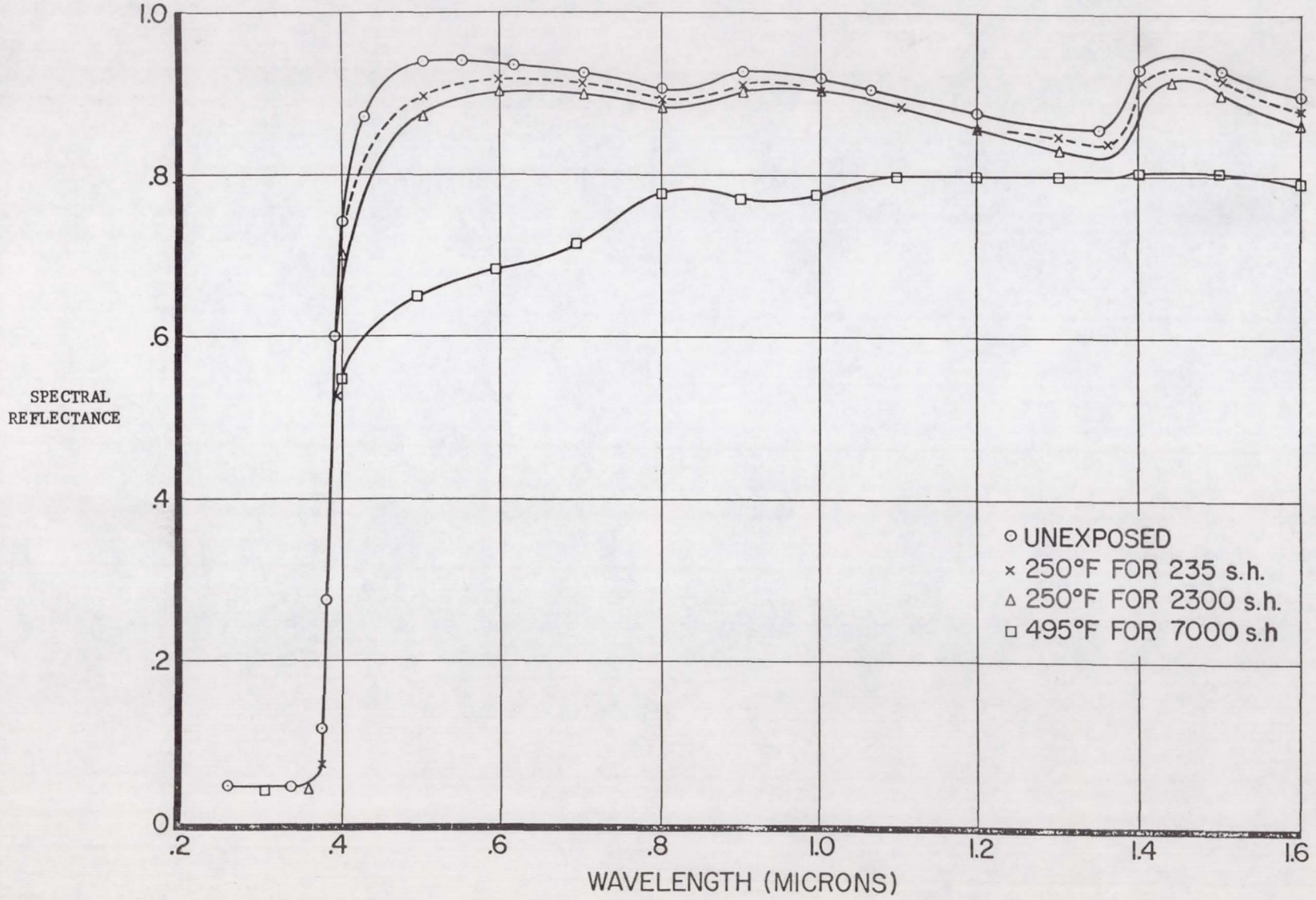

NATIONAL AERONAUTICS AND SPACE ADMINISTRATION
AMES RESEARCH CENTER, MOFFETT FIELD, CALIFORNIA

THE EFFECTS OF ULTRAVIOLET AND GAMMA RAYS ON THERMAL CONTROL COATINGS

Robert A. Jewell, George F. Pezdirtz, and Harold D. Burks
AMPD - Langley Research Center

INTRODUCTION

In conjunction with our initial ultraviolet-vacuum degradation studies of five white paints, a brief series of gamma-vacuum experiments was conducted on the same coatings to determine the extent of change in solar absorptance produced by each type of radiation. Four of these materials stem from our participation in the OSO Round Robin on UV Stability (Ref. 1) and the fifth is Zerlaut's (IIT) zinc oxide-silicone S-13 formulation. The ultraviolet and gamma exposures were not run concurrently, so their results are shown separately. All emittance values remained fairly constant, with the α_s change being of primary importance.

Ultraviolet-Vacuum Environmental System

The ultraviolet-vacuum environmental system used in these tests is shown schematically in figure 1. The stainless-steel front plate is integral with the glycol-water cooled specimen holder which can accomodate up to eight specimens for simultaneous irradiation. The temperatures of the test specimens ranged from 0°C to 15°C and were monitored periodically throughout the test with copper-constantan thermocouples mounted in the metal substrates of each coating. The vacuum chamber was mounted to a 1,200 liter/sec Ultek ion pump. A silicone rubber o-ring (Dow Corning Silastic #916 compound) was used to seal quartz window; the remaining seals were Viton (fabricated of

Parker Seal Co. V-495-7 compound). Chamber pressure was monitored throughout the test and maintained in the range of 1×10^{-6} to 6×10^{-7} torr. After irradiation, sample temperatures were allowed to return to ambient temperature and chamber pressure was then brought to atmospheric pressure using argon in an attempt to limit any oxidation effects prior to taking reflection measurements.

High-pressure mercury arc lamps (G.E. BH-6) were used as the source of ultraviolet radiation in these studies. The lamp manufacturer and others (reference 2) have reported on the fact that the spectrum of the BH-6 lamp is not completely similar to the solar spectrum. Figure 2 shows the ratio of the lamp intensity (at a distance of 25 cm) to solar intensity (at 1 A.U.) for different wavelengths in the 0.22- to 0.40-micron region. The cumulative average lamp intensity for this wavelength range is approximately 3 times the solar intensity. This figure is based on the geometry of this system and the manufacturer's data for BH-6 lamps (reference 3). The relative intensities of the BH-6 lamps were monitored during each run with a Westinghouse SM-200 ultraviolet photometer. The individual lamps were selected and changed as necessary so as to maintain relative intensities within 15 percent of a nominal intensity of 3 times solar intensity.

---

*The substrates for the titanium dioxide-epoxy coating were too thin to permit thermocouple mounting. Sample temperatures were assumed to be comparable to the average of the monitored samples.

Effect of Ultraviolet Radiation

The effect of UV on the solar absorptance of the five paints are noted in figure 2. The inorganic materials, in general, were more resistant to change. The change in α_s due to 300 equivalent sun hours (ESH) of ultraviolet exposure are end points taken from figure 3, which shows the rate of change of α_s over this period of about 2 weeks. Along the y-axis is plotted the ratio of solar absorptance after irradiation to solar absorptance prior to irradiation (α_{s_o}). Values of $\Delta\alpha_s$ were not used because somewhat erratic changes in α_s we found were, in a great part, linked to a wide spread on the initial α_s values.

In figure 4 initial solar absorptances are shown as related to coating thicknesses. For the thin coatings, such as the TiO_2-silicone, a small change in thickness can result in a large increase in α_s. Note that three specimens, one Sb_2O_3-potassium silicate and two TiO_2-epoxy samples, showed initial abnormalities in the sense that they did not fit their respective curves in figure . When irradiated these three samples degraded more severely than their companion specimens, which may have been due to the effects of surface impurities or contaminants. All reflectance measurements were taken in air within one hour after removal from vacuum. A Cary 14 spectrophotometer was used.

A brief series of exploratory experiments were conducted to determine the extent of bleaching after the samples had been removed from the ultraviolet-vacuum environment. Figure 5 shows portions of the spectral reflectance curves for zinc-oxide-silicone samples after some bleaching attempts. Samples previously degraded under UV-vacuum conditions almost returned to their original unirradiated values when exposed to as little as 6 ESH of ultraviolet in air. Other samples when exposed to ultraviolet radiation in dry nitrogen,

showed little change from the value obtained after UV degradation in vacuum. These curves tend to point up the healing effect of the earth's atmosphere. In Zerlaut's work (ref. 4) zinc oxide gave evidence of being reduced by ultraviolet-vacuum environment.

Gamma-Vacuum Environmental System

For the gamma radiation exposure a Cobalt-60 source was used. The flux of gamma photons in space is quite low, but this type of penetrating radiation does provide a convenient means of simulating the effects of optical surface damage from electrons and protons. Dose rate in the Gammacell-220 was approximately 1.5 Megarads per hour. Ambient temperature of the gamma cell was 47° Centegrade. A short series of 50°C thermal-vacuum tests showed no effect on the α_s values for the 5 materials listed in Table I. Figure 6 is a schematic of the Pyrex specimen container used for gamma exposures. During sealing off at the bottom of the tube and pinching off in the center under vacuum, noted by the dotted lines, care was taken to keep each specimen below 50°C to limit thermal effects.

Comparative Effects of Gamma and Ultraviolet Radiation

Five white coatings exposed to both types of radiation are listed in Table I in decreasing order of stability to these environments.

Comparative Effect of Gamma & Ultraviolet Radiation
on Solar Absorptance of Thermal Control Coatings

Table I

COATING		SOLAR ABSORPTANCE, α_s			
			Increase, $\Delta\alpha_s$		
Pigment		Original Value	Gamma MRAD		Ultraviolet, ESH
			77*	385*	300*
Zinc Oxide	Potassium Silicate	0.14	0.04	0.04	0.01
Zinc Oxide	Silicone plus Catalyst	0.17	0.04	0.04	0.04
Titanium Dioxide	Silicone Resin	0.25	0.12	0.18	0.03
Antimony Oxide	Potassium Silicate	0.26	0.10	0.26	0.08
Titanium Dioxide	Epoxy Resin	0.20	0.22	0.27	0.19

Note: (1) 77 Megarads approximate surface exposure in space of 12 weeks

(2) 385 Megarads approximate surface exposure in space of 60 weeks

(3) 300 ESH (equivalent sun hours, ultraviolet) approximates ultraviolet exposure in space of 2 weeks.

In comparing the ultraviolet effects at 2 weeks equivalent sun exposure of ultraviolet with an exposure of 12 weeks equivalent inner Van Allen belt absorbed dose of high-energy ionizing (gamma) radiation, the titanium dioxide-epoxy and the antimony oxide-potassium silicate coatings were found to be more susceptible to damage from ultraviolet radiation than from gamma radiation. To a lesser extent the remaining three, more stable coatings in Table III underwent a change in α_s due to ultraviolet radiation

equal to or greater than that obtained by extrapolation of change in α_s due to gamma radiation. The similarity of damage to the optical properties of a coating surface caused by gamma protons of 1.17 Mev and 1.33 Mev and by ultraviolet protons of approximately 5 ev can be noted from Figure 7, which is a plot of the effects of both types of radiation on the spectral absorptance versus wavelength for the titanium dioxide-epoxy coating.

For a short series of longer exposures to ultraviolet and gamma, the zinc oxide-silicone (S-13) paint was chosen. Batches of this material could be formulated in-house, allowing better pre-selection of specimens on the basis of initial α_s values. Also the S-13 had been studied at Langley as part of the Explorer XIX project. Portions of this satellite's surface were 2" diameter polka-dots of S-13 paint.

Figure 8 shows the extent of damage after longer exposures (10^3 hrs.) to ultraviolet and gamma radiation. For the S-13 samples exposed to gamma for an equivalent of 12 months time, α_s increased less than 0.2% from the original value of 0.22. Two months equivalent ultraviolet exposure caused approximately 5% increase in the original solar absorptance. The curves for the TiO_2-epoxy coating in this figure provide a closing remark on the comparative stability of these two materials. Less than five years ago, this particular TiO_2-epoxy coating was considered a most stable white paint. Based primarily upon results from terrestrial testing, this paint had been flown as part of the Explorer IX thermal control surfaces.

CONCLUSIONS

Gamma radiation, used to simulate the effects of electrons and protons, generally changes α_s less than ultraviolet radiation when a comparison is made on the basis of equivalent time exposures in space. More attention

should be given to additional studies of the effects of high-energy ionizing radiation on thermal-control coatings. These effects should be taken into account in the analysis of the results from thermal-control experiments aboard spacecraft, as well as in spacecraft design for long-term missions. A better understanding of the specific molecular changes which result from UV and high energy radiation damage to thermal control coating is needed to properly analyze engineering and environmental tests.

REFERENCES

1. Neel, C. B.; Arvesen, J. C.; and Shaw, C. C.: Preliminary Results From a Round-Robin Study of Ultraviolet Degradation of Spacecraft Thermal-Control Coatings.

2. Carroll, W. F.: Development of Stable Temperature Control Surfaces for Spacecraft. Progress Report No. 1. Jet Propulsion Laboratory, Technical Report No. 32-340.

3. General Electric Outdoor Lighting Dept: Application Data and Accessory Equipment-Capillary Type AH-6 Arc Lamp Bulletin. GET 1248 H, Hendersonville, N. C.

4. Zerlaut, G. A.; and Harada, Y.: Stable White Coatings, Interim Report Nos. ARF 3207-5 (April 1962) and ARF 3207-14 (Oct. 1962), Illinois Institute of Technology for Jet Propulsion Laboratory.

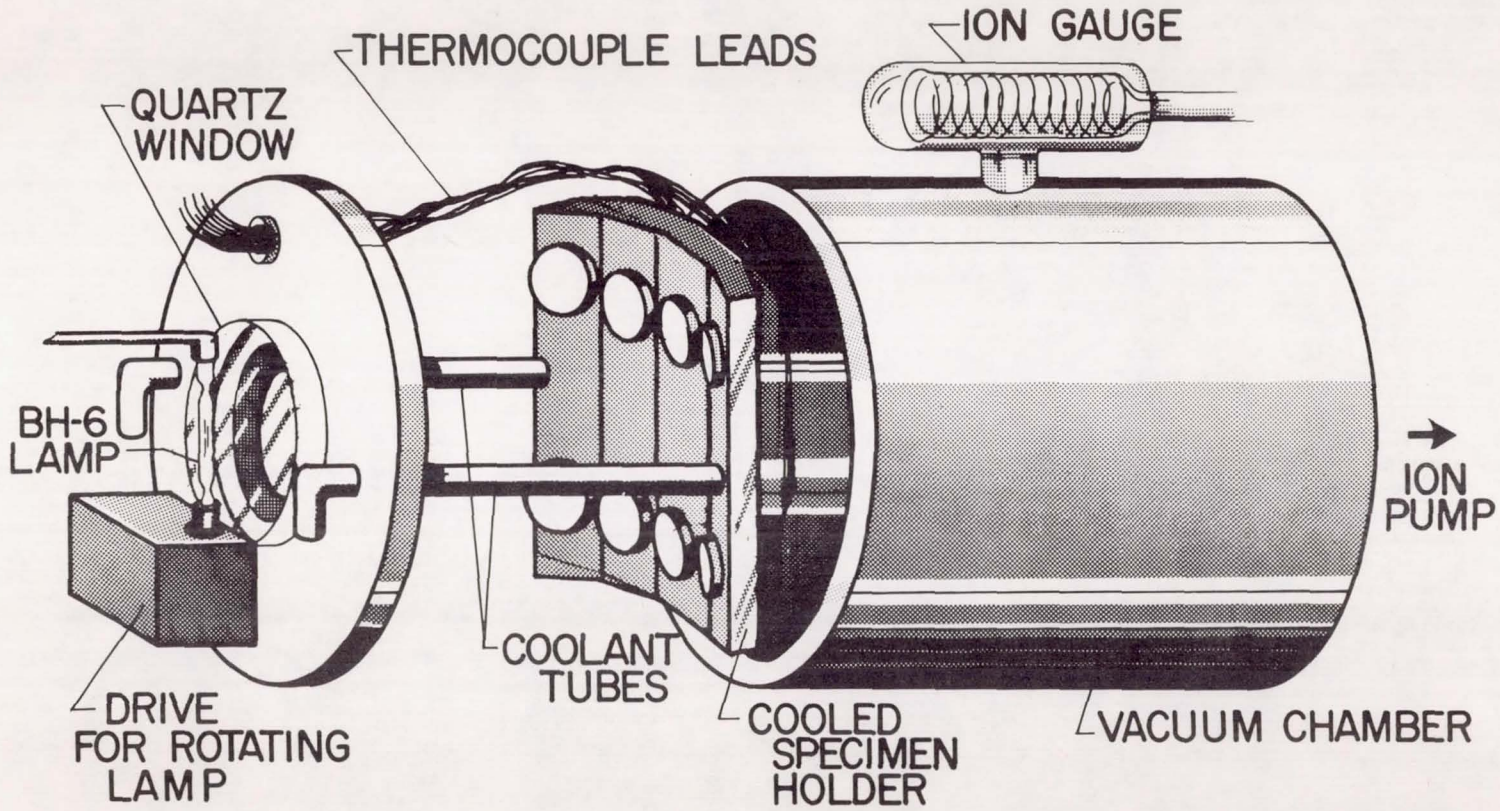

NASA

Figure 1.- Ultraviolet-vacuum chamber.

EFFECT OF UV AND GAMMA RADIATION ON SOLAR ABSORPTANCE

MATERIAL	INITIAL α_s	$\Delta\alpha_s$ AFTER 300 HR UV	$\Delta\alpha_s$ AFTER 77 MEGARAD DOSE*
1. ZnO - POT. SIL.	0.14	0.01	.00
2. ZnO - SILICONE	.22	.02	.00
3. TiO_2 - SILICONE	.25	.03	.08
4. Sb_2O_3 - POT. SIL.	.26	.08	.05
5. TiO_2 - EPOXY	.20	.19	.18

*77 MEGARAD DOSE APPROXIMATES 12 WEEKS ABSORBED SURFACE DOSE IN INNER VAN ALLEN BELT.

Figure 2

COMPARATIVE EFFECT OF UV & VACUUM EXPOSURE

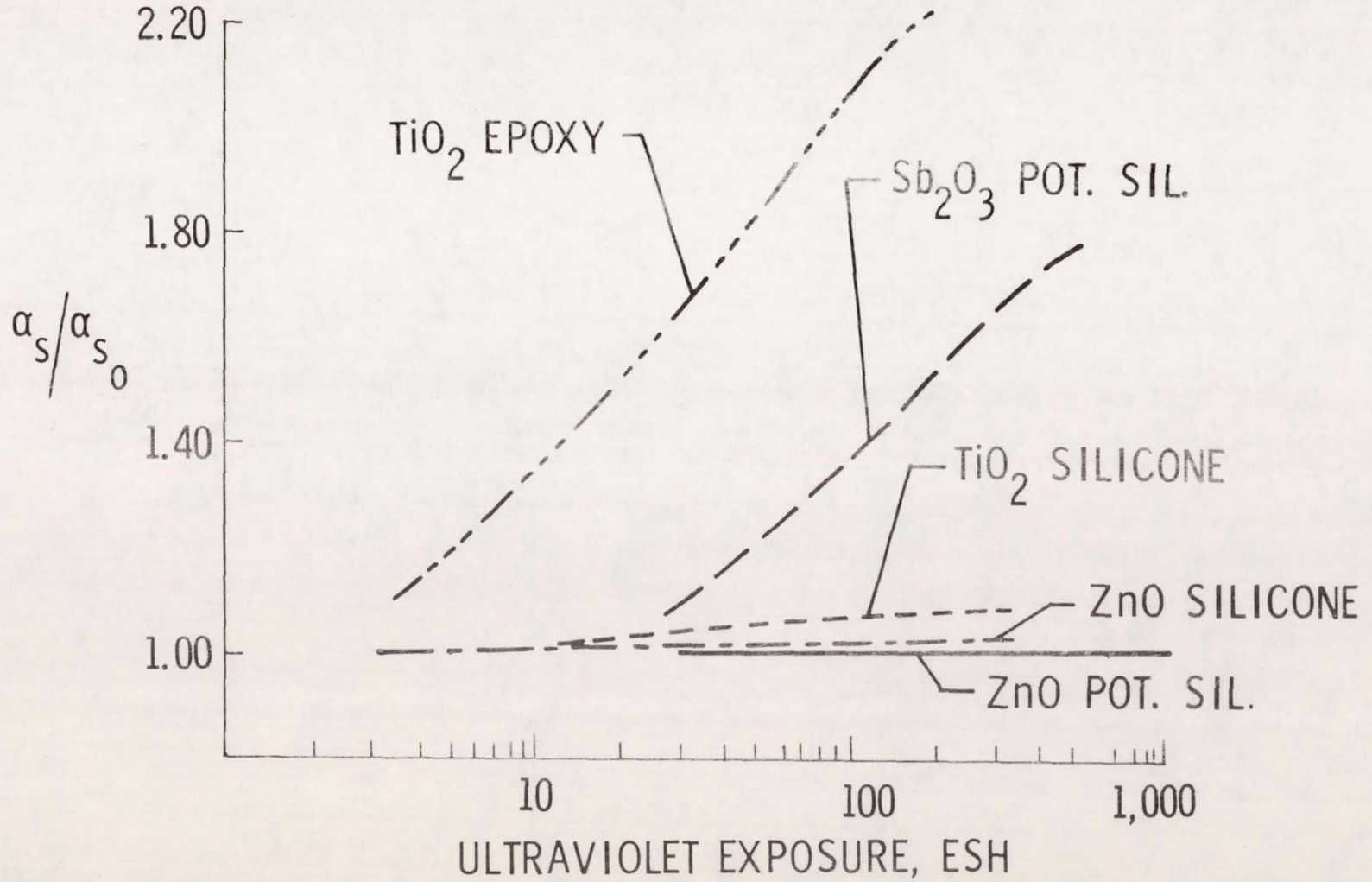

EFFECT OF COATING THICKNESS ON SOLAR ABSORPTANCE OF UNIRRADIATED SPECIMENS

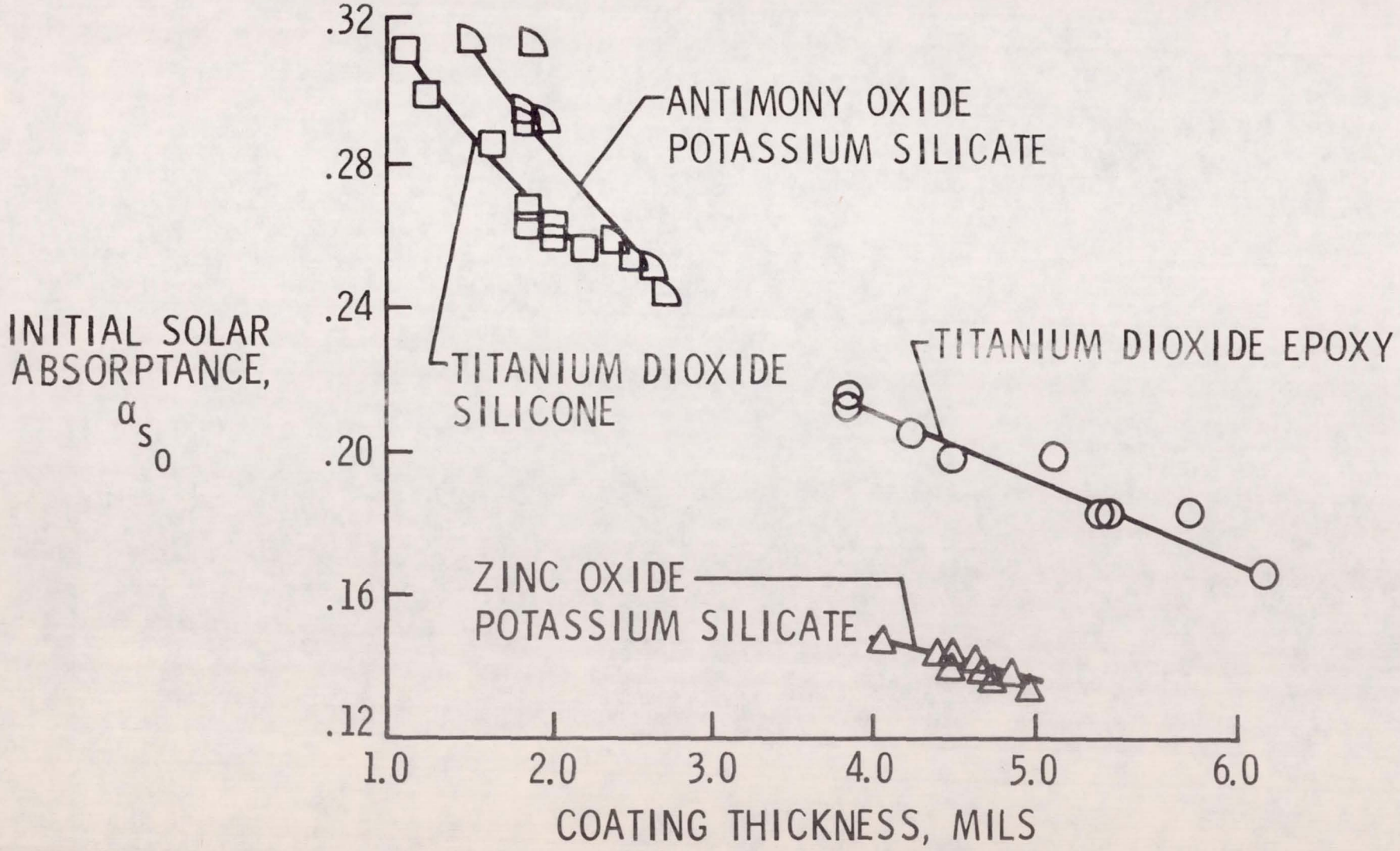

Figure 4

BLEACHING EFFECT ON S-13 COATINGS PREVIOUSLY DEGRADED BY ULTRAVIOLET-VACUUM EXPOSURE

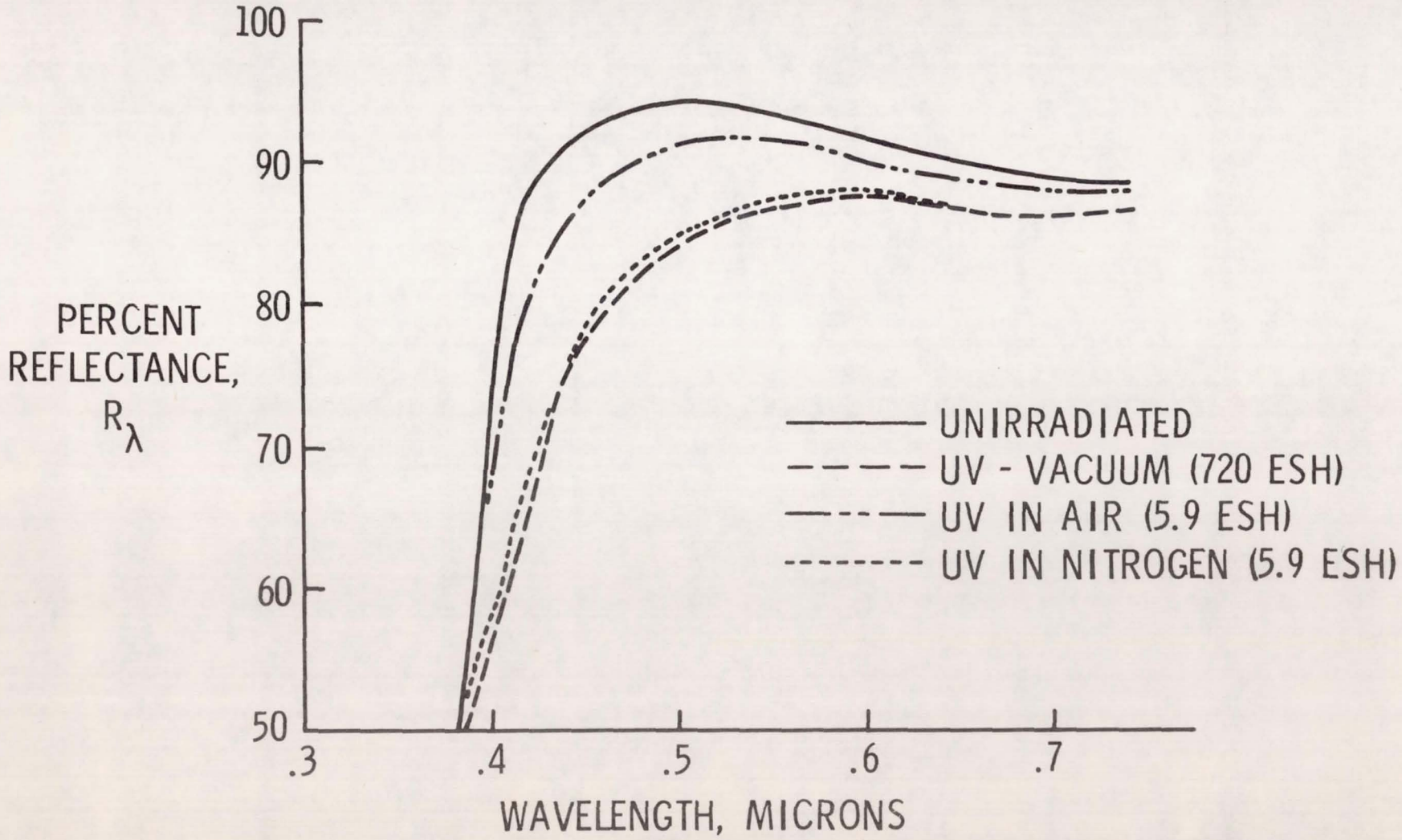

Figure 5

PYREX SPECIMEN CONTAINER FOR GAMMA IRRADIATION UNDER VACUUM

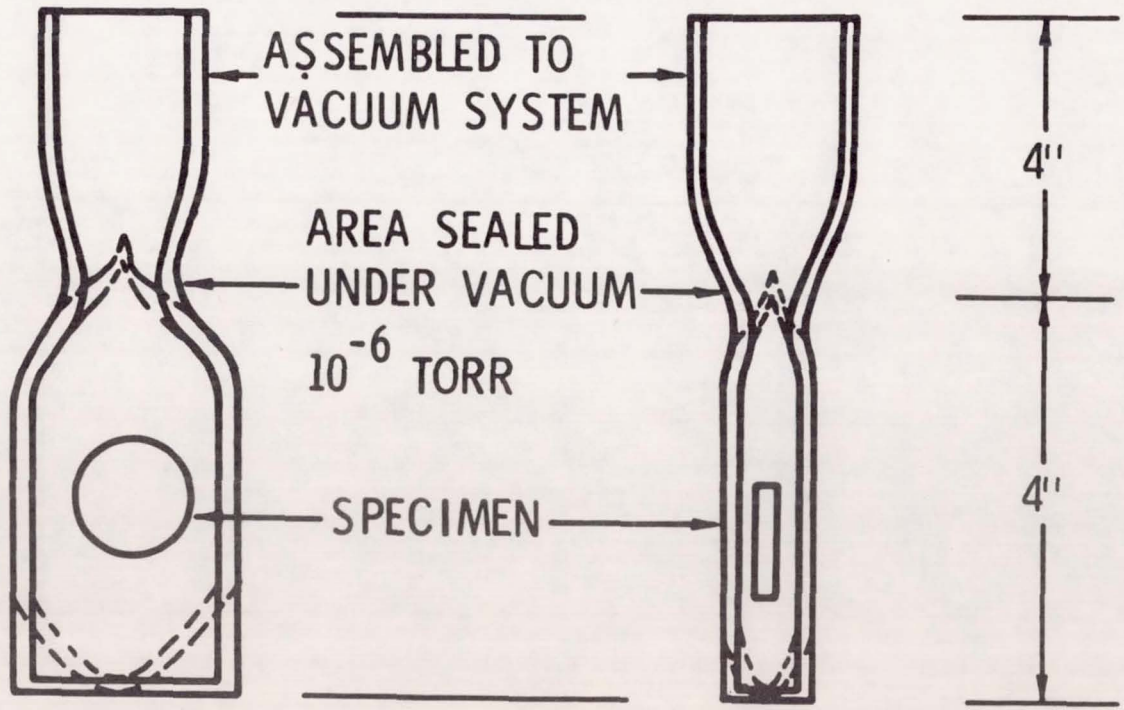

Figure 6

EFFECT OF RADIATION ON THERMAL CONTROL COATINGS

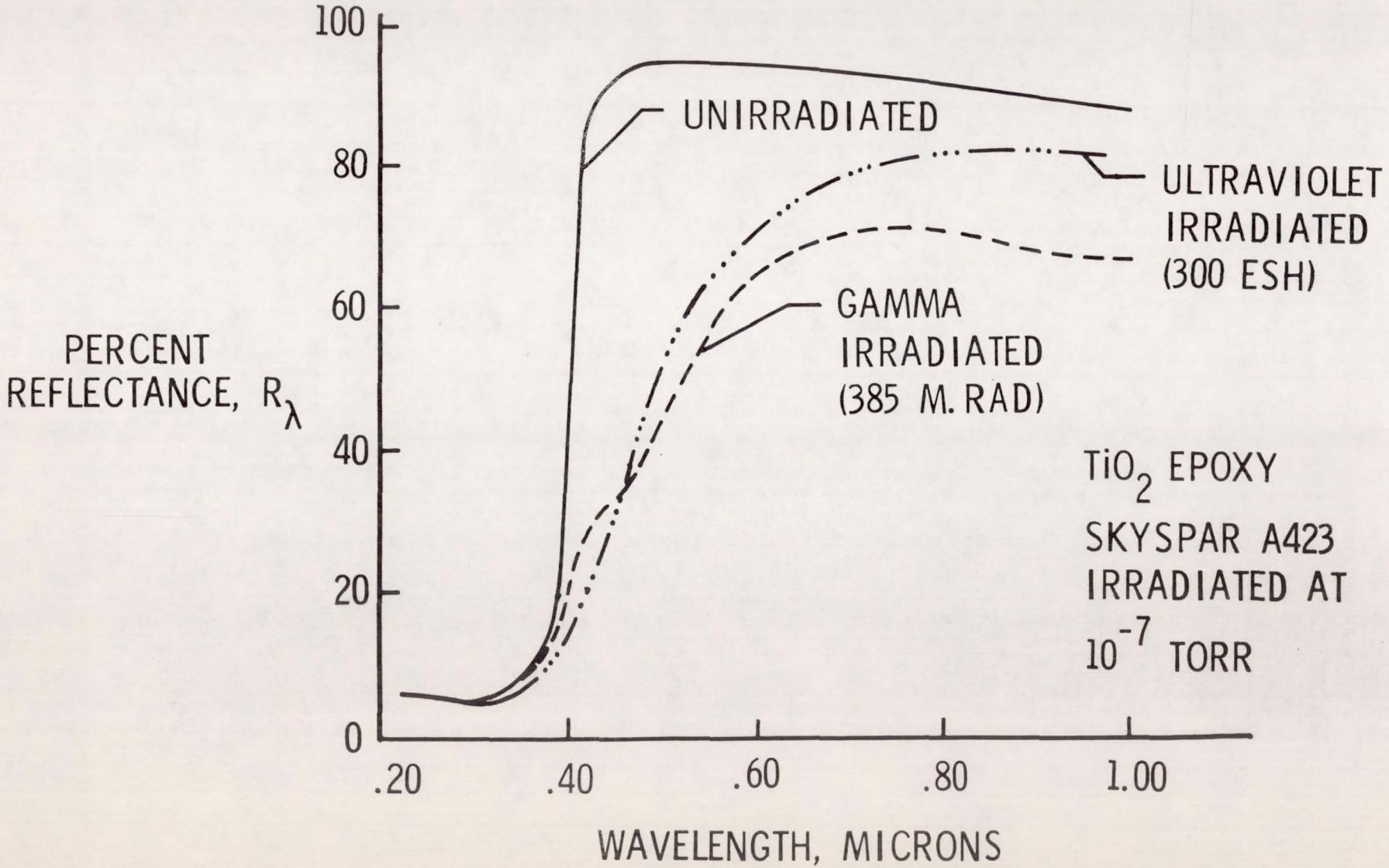

Figure 7

COMPARATIVE EFFECTS OF ULTRAVIOLET AND GAMMA RADIATION ON S-13 COATING

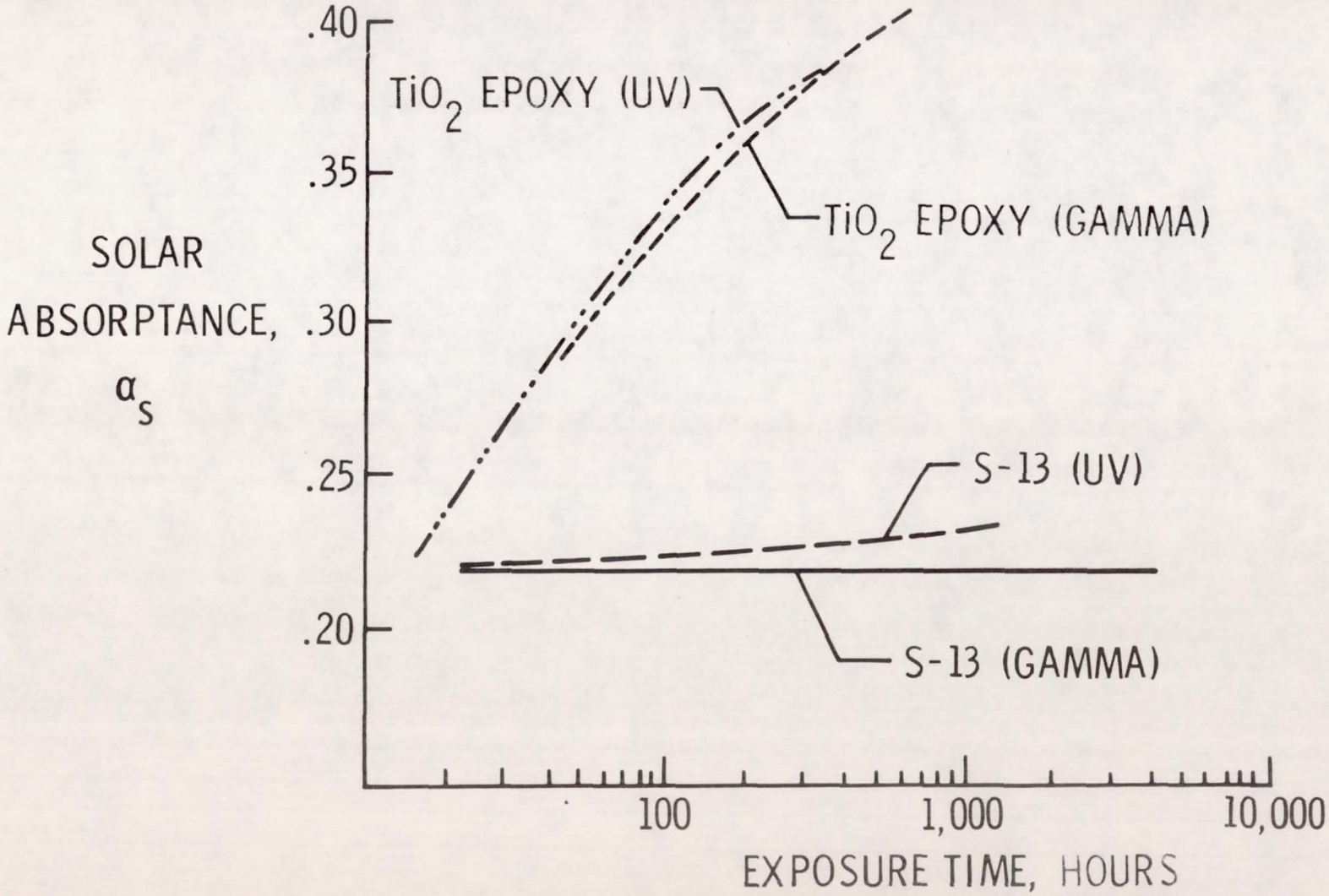

Figure 8

PRELIMINARY RESULTS FROM A ROUND-ROBIN STUDY OF ULTRAVIOLET DEGRADATION OF SPACECRAFT THERMAL-CONTROL COATINGS

By J. C. Arvesen, C. B. Neel, and C. C. Shaw

INTRODUCTION

In the past, comparisons of laboratory measurements of the rate of degradation of spacecraft thermal-control coatings with the limited data available from flight experiments have shown generally poor agreement (see ref. 1). The disagreement is believed to be the result of inadequacy in the laboratory simulation of the space environment and, in particular, solar-ultraviolet radiation. The need to resolve the problem of adequate simulation was recognized, and as a first step, a voluntary round-robin testing program was organized in November of 1962 to compare and evaluate existing capabilities for ultraviolet-degradation studies. Sixteen organizations are participating in this program and results from twelve had been received at the time of preparation of this paper. The purpose of this paper is to present these results and to discuss in a preliminary fashion their significance.

In the program, each organization was offered identical samples of four different low α_s/ϵ white thermal-control coatings with various degrees of color stability under ultraviolet irradiation. Each organization tested the samples at exposures up to the equivalent of 1,000 sun hours. Results of the rate of coating degradation were compared for the various test facilities. The results for two of the coatings were also compared with flight data.

The authors wish to thank the following organizations for their participation in the round-robin program:

Air Force Materials Laboratory - Wright-Patterson AFB

American Cyanamid Company

The Boeing Company

Fairchild Stratos Corporation

General Dynamics/Astronautics

General Electric Company

Hughes Aircraft Company

I. I. T. Research Institute

Jet Propulsion Laboratory

Lockheed Missiles and Space Company

Martin Marietta Corporation

McDonnell Aircraft Corporation

NASA-Langley Research Center

NASA-Marshall Space Flight Center

T. R. W.-Space Technology Laboratories

U. S. Naval Research Laboratory

The efforts of those persons directly involved in the tests are appreciated. In particular, Mr. William F. Carroll of the Jet Propulsion Laboratory should be acknowledged for his work in establishing the basic ground rules and enlisting participation for the program. Mr. G. Richard Blair of Hughes Aircraft Co., Mr. Louis A. McKellar of Lockheed Missiles and Space Co., and Mr. Jerry T. Bevans of T. R. W.-Space Technology Laboratories also aided in setting up the test requirements.

DESCRIPTION OF COATINGS

Four low α_s/ϵ white thermal-control coatings were chosen for study. The individual coatings were selected on the basis of pigment and binder composition, expected degradation processes, and previous flight and laboratory experience. All samples of a particular coating were prepared at the same time from the same batch and were distributed to the participants in light-tight containers in an effort to minimize variations in the initial undegraded state. The samples were prepared by three of the participants.

The first coating was composed of a rutile titanium-dioxide pigment in an epoxy binder (Andrew Brown Company; Skyspar A423; color SA 9185 untinted) and was chosen for study as an example of a coating with a stable pigment and an unstable binder that will degrade noticeably in a short period of time. These coating samples were prepared by Lockheed Missiles and Space Company.

The next coating was formulated and the samples were prepared by the Illinois Institute of Technology Research Institute. The coatings consisted of a rutile titanium-dioxide pigment in a more stable silicone binder (IIT designation: TC-50-19). Samples of both these coatings were flown aboard the first Orbiting Solar Observatory (OSO-I)(see ref. 1). Measurements of the rates of degradation of these coatings were made over a period of 16 months in orbit and, although the coatings were prepared from different material lots than the round-robin samples, the flight data serve as a preliminary basis for evaluating the laboratory simulation tests.

The next coating was composed of an antimony-trioxide pigment in a potassium-silicate binder, and was developed especially for the round-robin

by Hughes Aircraft Company. In contrast to the TiO_2 in epoxy, this coating has an unstable pigment in a stable binder. Consequently, its degradation mechanism was expected to be different from that of the epoxy-binder paints.

The last of the four coatings, also prepared by IIT Research Institute, was a stable zinc oxide pigment in potassium silicate (IIT designation: 441-2). The first, third, and fourth coatings are scheduled to be flown aboard the OSO-B2 Satellite near the end of the year. Thus, it is expected that information on their degradation in the actual space environment will also be available for correlation with the laboratory results.

TEST PROCEDURE AND EQUIPMENT

Procedure

The test procedure followed by the various organizations was basically the same, although specific simulation equipment and techniques differed considerably. The samples were first measured by each organization to obtain initial values of solar absorptance. They were then placed in a vacuum chamber and exposed to a source of ultraviolet radiation for varying periods of time up to the equivalent of 1000 hours in space. After irradiation, the samples were removed from the vacuum chamber and their solar absorptances were again measured.

Test Equipment and Conditions

The equipment used by the various participants and the conditions of test are listed in table I. It should be noted that the order of listing in this table is not the same as given previously for the participating organizations, which were listed alphabetically.

Both oil-diffusion and ion pumps were used about equally in the vacuum systems, along with various types of roughing pumps. These systems produced vacuums in the pressure range from 10^{-5} to 10^{-7} torr. One organization, however, used only a mechanical pump with liquid-nitrogen trapping, which resulted in a relatively high vacuum-chamber pressure of 10 microns of mercury (10^{-2} torr).

In some cases, sample temperature was controlled by cooling and in other cases no cooling was provided. This resulted in variations in sample temperature among the participants from 15° C to over 200° C.

All participants used a mercury lamp to simulate solar ultraviolet radiation. The General Electric BH-6 and AH-6 lamps were most commonly used. In an attempt to investigate the source-dependency characteristics of the coatings, one organization also conducted tests with a 2 kw xenon lamp. The comparison of the relative intensities of the BH-6 mercury lamp, the xenon lamp, and the sun in the ultraviolet region from 2000 to 4000 Å is shown in figure 1. The spectral distribution of the AH-6 lamp was not shown because it is similar to that of the BH-6 lamp. The spectrum of the BH-6 lamp consists largely of emission bands that may be many times the level of the solar continuum. The xenon lamp, on the other hand, offers a much better duplication of the solar spectrum below 4000 Å than does the mercury lamp. Because of this closer match, the xenon lamp was expected to provide more realistic coating degradation rates than the mercury lamps.

It was recognized by the round-robin participants that the mercury spectrum gives a poor duplication of solar ultraviolet radiation. However, the assumption was made that if the total output of the lamp below 4000 Å

was set equal to the solar output below 4000 Å, the same degradation would occur. This assumption was the basis for calculating the equivalent solar illumination level on the samples. Thus, for example, if the total radiation below 4000 Å incident on a sample is ten times the solar radiation in the same range, the illumination level is defined as ten "ultraviolet solar constants" or ten "suns."

The choice of the 4000 Å wavelength as the cutoff point was purely arbitrary. It was felt that 4000 Å represented the upper limit of damaging radiation for nearly all materials of interest. It is known, however, that many materials require higher photon energies, or shorter wavelengths, to cause degradation. Some materials may be particularly sensitive to certain portions of the spectrum. It can be seen from the plot of the BH-6 and solar spectra that below 3200 Å there is considerably more radiation from the mercury lamp than from the sun. Thus, a sample that is particularly susceptible to damage below 3200 Å would, in effect, have much more than the equivalent of one ultraviolet solar constant incident on its surface when the mercury lamp is used.

Another factor which may influence the degradation rate of some coatings is the possible bleaching effect resulting from exposure to longer wavelength radiation, as mentioned in references 2 and 3. This effect, which tends to offset the increase in solar absorptance resulting from ultraviolet radiation, apparently is caused by radiation in the visible region. The radiant intensity of the mercury-vapor lamps is well below solar intensity in the visible, and failure of the lamps to adequately simulate the bleaching effect could cause difficulties in simulation of the over-all degradation rate.

RESULTS AND DISCUSSION

Initial Values of Solar Absorptance

Values of solar absorptance of the test coatings, measured before exposure to ultraviolet radiation, are listed in table II. The various instruments used by the participants for the initial and subsequent measurements are also given. The order of listing in this table is the same as in table I. In all cases the solar absorptance of a coating was determined by a reflectance technique. The last two measurements shown were over limited spectral regions and thus are not indicative of solar absorptance. Agreement among the remaining measurements is generally within the normal experimental tolerances associated with reflectance measurements. It is apparent that, for coatings with low values of solar absorptance, the percentage deviations normally resulting from reflectance measurements are quite large. More effort is clearly needed to develop equipment and to refine the techniques that are necessary to accurately determine the solar absorptance of low α_s/ϵ materials.

Coating Degradation

The results of the coating degradation studies are presented in figures 2, 3, 4, and 5. These figures show the measured change in solar absorptance as a function of "Equivalent Sun Hours." In the studies, it was found that only the solar absorptance of the coatings was altered by exposure to ultraviolet radiation and that the emittance remained relatively unchanged.

In illustrating the results of the tests, an attempt was made to separate out the effects of what were felt to be two of the most important variables, that is, sample temperature and the radiant intensity of the ultraviolet source. In the figures, temperature is indicated by the color of the curves and the data have been divided into five different temperature intervals. The curves are dashed, the length of the dashes denoting the radiant intensity used in the tests. The short dashes indicate an intensity of one ultraviolet solar constant, whereas the longer dashes indicate multiples of the solar constant. In some cases the exposures were made at varying intensities, as indicated by the changing length of the dashes in the curve. With one exception, mercury-vapor lamps were used in all exposures. The single test with the xenon lamp is noted on the figures. The test at a pressure level of 10 microns also is shown.

Titanium dioxide - epoxy coating.- The results of the studies made on the titanium dioxide in epoxy coating are shown in figure 2. Also shown in the figure are the OSO I flight data which were obtained with the same type of coating.

The wide spread of the results in figure 2 illustrates the present level of uncertainty in solar ultraviolet-simulation tests. In view of the poor match of the mercury vapor lamps with the solar ultraviolet-intensity spectrum, it is perhaps not surprising to find general disagreement among the laboratory results and the flight data. It is rather surprising, however, that the tests with the xenon lamp, which matched the solar spectrum far better than the mercury lamps, did not agree with

the flight data as well as two of the tests with the mercury lamps. Even for these cases, the time required for the coating to be degraded by a given amount was about one-third the time required in flight. The remaining simulation tests all produced more rapid changes in solar absorptance than measured in flight, with the exposure time required for a given change in solar absorptance in some cases differing from the flight data by several orders of magnitude.

Although the exact causes of the wide variations in the test results are not immediately evident, the data reveal a number of interesting points. For example, after a large increase in absorptance shortly after the beginning of sample exposure, the rate of increase in absorptance in most cases became roughly equal to the rate obtained in flight. The magnitude of the initial increase in solar absorptance apparently was influenced by both sample temperature and lamp intensity, although it is difficult to separate out the relative importance of these two factors. Nevertheless, there appears to be a definite correlation between sample temperature and initial degradation rate, with the higher degradation rates being associated with the higher temperatures. There also appears to be a nonlinear correlation of degradation rate with lamp intensity, with the higher intensities producing a relatively higher rate of change of solar absorptance. In tests where the intensity was constant, the change in absorptance with time was almost linear when plotted on a logarithmic time scale. On the other hand, where the intensity was increased to obtain long equivalent exposures in a reasonable length of time the corresponding rate of change of solar absorptance increased by an even greater degree.

The curve for the tests made with a chamber pressure of 10 microns is high compared with the other curves for the same temperature level. The higher degradation rate may have been caused by the presence of oxygen or other impurities not present under the higher vacuum conditions of the other tests. Finally, one other possible cause of the higher degradation rates obtained in the laboratory should not be overlooked. This is the effect of bleaching due to visible or longer wavelength radiation which mercury-vapor lamps do not adequately simulate.

Titanium dioxide - silicone coating.- The results of ultraviolet irradiation on the more stable titanium dioxide in silicone coating are shown in figure 3. Note that the scale for the change in solar absorptance has been expanded to twice that for the epoxy coating to help emphasize differences in the results. This material apparently is not nearly as sensitive to intensity and temperature variations as the epoxy coating. In fact, with the exception of the high-temperature test, there appears to be no correlation of degradation rate with temperature or intensity. The large change in solar absorptance at the high temperature may have been the result of either thermal degradation or an increase in the ultraviolet sensitivity resulting from the excessive temperature. Tests with the xenon lamp at a low sample temperature and with a mercury lamp at a higher temperature show good agreement with the flight data. In constrast to the tests with the epoxy coating, the laboratory results gave both higher and lower degradation rates than were obtained in flight with the same type coating. The lack of any apparent trend in the data from the standpoint of temperature or intensity effects suggests that the spread in measurements are the result of differences in other experimental factors.

Antimony trioxide - potassium-silicate coating.- Results of tests of the antimony trioxide in potassium-silicate coating are shown in figure 4. There is an extreme diversity in the degradation rate, even greater than for the TiO_2-epoxy coating. For example, the measured values of the change in solar absorptance after 100 equivalent sun hours ranged from less than 0.1 to over 0.6. Incidentally, since the initial solar absorptance was 0.3, an increase in absorptance of about 0.7 would correspond to the sample becoming a perfect black absorber. The increase in solar absorptance appears to be extremely temperature and intensity sensitive. As with the epoxy coating, the degradation appeared to increase with increase in sample temperature. However, there is no evidence of a constant increase in absorptance after an initial change. Flight data for this coating are not yet available. However, samples of this material will fly on OSO-B2, and it is expected that flight data will be obtained for comparison with these results.

Zinc oxide - potassium-silicate coating.- Figure 5 shows the data for the zinc-oxide pigment in a potassium-silicate binder. Excluding the two cases of the excessively high sample temperature and the high chamber pressure, the tests show the coating to be very stable and fairly independent of intensity and temperature. It is interesting that the tests with the xenon lamp produced a higher degradation rate than the remainder of the tests performed with mercury-vapor lamps. Unfortunately, no flight data are yet available for comparison with these results, and it is not known whether the xenon or the mercury lamps give the better duplication of the solar degradation of this coating. The difference between the results with the xenon lamp and with the mercury lamps could be the result of a dependence of degradation upon wavelength for this coating.

As with the previous coatings, the highest rate of degradation at 200° C may have been due to increased ultraviolet sensitivity or thermal degradation, or possibly a combination of both factors. The test performed at a pressure level of 10 microns also resulted in a high degradation rate, and these data may reflect the influence of a high oxygen level.

CONCLUDING REMARKS

In reviewing the significance of the limited results obtained through the round-robin tests, a few facts are apparent regarding laboratory simulation of degradation of thermal-control coatings. It is important, for example, in testing some coatings to control sample temperature at a level reasonably near the expected operating temperature. The exposures should be made in an environment in which the pressure does not exceed about 10^{-5} torr. The validity of accelerated testing with lamp intensities many times the solar level is questionable for some coatings, and further investigation is required into the ramifications of this testing technique. The question of the importance of the spectral intensity distribution of the ultraviolet lamps has not yet been resolved, although it is hoped that the OSO-B2 flight tests may help in this regard. Without further evidence, it would appear at this time that the solar ultraviolet intensity spectrum should be matched as closely as possible, and that for some coatings it may even be necessary to simulate the visible and near-infrared regions of solar energy. The extent to which these various distribution requirements must be met is undoubtedly a function of the chemical degradation processes associated with each individual coating, and before this problem can be completely resolved, more must be learned about the mechanism of the degradation process.

REFERENCES

1. Neel, Carr B.: Research on the Stability of Thermal Control Coatings for Spacecraft. Proc. Fifth International Symposium on Space Technology and Science, Tokyo, Japan, 1963.

2. Zerlaut, G. A., and Harada, Y.: Stable White Coatings, ITT Research Institute Rep. no. IITRI-C207-25, 1963.

3. Olson, R. L., McKellar, L. A., and Stewart, J. V.: The Effects of Ultraviolet Radiation on Low α_s/ϵ Surfaces. Presented at the Symposium on Thermal Radiation of Solids, San Francisco, Calif., March 1964.

TABLE I.- TEST EQUIPMENT AND CONDITIONS

No.	Intensity "U.V. suns"	Temperature, °C	Lamp type	Vacuum system type	Pressure level, torr
1	3 to 14.4	27	B-H6	Sorption and ion	Below 10^{-6}
	1 to 7		xenon		
2	1	32	B-H6	Mechanical and diffusion to 10^{-4} sputter ion	10^{-7} to 10^{-8}
	5	100			
	10	157			
3	10	Not measured	B-H6	Mechanical and diffusion	5×10^{-5} to 7×10^{-6}
4	1 to 11	25	A-H6	Mechanical and ion	3×10^{-6} to 2×10^{-7}
5	2.7	5 to 65	B-H6	Mechanical and ion	10^{-6}
6	5 to 16	35	A-H6	Sorption, mechanical, and ion	10^{-7}
7	5	50	A-H6	Mechanical and LN_2 trap	10^{-2} (10 microns)
8	20	150	B-H6	Mechanical and diffusion	10^{-6}
9	15.5	Above 200	A-H6	Mechanical and diffusion	10^{-5}
10	7.1	86	B-H6	Mechanical and diffusion	10^{-5}
11	1	24	Hanovia 54A-10	Mechanical and diffusion	5×10^{-6}
12	1.5	15	UA-3	Mechanical and ion	10^{-5} to 10^{-6}

TABLE II.- INITIAL SOLAR ABSORPTANCE MEASUREMENTS

Instrument	Initial Solar Absorptance - α_{so}			
	TiO_2-Epoxy	TiO_2-Silicone	Sb_2O_3-Potassium Silicate	ZnO-Potassium Silicate
1. Gier - Dunkle Integrating Sphere	0.21	0.30	0.28	0.14
2. Gier - Dunkle Integrating Sphere	.22		.27	
3. Gier - Dunkle Solar Reflectometer	.22	.27	.29	.16
4. Cary 14 - Integrating Sphere	.22	.31	.30	.16
5. Cary 14 - Integrating Sphere	.21	.27	.28	.14
6. G.E. and P.E. - Integrating Sphere	.23	.30	.26	.16
7. Beckman DK-2A - Integrating Sphere	.16		.25	.10
8. Beckman DK-2A - Integrating Sphere	.26	.33	.27	.18
9. Beckman DK-2A - Integrating Sphere	.21	.28	.26	.16
10. Bausch and Lomb 505 - Integrating Sphere	.19	.26	.25	.13
*11. Bausch and Lomb 20 - Integrating Sphere	.08	.11	.14	.02
**12. Beckman IR-4 - Hohlraum	.14	.50	.34	.17

*4000 Å to 7000 Å only
**At 1.0 micron

FIGURE TITLES

Figure 1.- Comparison of ultraviolet spectral distribution of sun and lamps.

Figure 2.- Degradation of titanium dioxide - epoxy coating.

Figure 3.- Degradation of titanium dioxide - silicone coating.

Figure 4.- Degradation of antimony trioxide - potassium silicate coating.

Figure 5.- Degradation of zinc oxide - potassium silicate coating.

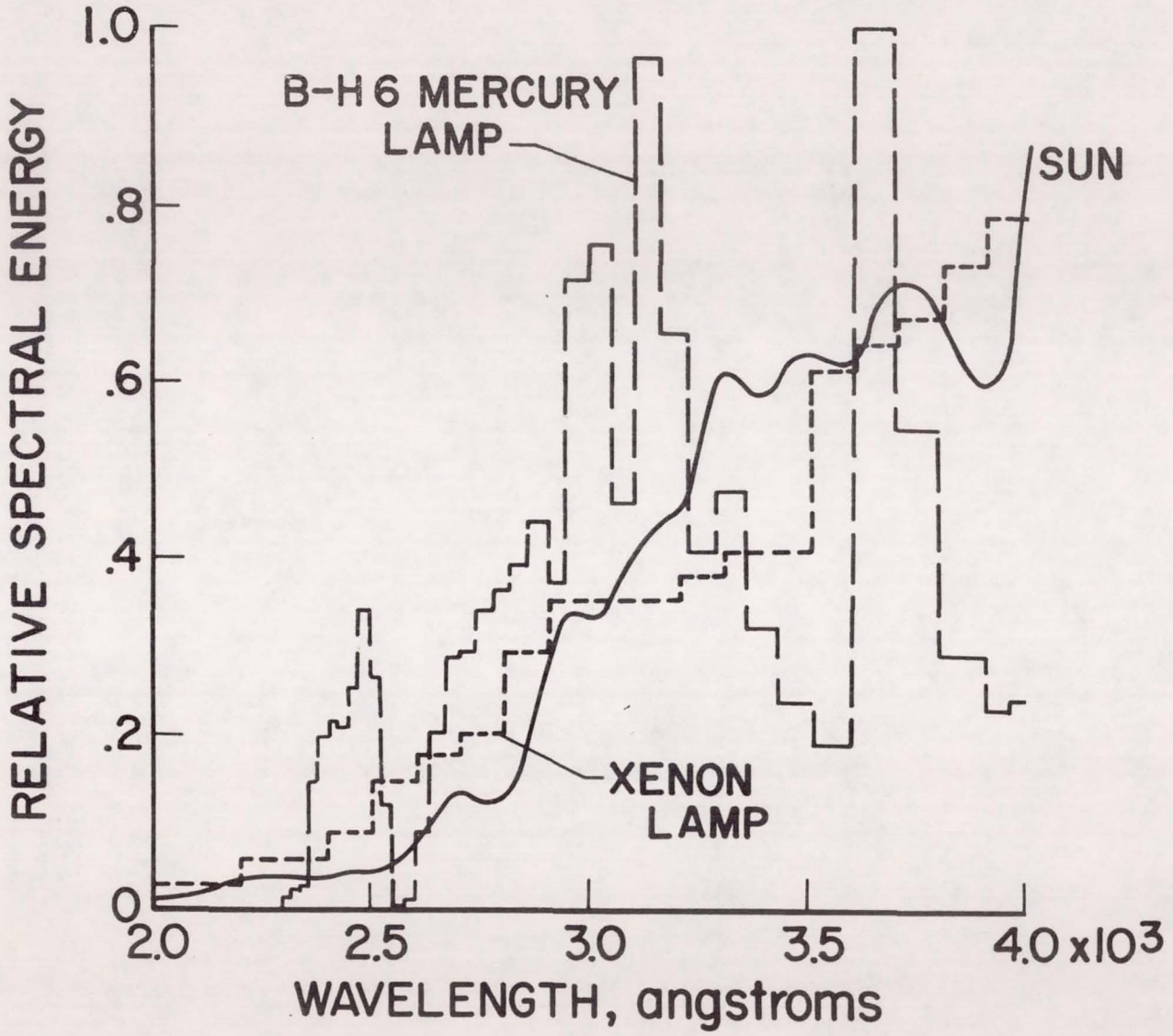

Figure 1.- Comparison of ultraviolet spectral distribution of sun and lamps.

NATIONAL AERONAUTICS AND SPACE ADMINISTRATION
AMES RESEARCH CENTER, MOFFETT FIELD, CALIFORNIA

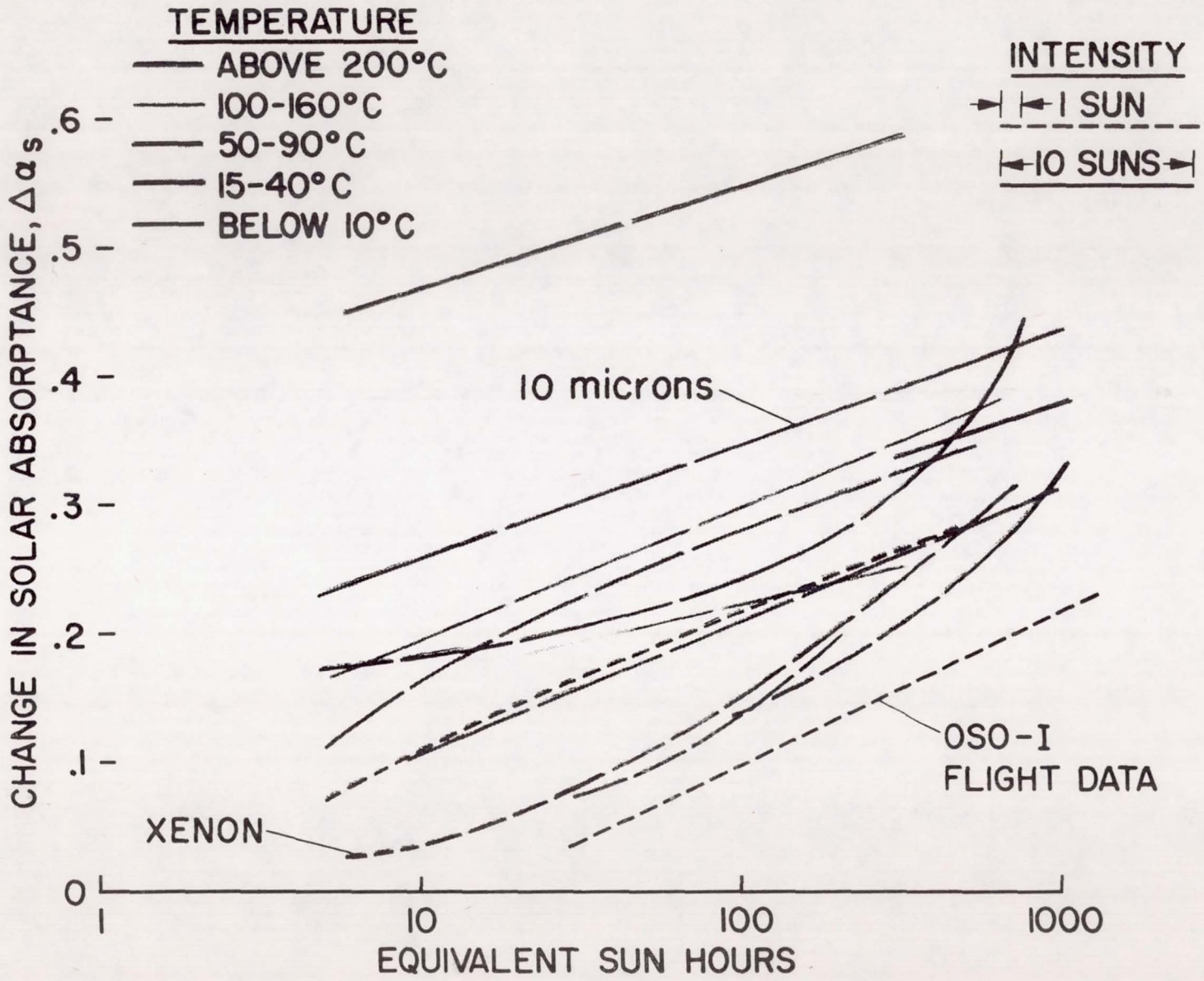

Figure 2.- Degradation of titanium dioxide - epoxy coating.

NATIONAL AERONAUTICS AND SPACE ADMINISTRATION
AMES RESEARCH CENTER, MOFFETT FIELD, CALIFORNIA

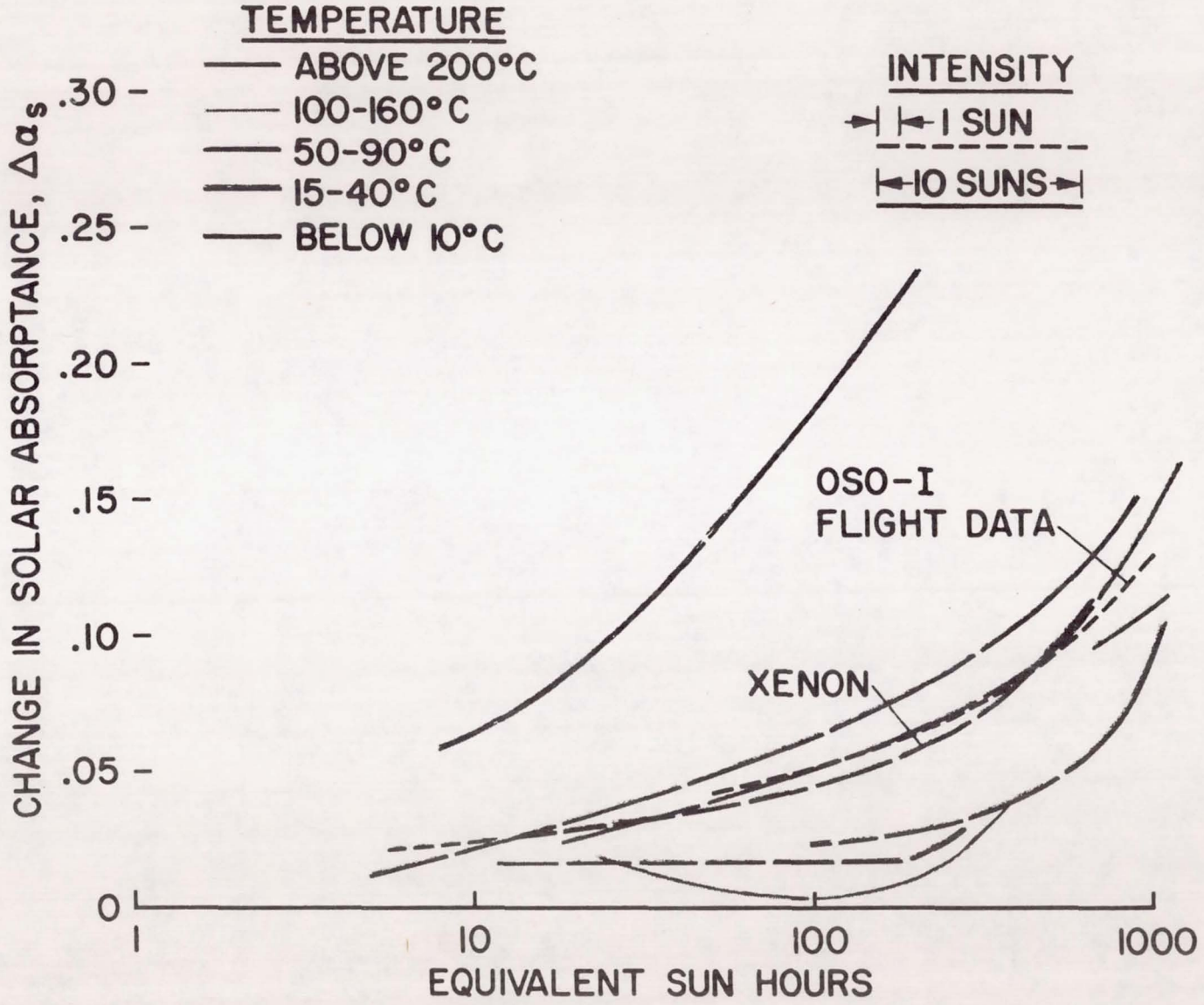

Figure 3.- Degradation of titanium dioxide - silicone coating.

NATIONAL AERONAUTICS AND SPACE ADMINISTRATION
AMES RESEARCH CENTER, MOFFETT FIELD, CALIFORNIA

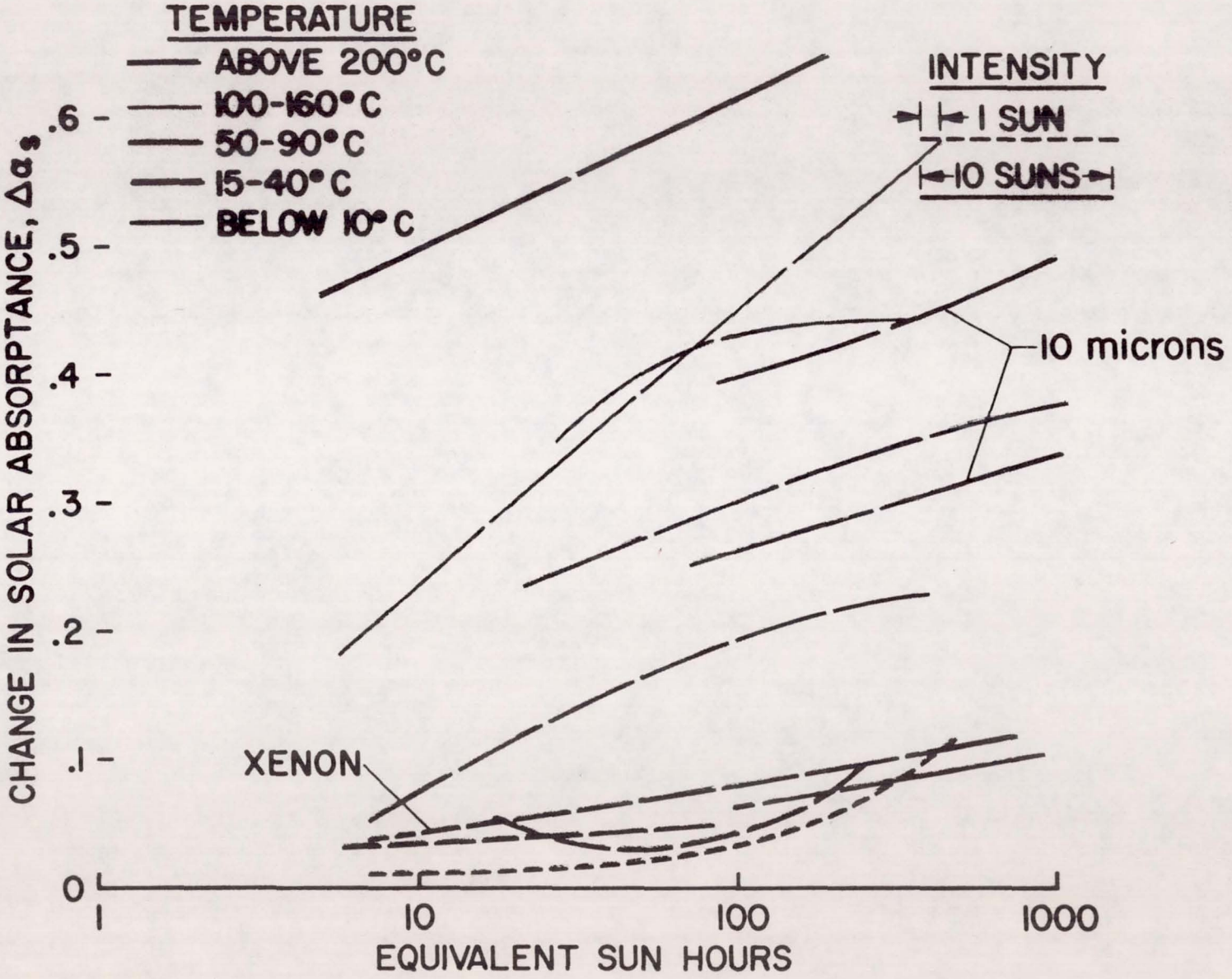

Figure 4.- Degradation of antimony trioxide - potassium silicate coating.

NATIONAL AERONAUTICS AND SPACE ADMINISTRATION
AMES RESEARCH CENTER, MOFFETT FIELD, CALIFORNIA

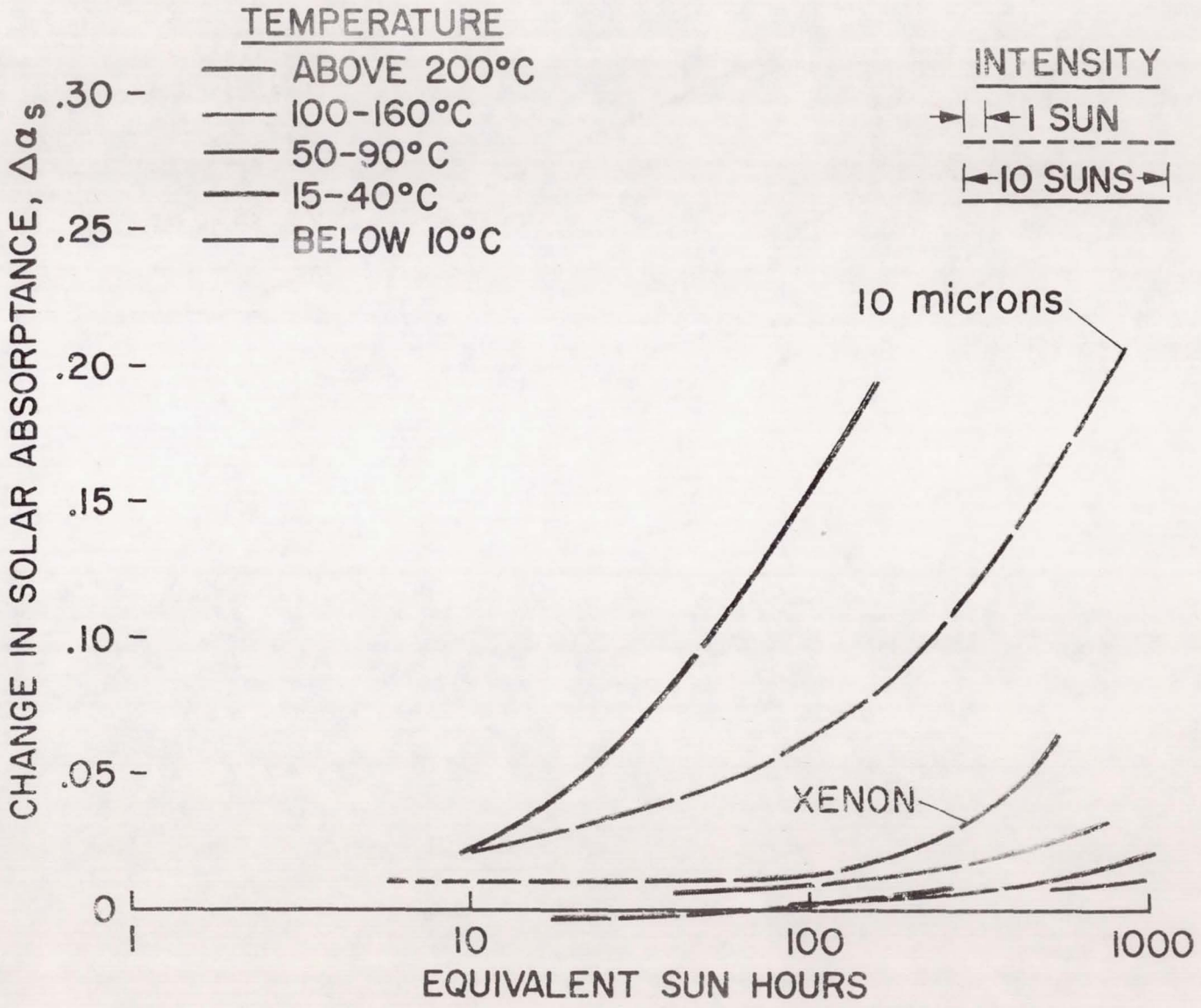

Figure 5.- Degradation of zinc oxide - potassium silicate coating.

NATIONAL AERONAUTICS AND SPACE ADMINISTRATION
AMES RESEARCH CENTER, MOFFETT FIELD, CALIFORNIA